UCGE Reports
Number 20171

Department of Geomatics Engineering

Development of an Ionosphere Monitoring Technique Using GPS Measurements for High Latitude GPS Users

(URL: http://www.geomatics.ucalgary.ca/links/GradTheses.html)

by

Mahmoud Lotfy El Gizawy

March 2003

THE UNIVERSITY OF CALGARY

Development of an Ionosphere Monitoring Technique Using GPS Measurements for High Latitude GPS Users

by

Mahmoud Lotfy El-Gizawy

A THESIS

SUBMITTED TO THE FACULTY OF GRADUTE STUDIES IN

PARTIAL FULFILMENT OF THE REQUIRMENTS FOR

DEGREE OF MASTER OF SCIENCE

DEPARTMENT OF GEOMATICS ENGINEERING

CALGARY, ALBERTA

March, 2003

ABSTRACT

Auroral activity is a significant concern for reliable operation of GPS positioning applications, at high latitudes. Auroral substorms are characterized by increased spatial and temporal decorrelations of ionospheric range delay. The loss of signal availability can occur during periods of ionospheric scintillations. In recent years, GPS precise positioning applications have been disrupted consistently in Northern Canada – at significant cost to commercial surveying operations. Given the number of GIS, exploration, and construction applications presently relying on GPS in Canada, a significant need exists to develop ionospheric warnings and alerts for the GPS user community.

In order to provide timely predictions of the auroral activity, and associated degradations in receiver tracking performance and positioning accuracies, a monitoring technique of the magnitude and extent of the ionospheric effects in Canada and Northern United States is developed. In addition, a real-time ionospheric warning and alert system for GPS users is established. The techniques presented here are based on dual frequency GPS observations from a network of permanent GPS reference sites in North America, using measurements from IGS network. Using dual-frequency measurements, a GPS-based index is introduced to describe the local ionospheric activity in the region where the observation line-of-sight penetrates the ionosphere. Statistical analysis is conducted to define the threshold values of the introduced index, and to define the corresponding spatial and temporal correlations of TEC. Regions of high, moderate, and quiet

ionospheric activity are identified according to the GPS-based index. A warning, therefore, is issued according to the user's location.

This technique has been implemented successfully to monitor the ionosphere during periods of high and moderate activity. Reliability of the monitoring technique has been investigated during a period of 8 months. The technique successfully monitored "active" ionosphere (i.e. high or moderate activity) more than 90% of the time.

It is intended that techniques developed in this thesis will be applied in the Canadian GPS Network for Ionosphere Monitoring (CANGIM) – currently being developed by the University of Calgary. This network will consist of a number of GPS Ionospheric Scintillation Monitors (GISM). Observations will be processed at a centralized control facility at the University of Calgary. It is intended that GPS users will access the real-time ionosphere warning service via the Internet.

ACKNOWLEDGEMENTS

I would like to express my deep appreciation to my supervisor Dr. Susan Skone for her continuous guidance and support every day of my graduate studies, for her patience and her confidence in me, and for the financial support. I was extremely lucky to have a supervisor like her. Dr. Yang Gao, and Dr. Brent Maundy are thanked for their constructive comments on my thesis.

IGS network is acknowledged for providing the data used in this thesis. My research was funded by Federal NSERC grants, Canadian Hunter award, and Department of Geomatics Engineering Graduate Research Scholarships.

Many thanks go to my colleagues: Natalya Nicholson, Paul Alves, Rob Watson, Sudhir Shreshta, Victoria Hoyle, and Yongjin Moon.

To my good friends in Calgary who are always there for me, many thanks for their endless support. Specifically, Dr Abouelmagd Noureldin, Ahmed Helmy, Ahmed Elmetwaly, Dr Husam Kinawi, Khaled Abdelrahman, Mohamed Abdelsalam, Mohamed Elhabiby, Dr Naser Elsheimy, Ramy Zaghloul, Sameh Nassar, Samer Adeeb, Sherif Saad, and Walid Noureldin.

Special thanks go to my friend Kara McCarty for her continual encouragement and support throughout my life in Calgary.

In the thesis guidelines provided by the Faculty of Graduate studies, an acknowledgement page is an option and it should not exceed a one page. If I want to thank my parents and my sister, I know I would write thousands and thousands pages trying to thank them. All that I am, and all that I will ever be, I owe to them.

TABLE OF CONTENTS

LIST OF TABLES

LIST OF FIGURES

LIST OF ABBREVIATIONS

1-D	one-dimensional
2-D	two-dimensional
2DRMS	two Distance Root Mean Square
C/A code	Coarse/Acquisition code
DGPS	Differential Global Positioning System
IGS	International GPS Service
IPP	Ionospheric Pierce Point
ISM	Ionosphere Scintillation Monitor
GIS	Geographic Information System
GPS	Global Positioning System
NOAA	National Oceanic and Atmospheric Administration
MPC	Modulated Precision Clock
P code	Precise code
PLL	Phase Lock Loop
PRN	Pseudo-Random Noise
Relative TEC	Relative Total Electron Content
RTEC	time Rate of change of Total Electron Content
RTECI	time Rate of change of Total Electron Content Index
RTK	Real-Time Kinematic
TEC	Total Electron Content (el/m^2)
TECU	Total Electron Content Unit (10^{16} el/m^2)
SED	Storm Enhanced Density
SNR	Signal-to-Noise Ratio
SSP	Standard Positioning Service (SPS)
UT	Universal Time
UTC	Universal Time Coordinated
UV	Ultra Violet

CHAPTER 1

INTRODUCTION

1.1 BACKGROUND AND MOTIVATIONS

In the early 1970s, the Global Positioning System (GPS) was established by the U.S Department of Defense (DoD). The GPS system was intended mainly for military purposes. The world-wide civil community has been quickly attracted to the usefulness of GPS in extensive applications and fields [*Parkinson at al.,* 1994]. Since the 1970's, researchers have focused on defining the different positioning error sources, studying their effects, and searching for methods to decrease, or possibly eliminate these errors in order to achieve better positioning accuracies.

The different GPS error sources have been defined as three types. First, satellite errors exist; these include ephemeris errors in the transmitted location of the satellite and satellite clock errors in the transmitted clock. Secondly, propagation errors also occur when GPS signals are transmitted through the ionosphere and troposphere. Finally, errors are associated with the reception of the signal, such as multipath errors that are caused by signals reflected prior to reaching the receiver antenna, and receiver measurement noise [*Parkinson et al.,* 1996].

One of the major error sources is the ionosphere, where GPS signals transmitted by satellites have to propagate through the dispersive ionosphere layers. In a high latitude region of the Earth's ionosphere, interactions between the solar wind and the Earth's magnetic field lead to creation of the auroral oval. While commonly observed in Canada and Northern Europe, the auroral oval can also expand several degrees equatorward over the Northern United States and Europe during periods of increased geomagnetic activity. In the auroral zone, irregular precipitation of energetic electrons occurs during substorm events – resulting in optical and UV emissions (Northern/Southern Lights). During such events, structured depletions/enhancements of total electron content (TEC) can occur in the auroral ionosphere (at E-region altitudes of 110 km). *Hunsucker et al.* [1995] determined that these features are medium-scale structures (20-130 km in wavelength) with amplitudes of 1-5 TECU for slant TEC series at lower elevation angles (16 – 80 cm ionospheric range delay on L1).

Ionization along terrestrial magnetic field lines also results in small-scale field-aligned irregularities in electron density at F region (350 km) altitudes. These irregularities have scale sizes on the order of 1 km or less, and can cause phase and amplitude scintillations. Phase scintillations are observed as high frequency fluctuations in GPS carrier phase observables. The resulting dynamic stress on the carrier tracking loops is associated with an increased probability that the GPS receiver will lose phase lock. Amplitude scintillation is observed as a random rapid fluctuation of the signal strength, leading to periods of reduced signal strength at the GPS receiver antenna – resulting in short term signal fading. In some cases, fading may be so severe that the signal level drops

below the receiver threshold. Extensive studies of scintillation effects on GPS signals have been conducted [*Knight and Finn,* 1996*; Bishop et al.,* 1998*; Nichols et al.,* 2000*; Doherty et al.,* 2000*; Skone et al.,* 2001].

Mitigation of the ionospheric effects during periods of enhanced ionospheric activity in auroral and sub-auroral regions is a challenge facing GPS users. If the location of the auroral oval can be identified, and the magnitude of auroral disturbances can be quantified, excellent insight into auroral effects on GPS may be gained. It therefore becomes possible to notify GPS users of the possible impacts on GPS signals. The auroral oval location and extent varies with solar and geomagnetic activity [*Hargreaves,* 1992].

The ionosphere activity can be monitored by considering TEC observations derived from a network of GPS stations using dual-frequency measurements [*Wanninger*, 1993; *Coker et al.*, 1995]. The rate of change of TEC may be derived from precise GPS carrier phase observations; this has been used as a measure of ionospheric disturbances at high latitudes [*Stewart and Langley*, 1999; *Pi et al.*, 1997]. The severe GPS signal phase fluctuations observed during auroral substorm events are directly observed in rapid rates of change of total electron content (RTEC). By using dual frequency GPS data, the time rate of TEC may be measured from precise carrier phase observables. This provides an opportunity to track the magnitude and the extent of auroral ionospheric effects in Canada and Northern United States by using measurements from a network of GPS stations. Development of such a method is the focus of this thesis research.

Furthermore, it becomes essential to provide a real-time ionosphere warning according to the GPS user location and the ionospheric activity level, as introduced in this thesis. The user will be able to identify the levels of the ionospheric activity and the possible impacts on GPS measurements. The objectives of this research are described in the following section.

1.2 RESEARCH OBJECTIVES

The availability of enormous amounts of TEC observations derived from a network of GPS stations, using dual-frequency GPS measurements, provides an excellent resource for monitoring the ionospheric activity. The lack of precise techniques for monitoring the extent and effects of the auroral region – particularly for GPS users during periods of enhanced ionospheric activity - is the motivation of this thesis work. This thesis work introduces a methodology for an online ionospheric warning service for GPS users, and achieves the following objectives:

1) Introduce a GPS-based index to describe the level of ionospheric activity. In turn, develop a method to track in real-time the magnitude and extent of the auroral oval, and identify levels of ionospheric activity in Canada and Northern United States.

2) Quantify the associated impacts on GPS applications. Determine temporal and spatial correlations in the disturbed high latitude ionosphere for various levels of

ionospheric activity – useful information for various GPS positioning applications, such as RTK and regional networks.

3) Based on Objectives 1 and 2, develop an ionospheric warning and alert system for GPS users in the Canadian sector, which can operate in near real-time and be accessed via the Internet.

1.3 THESIS OUTLINE

The research objectives have been stated in the previous section. Essential background material will be provided in Chapters 2 and 3 as fundamentals required to reach the desired objectives. Chapter 2 covers an introductory overview of GPS theory and GPS error sources. The second part of Chapter 2 provides essential background of ionosphere phenomena and characteristics.

Chapter 3 describes the impact of ionospheric activity on GPS signals and GPS applications. This chapter discusses the possible ionospheric effects on GPS signals, and the potential ionospheric impact on GPS positioning accuracies, as well as the receiver tracking performance – especially during periods of enhanced ionospheric activity. A description of different ionospheric regions is given, as well as an overview of the physical parameter called total electron content (TEC), and the derivation of an expression for ionospheric range delay.

Chapters 4 and 5 address the research objectives and contain the research analysis. Chapter 4 introduces the ionospheric GPS-based index, and investigates its correlation with the temporal and spatial properties of ionospheric activity in the auroral region. A description of the data set used in this investigation is provided. In Chapter 5, a technique is introduced for monitoring the magnitude and extent of the auroral oval, and identifying levels of ionospheric effects in Canada and Northern United States. This technique is demonstrated for three sample events presenting high, moderate, and quiet ionospheric activity. The ionospheric warning and alert system is also introduced, and demonstrated for the same scenarios. The reliability and efficiency of the proposed technique is also investigated in this chapter through extensive testing and analysis.

Finally, a summary of the research work is presented in Chapter 6. Potential future research and recommendations for future work are also provided in Chapter 6.

CHAPTER 2

GPS THEORY AND IONOSPHERE PHENOMENA OVERVIEW

A detailed definition of Global Positioning System (GPS) as given by *Wooden* [1985] reads: "The Navstar Global Positioning System (GPS) is an all weather, space based navigation system under development by the U.S. Department of Defense (DoD) to satisfy the requirements for the military forces to accurately determine their position, velocity, and time in a common reference system, anywhere on or near the earth on a continuous basis".

Despite the main military goal of GPS, it has attracted a broad spectrum of users. Moreover, it has become an essential component of various applications ranging from surveying and mapping as well as precise time determination, vessel navigations and oceanography to international air traffic management [*Parkinson et al.,* 1994].

Basically, GPS is comprised of three main segments: the space segment, the control segment and the user segment. The purpose of these segments is to provide continuous reliable positioning and timing services for GPS users. The space segment consists of 24 satellites orbiting around the earth at an altitude of about 20200 km and with a period of approximately 12 hours as illustrated in Figure 2.1 [*Hoffmann-Wellenhof et al*., 1994].

Each satellite transmits a signal that includes the navigation messages based on periodically uploaded data from the control segment. The control segment is a set of monitor stations, ground control stations, and a master control station (that is the central control node for GPS operations) and backup master control station. The user segment consists of GPS receivers from wide varieties of manufacturers. These receivers process the received GPS signals and compute the user position.

Figure 2.1 GPS satellite constellation

The GPS reference coordinate system is the World Geodetic System 1984 (WGS-84) [*Decker,* 1986]. The user's coordinates are determined in this frame and can then be transformed to other systems. Timing is the heart of GPS; GPS time uses an atomic time scale. GPS time is defined as the number of seconds elapsed from Saturday midnight of the present week. The GPS time was coincident with Universal Time Coordinated (UTC is maintained by the U.S. Naval Observatory USNO) at the GPS standard epoch of January 6,

1980. GPS time is synchronized with UTC at the microsecond level, within an integer number of seconds. The integer offset between GPS time and UTC arises because of the leap seconds periodically inserted for UTC [*Hoffmann-Wellenhof et al*., 1994].

Fundamentals of GPS signal structure, observations and error sources, as well as ionosphere characteristics and associated effects on GPS, are presented in the following sections. These fundamentals are directly relevant to the research presented in this thesis.

2.1 GPS SIGNAL STRUCTURE

The GPS signal is an electromagnetic wave generated by an oscillating electric force transmitted from GPS satellites. The signal strength decreases as the distance traveled between the satellites and GPS receiver increases. This is due primarily to geometric spreading and, to a lesser extent, attenuation in the ionosphere and troposphere.

Currently, GPS satellites broadcast ranging codes and navigation data on two main frequencies: L1 (f_{L1} = 1575.42 MHz) and L2 (f_{L2} = 1227.6 MHz). Two different codes are modulated on GPS signals. The precise code (P code) is modulated on both L1 and L2 signals. P-code is intended for military users, as it is encrypted with additional W-code. This Anti-Spoofing (AS) encryption denies civilian users access the P-code. The second code is the coarse acquisition code (C/A code), which is modulated only on the L1 signal and intended primarily for civilian users. The GPS signal spectrum is shown in Figure 2.2.

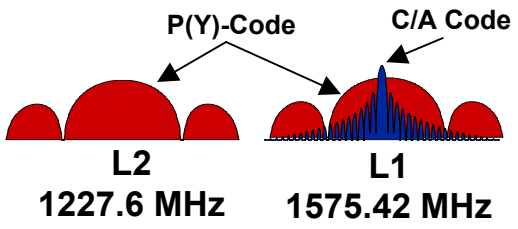

Figure 2.2 Signal spectrum for current GPS signals

Due to the dispersive nature of the ionosphere layer, having two GPS signals (i.e. L1 and L2) allows dual frequency users to remove the first order ionosphere dispersive effects. L1 and L2 signals are represented by the following equations [*Hoffmann-Wellenhof et al.*, 1994]:

$$L1(t) = a_1 P(t) W(t) D(t) \cos(2\pi f_1 t) + a_1 C/A(t) D(t) \sin(2\pi f_1 t) \quad (2.1a)$$

$$L2(t) = a_2 P(t) W(t) D(t) \cos(2\pi f_2 t) \quad (2.1b)$$

where

P(t), C/A(t)	= P(precise), C/A(coarse acquisition) codes,
$a_1\cos(f_1t)$,$a_2\cos(f_2t)$	= L1,L2 unmodulated carriers,
W(t)	= W-code, and
D(t)	= navigation message.

In 2003, it has been scheduled to add C/A code to the second GPS signal L2 as part of GPS modernization. Furthermore, the first set of Block IIF satellites will be launched in 2005 and will broadcast a third civilian frequency L5 at 1176.45 MHz [*Challstrom,* 1999].

While all GPS satellites transmit signals on the same frequencies (i.e. L1 and L2), each satellite transmits a different PRN code that allows GPS receivers to identify individual satellites. This technique is called Code Division Multiple Access (CDMA) [*Kaplan,* 1996].

2.2 GPS OBSERVABLES

The three GPS observables are the pseudorange P, the carrier phase Φ and the Doppler observable. The pseudorange is the range measurement derived using the time delay between the received PRN code and the code replicated by the receiver multiplied by the speed of light. The pseudorange would present the true geometric range between the satellite and the receiver antenna if satellite and receiver clocks were perfectly synchronized with each other, and all other error sources were negligible. However, the fact is that there is always a bias between the satellite and receiver clocks, and the pseudorange measurement does not represent the true geometric range. Also, due to the fact that the GPS signal does not travel through a vacuum, several atmospheric ranging errors exist in the GPS measurements. The observation equation of pseudorange and accompanied errors is expressed in as follows [*Wells et al.,* 1987]:

$$P = \rho + d\rho + c(dt - dT) + d_{ion} + d_{trop} + \varepsilon_{m_p} + \varepsilon_p \tag{2.2}$$

where

ρ = geometric range between the satellite and receiver antenna in metre,

$d\rho$ = satellite orbit error in metres,

c = the speed of light (metres/second),

dt = satellite clock error in seconds,

dT = receiver clock error in seconds,

d_{ion} = ionospheric delay error in metres,

d_{trop} = tropospheric delay error in metres,

ε_{ion} = code range multipath error in metres, and

ε_{p} = receiver code noise in metres.

The second observable is the carrier phase, which is made in the frequency domain. The carrier phase observable results from the difference between the received phase and the receiver-generated phase. This observable is ambiguous by an integer number of cycles, however it is more accurate than the pseudorange when the ambiguity is resolved. The carrier phase measurements are expressed mathematically as follows [*Wells et al.,* 1987]:

$$\Phi = \rho + d\rho + c(dt - dT) - d_{ion} + d_{trop} + \varepsilon_{m_\phi} + \varepsilon_{\phi} + \lambda N \qquad (2.3)$$

where

λ = carrier wavelength in metres,

N = integer ambiguity in cycles,

ε_{m_ϕ} = carrier phase multipath error in metres, and

ε_{ϕ} = receiver carrier noise in metres.

The third observable is the Doppler measurement. The Doppler frequency is a time rate of change of carrier phase observables, and it is a measure of the relative velocity between the satellite and the receiver. This measurement is not affected by cycle slips, nor does it have an integer ambiguity. The Doppler measurements are used for cycle slip detection and for velocity estimation. The observation equation can be expressed as follows:

$$\dot{\Phi} = \dot{\rho} + \dot{d}\rho + c(\dot{d}t - \dot{d}T) - \dot{d}_{ion} + \dot{d}_{trop} + \dot{\varepsilon}_{\phi} \qquad (2.4)$$

where the dots indicate the derivatives with respect to time.

2.3 GPS OBSERVABLE ERROR SOURCES

As indicated in Section 2.2, a number of error sources affect GPS measurements, which results in degradation of accuracy of GPS positioning. The error sources are briefly discussed below.

2.3.1 Orbital Errors

There are two ways to compute GPS satellite orbits: broadcast ephemeris, and precise ephemeris [*Hoffmann-Wellenhof et al.*, 1994]. The broadcast ephemeris is based on transmitting Keplerian and perturbation parameters in the navigation message, and then the

satellite's coordinates are computed from the broadcast ephemeris. The broadcast orbits are accurate to approximately 4 metres [*Jefferson et al.,* 2000].

The other way to compute the satellite coordinates is by using the precise ephemeris, which is provided by the IGS (International GPS Service). There are three forms of precise ephemeris categorized according to the achieved accuracies of the computed satellite coordinates. The most accurate orbital information is the final orbits, which can be accurate at the level of 5 centimetres [*IGS,* 2002]. The final orbits are available with delay of about two weeks. The second form of the precise ephemeris is the rapid orbits, which is available about two days after the observation period. The third form is the ultra-rapid orbits, which contains data of two days: the first day is data of post-mission orbits, and the second day is predicted data. The ultra-rapid orbits are the least accurate type of precise orbits, which can be accurate at level of 25 centimetres [*IGS,* 2002].

2.3.2 Clock Errors

GPS operates with its own time scale, which is referred to as GPS time. This time system is based on an atomic time scale, and is in reference to Coordinated Universal Time (UTC). GPS time varies between 0 and 604800 seconds. Each week GPS time is reset to zero at midnight on Saturday and the GPS week is incremented by 1. Sources of the clock errors can be due to drifts in either the satellite or receiver oscillators. Errors due to the satellite clock are the offset between the satellite clock and the GPS system time. This

offset arises from the instabilities in GPS satellite oscillators. Errors due to the satellite clock are generally less than 1 ms, and it can be eliminated by differencing the observations between two different receivers with respect to the same satellite [*Lachapelle,* 2001]. Additionally, this error can be estimated by the broadcast coefficients as part of the navigation message with typical accuracy in the range of 8 – 10 ns [*Lachapelle,* 2001]. The satellite clock error also can be estimated more accurately and provided by IGS network. The predicted clock errors by IGS are accurate to 5 ns, which is equivalent to 150 cm in range [*IGS,* 2002]. The accuracy of the computed precise clocks in post-mission by IGS can be accurate to 0.1 ns, which is 3 cm in range [*IGS,* 2002].

The offset between the receiver clock and the GPS system time produces the receiver clock error. Temporal variations in this error depend on the type of receiver oscillator. The magnitude of the receiver clock error ranges from 200 ns to several ms and depends on the receiver internal firmware [*Lachapelle,* 2001]. It can be eliminated by differencing the observations of the same receiver between two different satellites.

2.3.3 Receiver Noise

During the measurement process, the receiver produces noise, which is caused by a number of factors. These include dynamic stress on the receiver's tracking loops, code correlation method, thermal noise, and antenna gain pattern. Typically, the receiver noise ranges from 0.1%-1.0% of the observable wavelength [*Weisenburger,* 1997]. The error due to the receiver noise on the code measurements typically is at a level of tens of centimetres,

while it is a few millimetres on the carrier phase observable [*Van Dierendonck et al.,* 1992]. The uncorrelated nature of the receiver noise makes it a significant error source for differential GPS (DGPS) users.

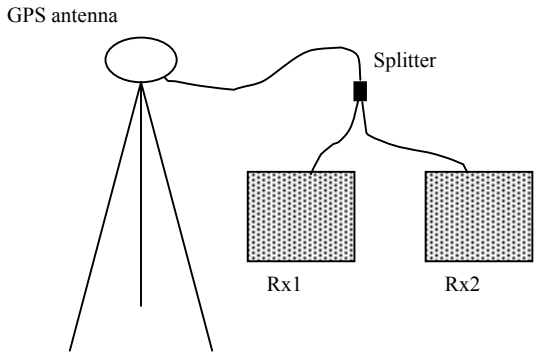

Figure 2.3 Zero-baseline test

The receiver noise strongly depends on the receiver itself, and it can be measured effectively though a zero-baseline test, where differences between observations derived at each receiver depend only on the internal receiver processing characteristics, as shown in Figure 2.3.

2.3.4 Multipath Error

Multipath errors are produced due to corruption of the directly received GPS signal by an indirectly received GPS signal. The GPS signal arrives at the receiver via multiple paths because of the reflection of the transmitted GPS signal by surrounding buildings, reflecting surfaces, and any objects that might reflect the signal, as illustrated in Figure 2.4.

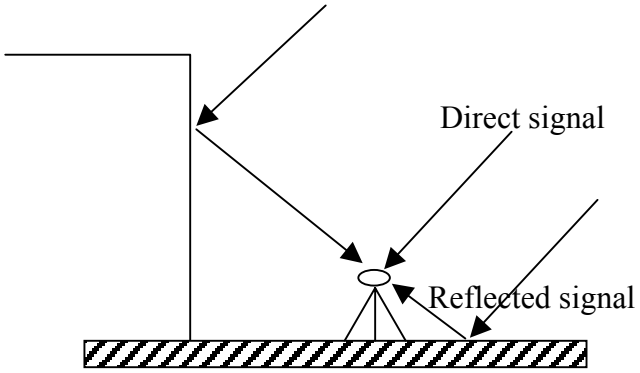

Figure 2.4 Direct and multipath signal

Observations at low elevation angles are more susceptible to multipath effects than those at high elevation angles. The magnitude of multipath errors is much greater for code measurements than for the carrier phase. In a severe multipath environment, the multipath can reach up to 15 m for code measurements, and approximately 5-6 cm for carrier phase measurements on L1 and L2 [*Ray,* 2000].

The simplest method to reduce the multipath errors is to avoid multipath environments by choosing a clear antenna location that is not near any reflecting surfaces. Also, multipath effects can be mitigated using a number of receiver processing technologies, such as narrow correlator spacing [*Van Dierendonck et al.,* 1992], Multipath Elimination Technology [*Townsend and Fenton,* 1994], and Multipath Estimating Delay Lock Loops [*Townsend et al.,* 1995]. Multipath errors can also be reduced by choosing an antenna with specific properties of signal polarization [*NovAtel,* 2000], as well as, using radio absorbent ground planes and choke rings at the antenna.

2.3.5 Troposphere Delay Error

The transmitted GPS signal travels through the atmosphere layers before it is received by the GPS receiver's antenna. The atmosphere consists of two main regions: the troposphere – which extends up to 50 kilometres above the earth's surface – and the ionosphere layers. The troposphere layer is a neutral part of the atmosphere, which causes attenuation, delay, and short-term variations (scintillation) of the GPS signals. The magnitude of the tropospheric delay errors depends on temperature, the atmosphere pressure, and the partial pressure of water vapor. The magnitude of delay errors is highly correlated with the satellite elevation angles, where it increases significantly with lower elevation angles.

The tropospheric delay is the sum of dry and wet components. It can be expressed mathematically as follows:

$$d_{trop} = d_{dry}.m_{dry} + d_{wet}.m_{wet} \tag{2.5}$$

where

d_{trop} = total tropospheric delay,

d_{dry} and d_{wet} = dry delay and wet delay respectively at zenith, and

m_{dry} and m_{wet} = the corresponding mapping factors to map the zenith delay to the slant direction of satellite-receiver line-of-sight.

The dry component contributes approximately 80%-90% of the total tropospheric delay, and it can be accurately estimated, while the wet component contributes 10%-20% of the delay. The wet component is difficult to estimate due to the unpredictable nature of atmospheric water vapour. The dry delay at the zenith is about 2.3 metres, while the wet delay is approximately 1-80 centimetres [*Spilker,* 1996].

The troposphere layer is a non-dispersive medium for GPS frequencies, which means that the tropospheric range errors cannot be cancelled through the use of dual frequency GPS measurements - unlike the ionospheric delay as it will be discussed in section 2.3.6. The tropospheric range delay can be estimated using a number of models [i.e. *Hopfield*, 1969; *Saastamoinen*, 1973; *Goad and Goodman*, 1974; and *Black*, 1978]. The dry delay can be estimated with an accuracy of less than 1%, while the wet part can only be estimated with accuracy of 10%-20% [*Mendes,* 1999].

2.3.6 Ionosphere Delay Error

The second region of the atmosphere is the ionosphere, which extends approximately 50 to 1500 kilometres above the surface of the earth. The ionosphere is an ionized layer consisting of ions and electrons. In this region the group and phase velocities are not the same as the speed of light. This fact introduces an ionospheric range delay error. This delay has an equal magnitude and opposite sign for the pseudorange and carrier phase measurements. In addition to the range delay error, there are other effects of the ionosphere on GPS signals such as range-rate errors, and phase and amplitude scintillations.

The fact that the ionosphere is a dispersive medium, unlike the troposphere, allows correction of the first order ionospheric range delay errors. These errors can be evaluated by integrating the electron density along a 1-m^2 column along the signal path using the following equation.

$$d_{ion} = \frac{40.3}{f^2} TEC \tag{2.6}$$

where f is the signal frequency, and TEC is the total electron content along the signal path. The calculation of the absolute TEC is presented in Equation (2.7) for the case where range measurements are available on two separate frequencies.

$$TEC = \frac{1}{40.3}\left(\frac{1}{f_1^2} - \frac{1}{f_2^2}\right)^{-1} (P_1 - P_2) \quad (\text{el/m}^2) \tag{2.7}$$

where

P_1 = pseudorange observable on L1 signal,

P_2 = pseudorange observable on L2 signal, and

el = number of electrons.

Typical magnitudes of the range delay error are a few metres to tens of metres [*Klobuchar,* 1996], and vary according to several factors such as the user's location, elevation angle, the time of the day, the time of the year, and solar cycle. Details on the ionosphere characteristics and ionospheric effects on GPS signals and applications are discussed in later sections.

2.4 IONOSPHERE CHARACTERISTICS

As mentioned in section 2.3.6, the ionosphere is the ionized layer of the earth's atmosphere. This electronically charged layer disperses the radio-wave signal according to the free electron density and the signal frequency – as expressed in equation 2.6.

2.4.1 Ionization Process

The solar emissions directed towards the earth's atmosphere play the main role in the ionization process. The sun's ultra-violet (UV) emissions ionize the gaseous O, O_2, and N_2 molecules and produces free electrons and ionized particles as shown in Figure 2.5 [*Bugoslavskaya,* 1962]. The free electron content is proportional to the ionization versus recombination. The recombination occurs if a free electron is near to an ion, so that they reform into molecular constituents.

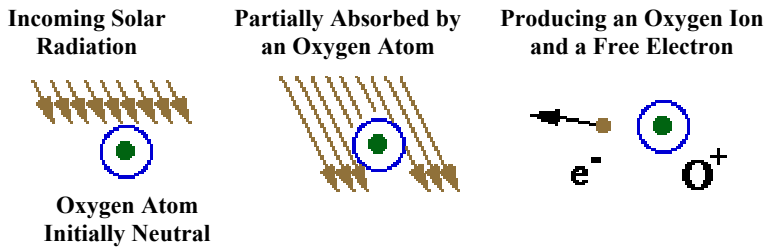

Figure 2.5 The ionization process

The fact that solar radiation is responsible for the ionization process results in maximum free electron content of the ionosphere at 1400 local time, just after local noon. The ionosphere electron density increases dramatically on the day side due to the increase of the UV, X-ray and gamma-ray photons. Some electrons precipitate into the ionosphere in the high latitude region, which causes an increase in the electron density at polar and auroral regions. The ionosphere effects on the GPS signal can increase during storm events and become a significant concern for GPS users.

The molecular absorption of the solar radiation increases with increasing altitude, and different vertical density layers are stratified. A discussion of the different ionosphere layers is presented in the next section.

2.4.2 Ionosphere Structure

The ionosphere consists of different regions: D, E, F1, and F2. The ionospheric processes and effects have different characteristics between these regions [*Rishbeth and Garriott,* 1969]. The free electrons are considered to be the most important parameter affecting GPS applications, and the vertical electron density profile is shown in Figure 2.6 [*Davies,* 1990].

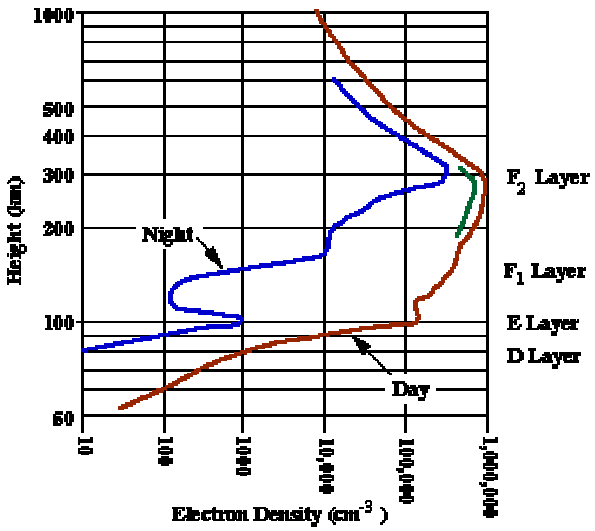

Figure2.6 The electron density profile as function of altitude

The D region lies above 60 km and below 90 km. The D region's ions are produced by the X-ray radiation. This region vanishes at night due to the recombination of ions and electrons, and is of little concern for GPS users.

The E region extends 90 to 150 km above the earth's surface, and has lower electron density than the F1 and F2 regions. The electron density in the E region has irregular structure at high latitude, produced by precipitation of energetic electrons, which creates the auroral oval.

The highest region of the ionosphere is known as F region, which extends 150 to 1000 km above the earth. The F region is divided into F1 and F2 sub-regions. The F1 region disappears at night, while the F2 region has the highest electron density at a height of approximately 350 km in altitude. This peak of the electron density highly depends on the time of the day, the season, and the year of the solar cycle (see section 2.4.3). The F2

region is of main concern for GPS users - due to the absolute ranging errors caused by the larger electron densities in this region.

2.4.3 Solar Cycle

Solar activity is associated with the sunspots that are cooler, dark patches on the sun's surface. Sunspots go through a cycle of high and low activities periodically repeated in an 11-year cycle, known as a solar cycle. The ionospheric electron density profiles highly depend on the solar cycle due to the fact that the high sunspot activity is associated with an increase of solar flares (enormous release of electromagnetic energy from the sun) and overall enhanced solar electromagnetic radiation. The current solar cycle has peaked in the middle of the year 2000 as illustrated in Figure 2.7.

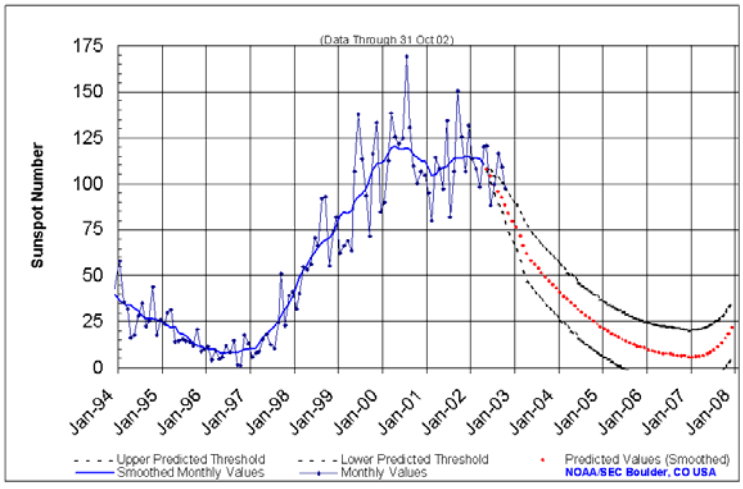

Figure 2.7 The current solar cycle sunspot number progression

(NOAA/Space Environment Center)

There is a significant increase of the occurrence and magnitude of the magnetic storms associated with enhanced solar flare activity during periods of maximum solar cycle. The magnetic storm is a global disturbance in the earth's magnetic field in the mid- and low-latitude regions. These events may be associated with substorm and aurora, where the solar energetic particles interact with earth's magnetic field and cause significant changes to the ionosphere's electron density. Such effects occur in regions of high latitude.

2.4.4 Local / Global Geomagnetic Activity Index "K/Kp"

During periods of enhanced auroral activity, the presence of strong electric currents is reflected in the Earth's magnetic field variations. Such currents fluctuate in response to transient storm events. Therefore, ionospheric activity in auroral and sub-auroral latitudes can be described approximately by geomagnetic variations. Geomagnetic indices are derived using measured variations in Earth's magnetic field strength at ground-based magnetometer stations.

Local K indices are derived at a given station by computing the maximum range between the lowest and highest observed magnetic field values during a three-hour time interval. This range is then converted into an integer value ranging from 0 to 9, with 0 representing the lowest level of ionospheric activity. The global Kp indices are the mean value of all K indices – for a given three-hour interval - derived from thirteen globally distributed stations in the sub-auroral region [*Mayaud,* 1980]. In this thesis, local North

American K indices (from Boulder, Colorado) are used to identify periods of high ($K \geq 7$), moderate ($K = 3 – 6$), and quiet ($K \leq 2$) ionospheric activity levels.

2.5 SUMMARY

In the last two decades, GPS applications have been growing rapidly, proving the availability and reliability of the Global Positioning System. However, the GPS positioning accuracies are affected by different error sources. A major error source results from the signal transmission through the ionosphere layers. This error can be dominant during periods of enhanced ionospheric activity. These periods of high ionospheric activity are usually accompanied by significant degradation of positioning accuracy, and degradation of receiver tracking performance. However, the severity of the ionospheric effects is a function of various factors, such as the user location, season, time of day, and the receiver type. In Chapter 3, potential ionospheric impacts on GPS applications are discussed in detail. Descriptions of the various factors that affect the severity of ionospheric effects are also provided in this Chapter.

CHAPTER 3

IONOSPHERIC EFFECTS ON GPS APPLICATIONS

During the GPS signal transmission from satellite to receiver, the signals propagate through the ionosphere, which has several effects on GPS signals. One of the most important parameters to characterize the ionosphere layer is the index of refraction. Understanding the index of refraction of the ionosphere is essential when studying the possible propagation effects of ionosphere on GPS signals.

3.1 IONOSPHERE INDEX OF REFRACTION

The wave propagation through the medium is characterized by index of refraction, and can be expressed as follows:

$$n = \frac{c}{v} \tag{3.1}$$

where c is the speed of light, and v is the velocity of the wave in a vacuum.

The ionosphere is not a homogenous medium. The phase index of refraction at a given location in the ionosphere, n_p, can be expressed by the Appleton-Hartree formula [*Rishbeth and Garriott,* 1969]:

$$n_p^2 = 1 - \frac{X}{1 - iZ - \frac{Y_T^2}{2(1 - X - iZ)} \pm \left[\frac{Y_T^4}{4(1 - X - iZ)^2} + Y_L^2 \right]^{\frac{1}{2}}} \tag{3.2}$$

where

$X = Ne^2 / \varepsilon_o m\omega^2 = f_n^2 / f^2$,

$Y_L = eB_L / m\omega = f_H \cos\theta / f$,

$Y_T = eB_T / m\omega = f_H \sin\theta / f$,

$Z = \nu / \omega$,

$\omega = 2\pi f$,

f = the radio-wave frequency,

f_H = the electron gyro frequency,

f_n = the electron plasma frequency,

N = Electron density (el/m^3),

e = electron charge = -1.602 x 10^{-19} Coulomb,

ε_0 = permittivity of free space = 8.854 x 10^{-12} Farads/m,

θ = the angle between the wave direction and the Earth's magnetic field,

m = the mass of a electron = 9.107 x 10^{-31} kg,

ν = the electron neutral collision frequency, and

B = ambient magnetic field.

Equation 3.2 can be simplified by ignoring higher order terms, where it has been concluded that higher order terms only contribute 1 to 2 mm of range error for GPS users during maximum solar condition [*Brunner and Gu,* 1991]. The first order term of the phase index of refraction can therefore be expressed by:

$$n_p = 1 - \frac{X}{2} = 1 - \frac{(2\pi)^2 N_e e^2}{2m\varepsilon_o (2\pi)^2 f^2} \tag{3.3}$$

By substituting values of constants e, m, and ε_0 in Equation 3.3, the phase index of refraction can be expressed by:

$$n_p = 1 - \frac{40.3N}{f^2} \tag{3.4}$$

Therefore, the phase index of refraction mainly depends on the electron density N, and the radio-wave frequency.

The propagation velocity of the code signal is defined by the group velocity. The group index of refraction can be derived from the relation:

$$n_g = n_p + \frac{f d_{n_p}}{df} = (1 - \frac{40.3N}{f^2}) + \frac{80.6fN}{f^3} = 1 + \frac{40.3N}{f^2} \tag{3.5}$$

Deriving the index of refraction for the ionosphere is essential in order to quantify the group delay of the code modulation, the phase advance of carrier signal, the Doppler shift, and any potential effects of Faraday rotation.

3.2 IONOSPHERIC IMPACTS ON GPS SIGNALS

The ionosphere layer produces range errors for GPS measurements. As discussed in Section 2.2, the carrier phase range, Φ, is derived by multiplying the number of carrier phase cycles by wavelength in the medium as shown in Equation 3.6. The pseudorange, *P* is derived by multiplication of code group delay in seconds by speed of light in the medium, as expressed in Equation 3.7.

$$\Phi = \int_{path} \lambda dN = \int_{path} \frac{\lambda_0}{n_p} dN \qquad \text{(cycles)} \qquad (3.6)$$

$$P = \int_{path} v_g dt = \int_{path} \frac{c}{n_g} dt \qquad \text{(metres)} \qquad (3.7)$$

The variable λ denotes the wavelength in the ionosphere, λ_o is the wavelength in a vacuum, v_g is the group velocity, and dN is the differential number of cycles.

3.2.1 Group Delay and Phase Advance

GPS pseudorange and carrier phase range measurements are estimated based on assumptions that the signal velocity and wavelength are equal to those values valid for an electromagnetic wave propagating in a vacuum. Due to the physical properties of the ionosphere, however, the ionosphere index of refraction has a non-unit value. Therefore, the assumption that the GPS signal travels at the speed of light in a vacuum - and with wavelengths equal to the wavelength in a vacuum – is incorrect. The apparent phase velocity is larger than the speed of light in a vacuum, causing the phase advance. The group velocity, however, is less than the speed of light, and causes the group delay. The phase and group velocities can be derived as follows:

$$v_p = \frac{c}{n_p} = \frac{c}{1 - \frac{40.3N}{f^2}} \approx c\left(1 + \frac{40.3N}{f^2}\right) \tag{3.8}$$

$$v_g = \frac{c}{n_g} = \frac{c}{1 + \frac{40.3N}{f^2}} \approx c\left(1 - \frac{40.3N}{f^2}\right) \tag{3.9}$$

The phase ionospheric range delay, $\Delta\Phi$, and the group range delay, ΔP, which are caused by the phase advance, and the group delay respectively, can therefore be derived by subtracting the assumed velocity, *c,* and the true velocities (i.e. v_p and v_g) multiplied by the travel time of the signal, and can be expressed as follows:

$$\Delta\Phi = \int_{path}(c - v_p)dt = \int_{path}(\frac{c}{v_p} - \frac{v_p}{v_p})dl = \int_{path}(n_p - 1)dl = -\frac{40.3}{f^2}\int_{path} Ndl = -\frac{40.3}{f^2}TEC \quad (3.10)$$

$$\Delta PR = \int_{path}(c - v_g)dt = \int_{path}(\frac{c}{v_g} - \frac{v_g}{v_g})dl = \int_{path}(n_g - 1)dl = \frac{40.3}{f^2}\int_{path} Ndl = \frac{40.3}{f^2}TEC \quad (3.11)$$

The magnitude of the range errors is equal for both carrier phase and pseudorange measurements but with the opposite sign. The quantity $\int_{path} Ndl$ can be evaluated by integrating the electron density along the signal path, *l*. This quantity represents the total electron content (TEC). Thus, the magnitude of the range errors is a function of the TEC along the signal path. Details of TEC estimation are presented in Section 3.3.

3.2.2 Doppler Shift (Range-Rate Errors)

There is a phase change (Doppler shift) of the received GPS carrier signal due to the satellite motions and due to the time rate of change of TEC (RTEC). The Doppler shift due to the RTEC can be computed by:

$$f_D = \frac{1}{2\pi}\frac{d\Phi}{dt} = \frac{8.44\times10^{-7}}{2\pi f}\frac{d(TEC)}{dt} = \frac{1.34\times10^{-7}}{f}RTEC \quad \text{(Hz)} \quad (3.12)$$

During periods of quiet ionospheric activity, RTEC is small (e.g. average 0.2 TECU/s), while during periods of high ionospheric activity, it has higher values due to the

rapid change of TEC [*Klobuchar,* 1996]. As an example, for L1 signal f = 1.5GHz, and assuming RTEC = 0.2TECU/sec. The additional frequency shift therefore is 0.18Hz, which is normally smaller than the receiver carrier phase tracking loop bandwidth. The additional Doppler shift would be of high concern, primarily for L2 users during periods of high ionospheric scintillation, where there is a rapid change of RTEC (i.e. RTEC > 1 TECU/s). The additional Doppler shift in some cases (i.e. $\Delta f > 1$ Hz) might not allow the receiver phase tracking loop to maintain a lock on GPS signal phase and would result in losing lock on the signal phase, and therefore cause cycle slips [*Skone,* 2001].

3.2.3 Scintillations

Ionospheric scintillations are rapid random variations in phase and amplitude of the received GPS signal, which are caused by electron density irregularities along the signal path through the ionosphere. Periods of scintillation are associated with the existence of regions of small-scale electron density irregularities in the ionosphere layer, as demonstrated in Figure 3.1. These patterns of irregularities can move through the ionosphere and the GPS satellite-receiver line-of-sight also moves relative to the irregularities. Rapid variations in refraction of the signal take place and the signal is diffracted at the irregularities. The emerging wavefront exhibits mutual interference and resulting variations in phase and signal amplitude are observed at the receiver. The severity of scintillation effects is related to the density and the size of such patterns of irregularities in electron density.

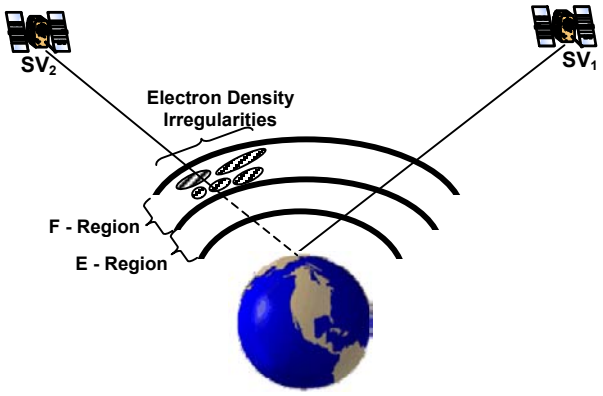

Figure 3.1 Electron density irregularities in the ionosphere

The amplitude scintillation (random rapid fluctuations of the signal strength) can lead to periods of reduced signal power at the GPS antenna. These fluctuations can cause short-term signal fading. Such fading can be so severe that the GPS signal-to-noise-ratio (SNR) drops below the receiver-tracking threshold, resulting in a loss of code lock. The phase scintillation is characterized by random rapid fluctuations of the signal phase, which can cause rapid carrier phase changes in the GPS signal. In turn, this increases the dynamic stress on the phase lock loops (PLL). If the scintillation produces a phase change faster than the receiver carrier tracking bandwidth can allow, the receiver will lose phase lock.

The ionosphere scintillation is of significant concern to GPS users during periods of high solar activity. The solar activity relates to the 11-year solar cycle as described in Section 2.4.3 (the peak of the current solar cycle was observed in the year of 2000 - 2001). In addition, the scintillation effects vary according to the user's location (i.e. geomagnetic latitude). During high ionospheric activity, these effects can be a serious problem for GPS users in some regions, such as polar and equatorial latitudes, while users in other regions

are not affected to a large extent. A discussion of the different regions and associated ionospheric effects is presented in Section 3.4.

3.3 TOTAL ELECTRON CONTENT (TEC)

The main parameter that describes the ionospheric effects on GPS signals is TEC. It is defined as the number of electrons in a vertical column that extends from the satellite to the receiver, and having a cross section of 1-m^2. The dispersive nature of the ionosphere allows calculations of TEC and rate of TEC using dual-frequency GPS measurements. Absolute TEC can be derived by forming a linear combination of the code measurements on L1 and L2 frequencies as expressed in Equation 3.13. The "absolute" TEC derived using code measurements are noisy; however, they can be smoothed by considering carrier phase ranges. The "relative" TEC derived using carrier phase measurements are not absolute, and are offset by a bias dependent on the L1 and L2 integer ambiguities.

In this thesis, the "relative" TEC are used, and are computed using only carrier phase observations as expressed in Equation 3.14. TEC values are measured in TEC Units (TECU). One TECU is equal to 10^{16} electrons/m^2. TEC values can be converted to ionospheric range for the L1 and L2 frequencies, using equation 3.11. One TECU is equal to 0.16 metres of range delay on L1, and is equal to 0.27 metres of range delay on L2.

$$TEC_P = \frac{1}{40.3}\frac{f_1^2 f_2^2}{f_2^2 - f_1^2}(P1 - P2) \qquad \text{(TECU)} \qquad (3.13)$$

$$TEC_{\Phi} = \frac{1}{40.3}\frac{f_1^2 f_2^2}{f_2^2 - f_1^2}[(\Phi_1 - \Phi_2) - \varepsilon_{\Phi,12} - b_r^{'} + b_s^{'} - \lambda_1 N_1 - \lambda_2 N_2] \quad \text{(TECU)} \qquad (3.14)$$

where

$\varepsilon_{\Phi,12}$ is carrier phase noise, and

$b_r^{'}, b_s^{'}$ are receiver and satellite interchannel biases, respectively, on the carrier phase measurements

For the purposes of this thesis, TEC is derived in geomagnetic latitude and magnetic local time (i.e. Sun-fixed coordinate system). The Solar-fixed coordinate system is often preferred rather than the Earth-fixed system, where the ionosphere activity depends on the solar radiation and the geomagnetic field. In addition, the auroral oval (discussed in Section 3.4.2) is approximately centered on the geomagnetic pole [*Skone,* 1998]. The geomagnetic coordinate calculations are discussed in Appendix B.

3.4 REGIONS OF IONOSPHERIC EFFECTS

Ionospheric effects vary with latitude, where various ionospheric phenomena take place in different regions of the ionosphere. The regions are identified as equatorial, mid-latitude, and high latitude regions as illustrated in Figure 3.2:

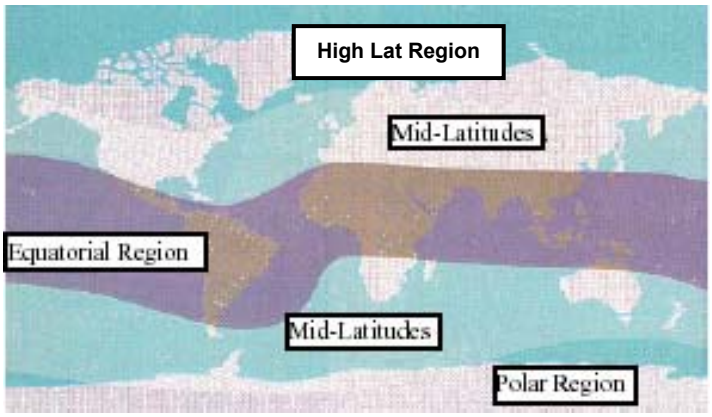

Figure 3.2 Ionospheric regions of the world [*Knight et al.*, 1999]

3.4.1 Equatorial Region

Significant effects of scintillation are observed in equatorial regions that extend $\pm 30^{o}$ on either side of the Earth's magnetic equator. The strongest effects are at approximately $\pm 10^{o}$ magnetic latitude [*Basu et al.,* 1988]. The distinct feature of ionospheric activity in the equatorial region is called the equatorial, or Appleton, anomaly [*Appleton,* 1954]. Equatorial scintillation is caused by rapid electron-ion recombination, which reaches its maximum activity during the hours after local noon. Since this recombination does not occur uniformly, large gradients appear. These gradients cause instabilities leading to small-scale irregularities (from a few metres to a few kilometres), which induce scintillation [*Hargreaves,* 1992*; Wanninger,* 1993a].

The equatorial ionospheric activity is highly correlated with local time, and generally begins to develop at 0900-1000 local time, reaching its maximum activity at 1400-1500 [*Huang and Cheng,* 1991]. The activity tends to have a secondary peak at about

2100 local time, with large TEC gradients in the north-south direction [*Wanninger,* 1993a]. Furthermore, the equatorial anomaly has seasonal peaks, where the strongest effects occur during winter months (September – March) [*Skone et al.,* 2001].

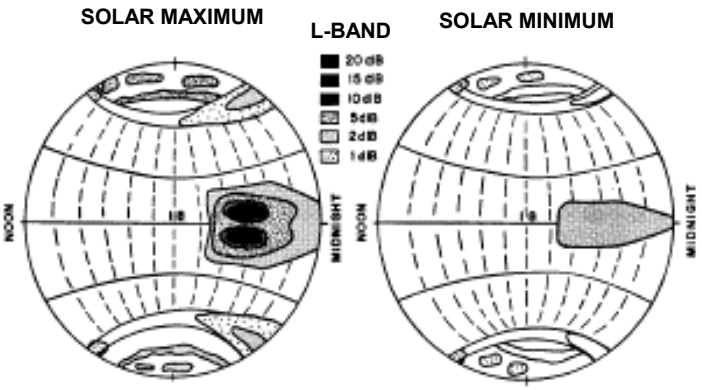

Figure 3.3 A global scale of scintillation fading depth during solar maximum and minimum [*Basu et al.*, 1988]

The global scale of the relative strength of ionospheric scintillation is presented in Figure 3.3. It is clear that the dependency of the scintillation occurrence is on solar activity, local time, and latitude [*Basu et al.,* 1988]. Equatorial scintillations were observed to be much stronger (with greater impact on receiver tracking performance) than high latitude scintillations [*Skone et al.,* 2001].

3.4.2 High Latitude Region

The high latitude region includes polar cap, auroral, and sub-auroral regions.

3.4.2.1 Polar Cap

The polar cap region is located at latitudes above the auroral region (i.e. > 75^{o} magnetic latitude). At these latitudes, the magnetic field lines are open such that it allows the flow of the solar wind plasma into the polar cap latitudes, which results in large patches of enhanced electron density with a horizontal scale size in the range of 50 – 1000 km [*Hargreaves, 1992*]. Within these patches, there are small-scale irregularities that cause scintillations, with sizes of a few metres up to 1 km. The enhanced electron density patches in the polar cap region are concentrated in the F region at altitudes 250-400 km.

3.4.2.1 Auroral Region

The auroral region is limited in its latitudinal extent, and is located 60^{o}-75^{o} geomagnetic latitude (night side) as shown in Figure 3.4. It has an average width of 5-7 degrees [*Rostoker and Skone,* 1993]. The auroral oval may expand to twice this width at the night side, during periods of storm conditions. The auroral region covers Canada, Alaska, Northern Europe, and some parts of Russia. In this thesis, the proposed ionospheric warning system focuses on monitoring the auroral region in the Canadian (and North American) sector, with a focus on quantifying the ionospheric activity in this region.

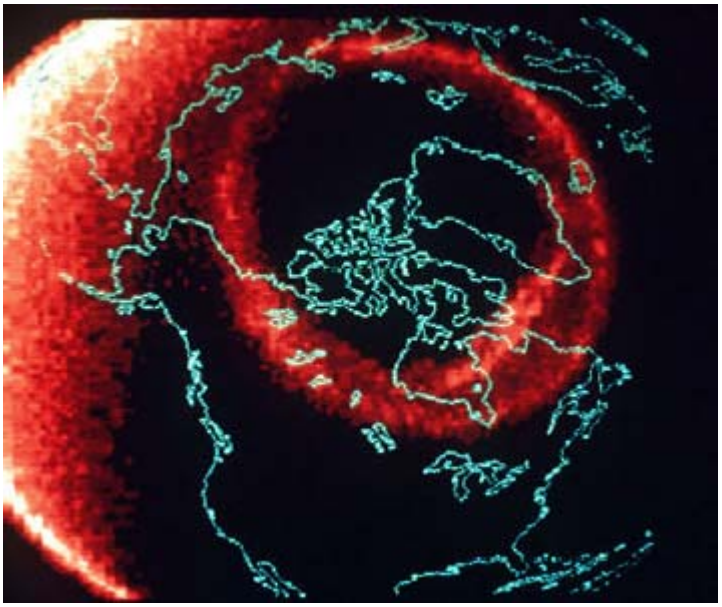

Figure 3.4 Satellite image of the auroral oval

[courtesy of L.Frank, University of Iowa]

The physical processes creating the auroral oval are different from those creating the equatorial anomaly. The interaction between charged energetic particles flowing outwards from the Sun (solar wind) and the Earth's magnetic field creates an acceleration of electrons in regions near the Earth. Energetic electrons precipitate into the high latitude ionosphere, along the Earth's magnetic field lines. The electrons energized through this interaction result in optical and UV emissions known as the aurora ("Northern Lights"). The geomagnetic substorm phenomenon is characterized by the aurora.

During periods of substorm events, the auroral oval can expand several degrees towards the equator. The irregular precipitation of electrons, and the presence of localized electric currents results in structural enhancements of TEC in the auroral region at altitudes of 110 km (E-region). These features are medium scale structures with a 20-130 km

wavelength [*Hunsucker et al.,* 1995]. Scintillations are often observed in conjunction with these features during substorm events [*Basu et al.,* 1983].

As a result of the ionospheric scintillation and structured irregularities during substorm events, it may be difficult to resolve ambiguities for precise positioning and regional network applications. A significant degradation in DGPS positioning accuracies as well as in receiver tracking performance has been observed during such events [*Skone and Knudsen,* 2001; *Skone at el.,* 2001].

In addition to the medium scale structure of the ionospheric irregularities, small-scale irregularities also can exist in electron density at F-region at altitudes of 350 km due to the ionization along the Earth's magnetic field. These structures have scale sizes ranging from several metres to 10 km [*Hunsucker,* 1992], and are associated with scintillation frequencies on the order of 0.5-1.0 Hz [*Hargreaves,* 1992]. The data recorded for this thesis is done at 30s intervals, which is not sufficient to study such effects on GPS measurements. However, it is recommended in the future to use an Ionospheric Scintillation Monitor (ISM) that extracts phase and amplitude scintillation parameters at 1 Hz. The ISM receiver is a single frequency GPS L1 receiver that was designed to monitor the level of ionospheric scintillation in real time. The ISM receiver calculates several parameters, such as a normalized standard deviation of the amplitude of the incoming signal, S4 [*Dierendonck et al.,* 1993]. Also, it calculates the standard deviation of the signal phase, σ_ϕ, and spectral density of the amplitude and phase noise.

The occurrences of the auroral scintillations are strongly correlated with substorm events; this is unlike the equatorial scintillations that are associated with seasonal and diurnal variations of TEC.

3.4.2.3 Sub-Auroral Region (Trough and Strom Enhanced Density)

The sub-auroral region is located several degrees south of the auroral oval. Electron densities in this region are much less then those at the auroral region, which results in sharp gradients in TEC between the aurora and trough boundary. There is a significant degradation in DGPS positioning accuracies in this region, due to the differential ionospheric range errors. Differential ionospheric range residuals of 15 ppm were observed in the trough region [*Foster,* 2000]. This trough feature may be significant in the nightside local time sector.

During events of storm enhanced electron density (SED), the ionospheric plasma transports from night-side to the day-side causing large enhancements of TEC. This enhancement occurs in the day-side local time sector with TEC gradients as large as 70 ppm [*Foster,* 2000].

3.4.3 Mid Latitude Region

This region is located between the equatorial and high latitude regions, and covers the geographic latitude range from approximately 30^{o} up to 50^{o}. The mid-latitude region has less effects of ionospheric activity on GPS signals. Generally, this region is not as

much of a concern to GPS users as equatorial and high latitude regions. However, severe substorm events can have a great impact on GPS applications in the mid-latitude region, where region of electron densities irregularities may extend equatorward across mid-latitude region [*Foster,* 2001].

3.5 IONOSPHERIC EFFECTS ON POSITIONING ACCURACY

3.5.1 Single Point Positioning Accuracies

GPS signal specifications for the Standard Position Service (SPS) allow single point GPS users to reach accuracies of 22 m horizontal and 33 m vertical at 95% (2DRMS) [*Shaw et al.,* 2000]. Several sources of error contribute to single point positioning accuracies, the ionosphere being the main source for single frequency users. In *Shaw et al.* [2000] the ionosphere range error is assumed to contribute 7 m of the total range error budget. The accuracy of single point positioning can be degraded significantly during periods of high ionospheric activity, while the GPS range error depends directly on absolute TEC values. In such cases the broadcast ionosphere model [*Klobuchar,* 1987] does not adequately represent local ionospheric features. Therefore, as the ionospheric activities vary according to the region and the season, so do the single point positioning accuracies.

A recent study was conducted to investigate the ionospheric effects on single point positioning accuracies [*Skone et al.,* 2001]. Three locations were chosen to represent

equatorial (Arequipa at 16.46° S, 71.49° W), middle (US Naval Observatory at 38.91° N, 77.06° W), and high latitude (Churchill at 58.75° N, 94.04° W) regions. The single point positioning solutions were computed for each station using L1 code measurements, and were then compared with known station coordinates. The 95th-percentile statistics were computed for every 30 minutes using position estimates every 30 s. Horizontal and vertical positioning accuracies for the three stations are presented in Figure 3.5 for one year of observations (May 2000 – May 2001).

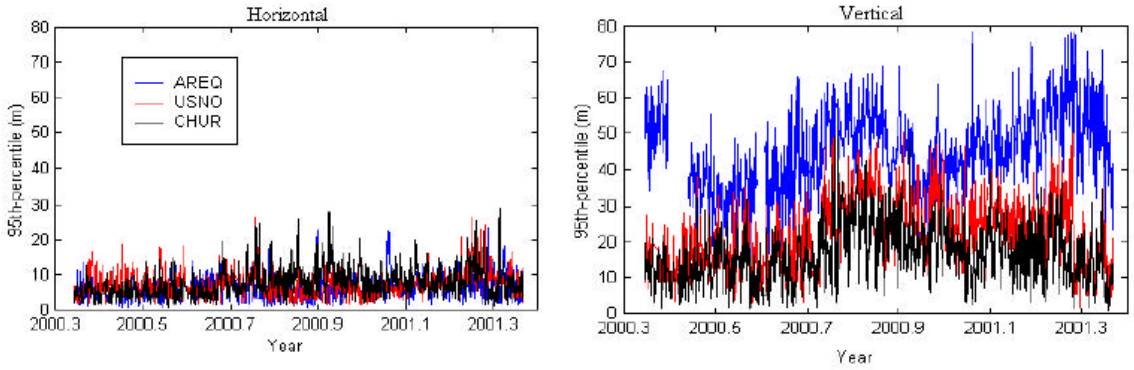

Figure 3.5 Horizontal and vertical positioning accuracies (95th-percentile) for the high (CHUR), middle (USNO) and low (AREQ) latitude stations [*Skone et al.*, 2001]

The positioning accuracies presented are values only for 1330 to 1430 local time sector to show the maximum diurnal values. The dayside vertical positioning accuracies can reach up to 60 m depending on the season and the location of the station [*Skone et al.,* 2001]. Significant large positioning errors were observed at low latitudes, associated with seasonal variations in the vertical positioning accuracies.

The dayside horizontal positioning accuracies are generally less than 20 m for the three stations. Unlike the vertical positioning accuracies, the horizontal accuracies show minimal dependency on absolute TEC values due to the compensation of the correlated ionosphere range errors in the horizontal plane through the horizontal geometry of the range observations. However the horizontal positioning accuracies can be corrupted severely during periods of storm events. As an example, a severe global storm took place in July 15-16 of the year 2000. Position solutions were computed at three stations in the United States and the Caribbean: Cape Canaveral, Florida (CCV3); Kingston, Jamaica (JAMA); and US Naval Observatory (USNO) as presented in Figure 3.6.

Horizontal position errors in the range 30-50 m were observed at the three stations during the peak of the ionospheric activity during the storm event. The vertical position errors were observed in the range of 50-70 m at the same time of the enhanced ionospheric activity. The observed position errors indicate significant impacts of the ionosphere on GPS users during periods of high ionospheric activity.

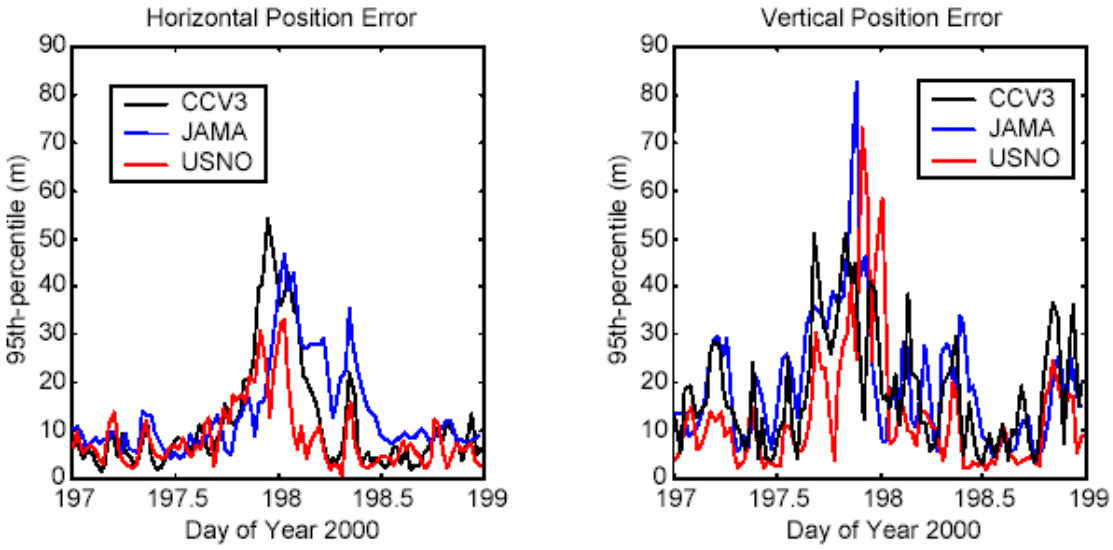

Figure 3.6 Horizontal and vertical positioning accuracies (95th-percentile) for the middle (USNO) and low (CCV3 and JAMA) latitudes stations [courtesy *S. Skone*]

3.5.2 DGPS Positioning Accuracies

Differential GPS (DGPS) is often used to reduce atmospheric and satellite dependent errors, and to obtain better positioning accuracy. This technique includes two GPS receivers (i.e. reference station receiver and rover receiver). The position of the reference station is known very accurately; therefore, the range errors of the observed pseudoranges can be computed for each satellite in view. GPS users receive range corrections from a reference station, and apply these corrections to the observed range measurements. Ionospheric range errors can be reduced using this technique. However, periods of high geomagnetic activity are usually associated with steep gradients and localized irregularities in electron density at equatorial, auroral, and sub-auroral regions. The typical large-scale gradients in TEC can result in differential range errors in the order

of 1-2 ppm [*Parkinson and Enge,* 1996]. Much larger differential errors are observed during periods of enhanced ionospheric activity.

Medium-scale irregularities in electron density exist in E-region at altitudes of 110 km, during the larger substorm events at auroral latitudes. In turn, differential ionospheric errors increase significantly in the precise positioning applications. This results in complicating the ambiguity resolution process, particularly for real-time applications. Electron density gradients can be significantly large and result in ionospheric range delays on the order 10 ppm up to 70 ppm during storm enhanced density (SED) at sub-auroral regions [*Foster,* 2000], and on the order of 32-48 ppm at equatorial regions [*Skone et al.,* 2001]. As a result, DGPS positioning accuracies are severely corrupted in regions of steep TEC gradients.

DGPS horizontal and vertical positioning errors were observed in the range of 10 – 50 m (95^{th} – percentile) for a baseline length of 430 km aligned approximately north-south direction in the equatorial anomaly region, as illustrated in Figure 3.7 for March 2000. The DGPS positioning errors were also observed for the same baseline in June 1999 to be in the order of 1-10 m [*Skone et al.,* 2001b]. During this month, the TEC values were lower, and large TEC gradients do not exist. The seasonal equinoctial enhancement of the equatorial anomaly is evident.

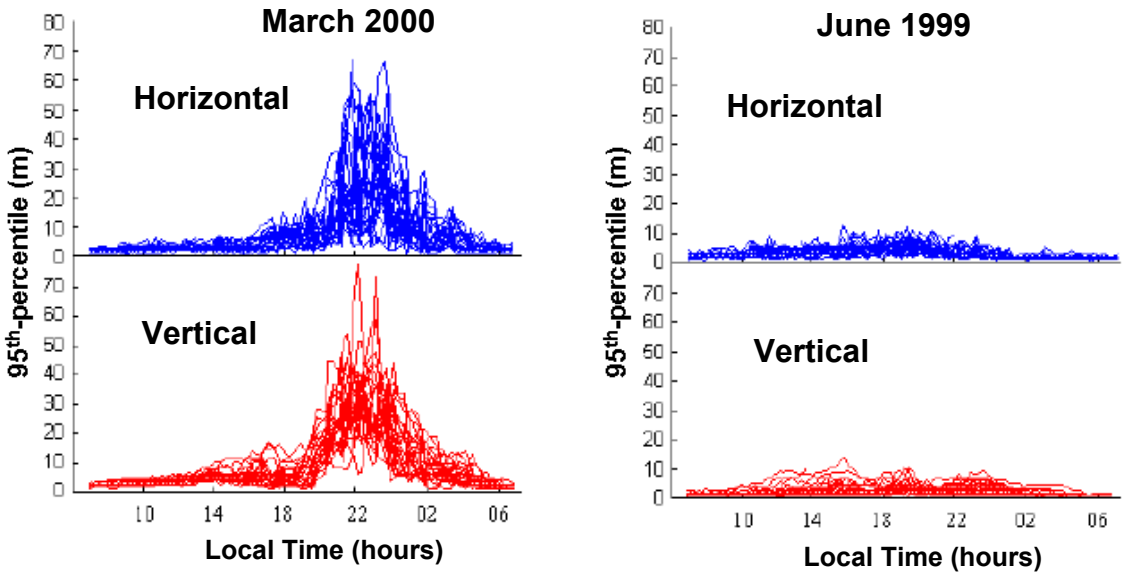

Figure 3.7 DGPS horizontal and vertical positioning accuracies (95th – percentile) during March 2000 (steep TEC gradients) and June 1999 for 430 km baseline (UEPP-PARA) [*Skone et al.*, 2001]

3.5.3 Receiver Tracking Performance

As discussed in Section 3.2.3, GPS receiver tracking performance can be affected during periods of ionospheric scintillation. Phase scintillations produce rapid carrier phase changes in GPS signal. The receiver may lose lock on the signal if the rapid changes exceed the bandwidth of the phase lock loop (PLL). Additionally, the signal strength may drop below the receiver tracking thresholds during periods of amplitude scintillation, leading to the loss of the lock on signal code.

L1 tracking performance is not affected as significantly as L2 during scintillation events. This relation is expected due to the narrow bandwidth of the L2 loop [*Nichols et al.,* 2000]. Loss of lock for L2 loops strongly affects dual-frequency applications. Those applications depend on the dispersive nature of the ionosphere to detect ionospheric delay. Therefore, it becomes necessary to monitor the ionospheric scintillation during periods of high ionospheric activity.

Scintillation impact on GPS receiver performance does not depend entirely on scintillation magnitude, but also on the type of GPS receiver. Codeless receiver technology is affected to a greater extent than semi-codeless receiver technology. The semi-codeless receivers have some knowledge of the encrypted code on the L2 signal, therefore they can reduce the squaring loss generated during cross-correlation tracking. In turn, semi-codeless receivers have a better performance than codeless receivers through high scintillation activity [*Knight et al.,* 1999; *Nichols et al.,* 2000].

3.5.3.1 Equatorial Region

A long-term study of the receiver tracking performance in the equatorial region was conducted during the period from January 1998 to April 2000 [*Skone and Knudsen.,* 2001]. The percent of missing L2 observations, and cycle slip occurrences, are computed at four reference stations in the Brazilian RBMC geodetic network. The percentages are derived for local times 2000-2300 in order to reflect the scintillation effects present at the secondary peak of the equatorial anomaly.

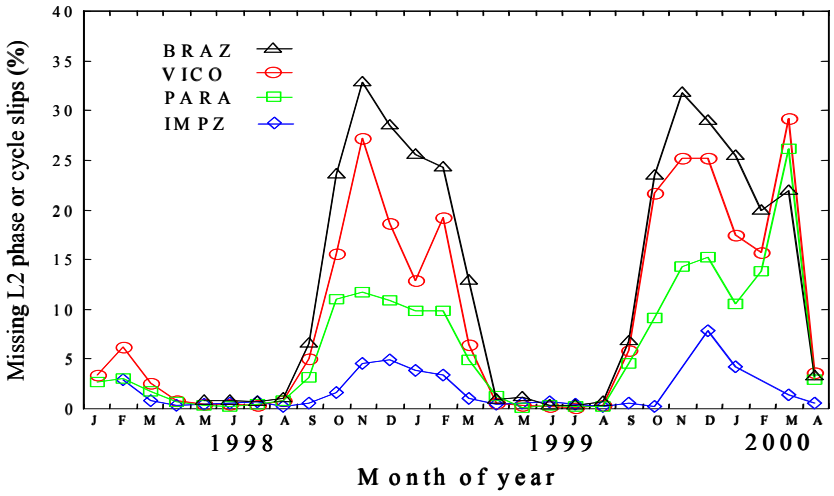

Figure 3.8 Monthly percentages of corrupt L2 phase observations in the local time sector 2000-2300 for the period 1998-April 2000 [*Skone and Knudsen*, 2001]

In Figure 3.8, peak degradations in L2 tracking performance occur primarily during the winter months (September – March). Additionally, the percentages of corrupted L2 observations were significantly increased in late 1998, versus early 1998, which shows evidence of solar cycle dependence. Generally, monthly averages of corrupt observations are in the range of 20-35 percent during the winter months, and are greater than 40 percent on many days. The largest scintillation effects occurred during the 2100-2200 local time sector [*Skone and Knudsen,* 2001].

3.5.3.2 High Latitude Region

The ionospheric scintillation monitor (ISM) provides measurements of scintillation parameters as well as dual-frequency GPS measurements. ISM data were collected at

Churchill, Manitoba from March 15 to March 22 during the year 2001. Churchill is located in the auroral region. A geomagnetic storm took place on the 20th of March. Analyzing the receiver tracking performance during this geomagnetic storm event allows an analysis of the possible impact of ionosphere. Figure 3.9 presents L2 tracking performance (lower panel) along with phase scintillation parameters (upper panel). Cycle slips are indicated by the blue circle with values of "2". It is evident that high phase scintillation values are generally associated with cycle slips on L2. However, there is no indication of any cycle slip detected on the L1 signal.

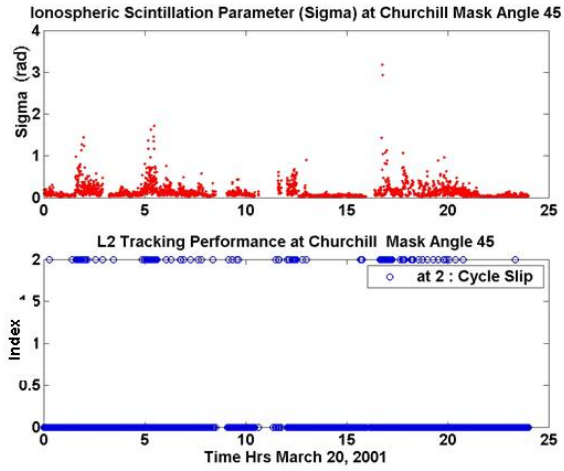

Figure 3.9 Phase scintillation parameter (upper panel) and cycle slip detection on L2 (lower panel) at mask angle 45 degree

A severe geomagnetic storm took place on day 197 – 198 (July 15 – 16) of the year 2000. The percent of corrupt L2 measurements were studied during this event. Observations were collected at two different stations located in Alaska. The two stations are part of the Continuously Operating Reference Stations (CORS) network. One station is

located in Glennallen (GNAA at 62.11^{o} N, 145.97^{o} W), and is equipped with a codeless receiver (presented by the cyan color in Figure 3.10). The other station is located at Potato Point (POT3 at 61.06^{o} N, 146.7^{o} W), and equipped with a semi-codeless receiver (presented by the blue color).

Rate of change of TEC (RTEC) is derived at each station during July of the year 2000 using dual-frequency measurements. Derivation of RTEC is discussed in Section 4.1.1. RTEC at POT3 and GNAA are presented in the middle and lower panels, respectively, on Figure 3.10. A high percent of corrupted L2 observations are highly correlated with the rapid change of RTEC. This highest percent of corrupted L2 measurements are observed during the ionospheric storm event (days 197 – 198), and therefore associated with the highest RTEC values.

The severity of the impact on L2 observations can depend on receiver type. RTEC values are almost similar at the two stations (i.e. POT3 and GNAA), resulting in similar ionospheric effects on the receiver tracking performance at both stations. However the percent of corrupted L2 observations are not similar. The percent at GNAA is always higher than at POT3, due to the codeless receiver technology at GNAA versus semi-codeless receiver technology at POT3. These results are consistent with the conclusions in *Knight et al.* [1999] and *Nichols et al.* [2000].

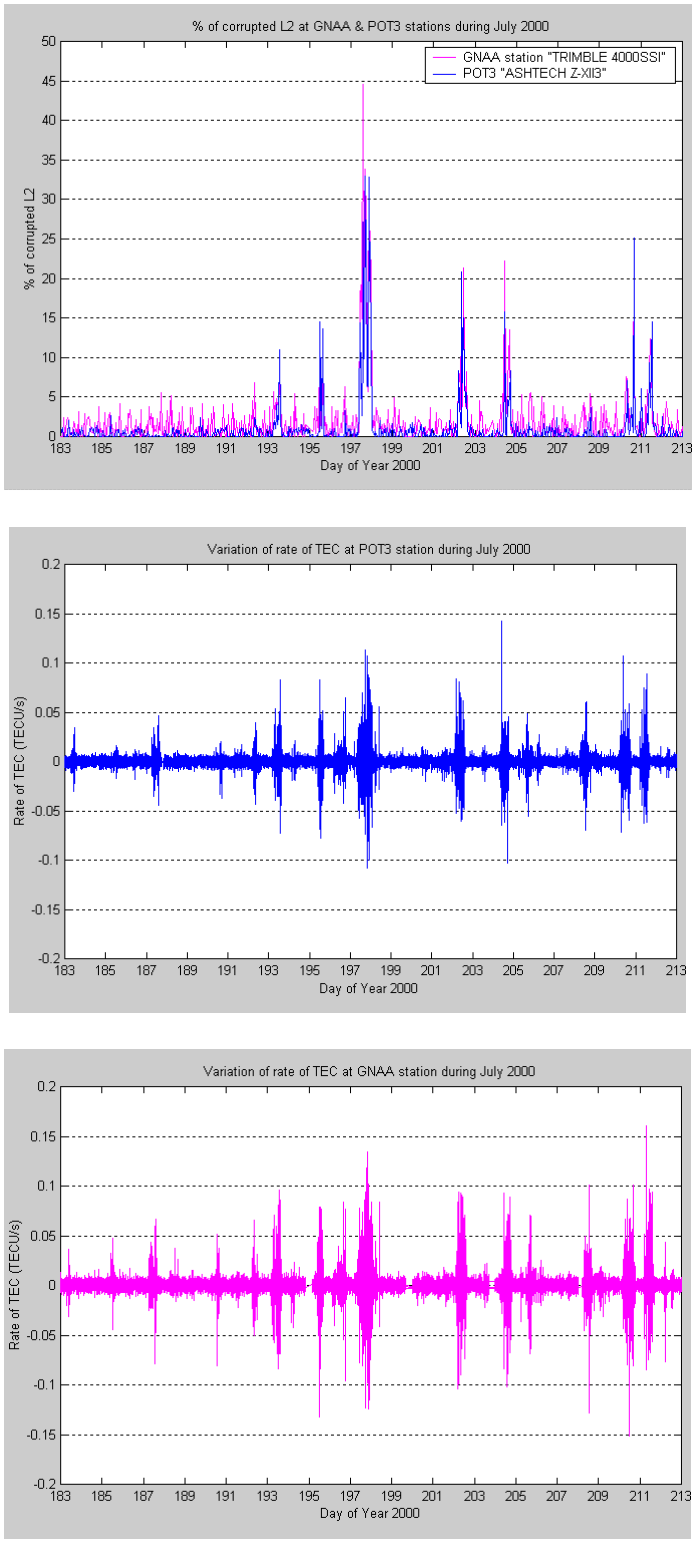

Figure 3.10 Percent of corrupted L2 observations during July of the year 2000 (upper panel), RTEC at POT3 (middle panel), and RTEC at GNAA (lower panel)

3.6 SUMMARY AND MOTIVATIONS

The ionosphere can have a severe impact on GPS observations. Single point positioning, differential GPS, and precise positioning applications experience degradations in accuracy during periods of high ionospheric activity. Moreover, the GPS receiver may lose lock on phase and/or amplitude of the signal when local irregularities in electron density are present in the ionosphere.

The ionospheric activity at equatorial regions has regular seasonal and diurnal variations. At high latitude regions, the ionospheric activity is strongly correlated with substorm events, however, which are difficult to predict. The degree of high latitude ionospheric impact on GPS applications cannot always be accurately predicted using conventional space weather observations. High latitude ionospheric activity may be observed in dual frequency GPS observations. Dual-frequency GPS observations provide an excellent measure of the ionospheric activity due to the dispersive nature of the ionosphere.

In the proposed technique, the ionosphere at auroral and sub-auroral regions will be monitored in real time using dual-frequency GPS measurements. The observations are available in a network of several stations covering the Canadian sector. Spatial and temporal ionospheric variations are modeled in real-time. It is intended to employ the proposed monitoring technique in future implementations of a real-time service to GPS users at auroral and sub-auroral regions in North America. This service will alert the user

about the degree of the ionospheric activity, regions of high/moderate/low ionospheric activity, and the possible impact on DGPS/precise positioning applications.

CHAPTER 4

IONOSPHERE MONITORING USING GPS MEASUREMENTS

In order to track the magnitude and the extent of auroral ionospheric effects in Canada and Northern United States, a measure of the ionospheric activity using GPS measurements is developed. Given that the ionosphere is a dispersive medium, the use of dual frequency GPS measurements allows calculation of the integrated total electron content (TEC) through the ionospheric layers along each satellite-receiver line-of-sight. Deriving the TEC provides a good reflection of the ionospheric activity at the region where the satellite-receiver line-of-sight crosses the ionosphere. Therefore, the ionospheric activity can be monitored by considering the TEC observations derived for a network of GPS stations using dual-frequency GPS measurements, such as the International Geodynamics Service (IGS) network. While the main objectives of the IGS are earth rotation monitoring and orbit determination, the enormous amount of continuous dual-frequency GPS tracking data provides an excellent resource for developing techniques to monitor the ionospheric activity [*Wanninger,* 1993a*; Coker et al.,* 1995]. As described in Section 3.3.2, high latitude scintillation is of concern for precise positioning applications, where the ionospheric scintillation causes cycle slips and the strong gradients in the

electron distribution complicates the ambiguity resolution process for regional network of baseline as short as 10 km [*Wanninger,* 1993a].

By differencing precise GPS carrier phase observations between successive epochs (for a given satellite) the rate of change of TEC (RTEC) may be derived. This has been used as a measure of ionospheric disturbances in the high latitude region, [*Wanninger,* 1993a*; Stewart and Langley,* 1999]. An example in Figure 4.1 presents two RTEC time series derived using measurements from the same satellite (PRN 17). The measurements were collected at the Yellowknife reference station, which is located at latitude 62.48 degrees and longitude -114.48 degrees. The upper panel presents one RTEC time series for day 154 of the year 2000 for a period of quiet ionosphere. The lower panel presents the RTEC time series for a period of high ionospheric activity on day 197 of the year 2000. In the upper panel, the RTEC time series is smooth with low values that indicate an undisturbed ionosphere, while the lower panel shows fluctuations with larger absolute values in the RTEC time series, which would indicate a region of ionospheric disturbance. The quiet and high ionospheric activities were determined according to the geomagnetic activity index "K". In the upper panel, K values were 2 and 3, while K values of 8 and 9 were recorded during the period of the measurements in the lower panel.

The TEC time series of PRN 17 are also presented in Figure 4.2 for the same periods as in Figure 4.1. In the upper panel, the low frequency variations dominate the TEC series; such variations arise from changes in the satellite elevation angle – and associated long-term variations in the line-of-sight path length through the ionosphere. In the lower

panel, high frequency variations in the time series of relative TEC arise from temporal changes in the number of ionospheric electrons, and the spatial distribution of irregularities in electron density (day 197).

The impact of such ionospheric disturbances on the receiver tracking performance is presented in the same figure, where the occurrence of a cycle slip on L2 signal is presented by a blue circle. There was no occurrence of cycle slips during the period of quiet ionosphere activity. However, several cycle slips were recorded on day 197 due to the observed high frequency variations in the relative TEC time series.

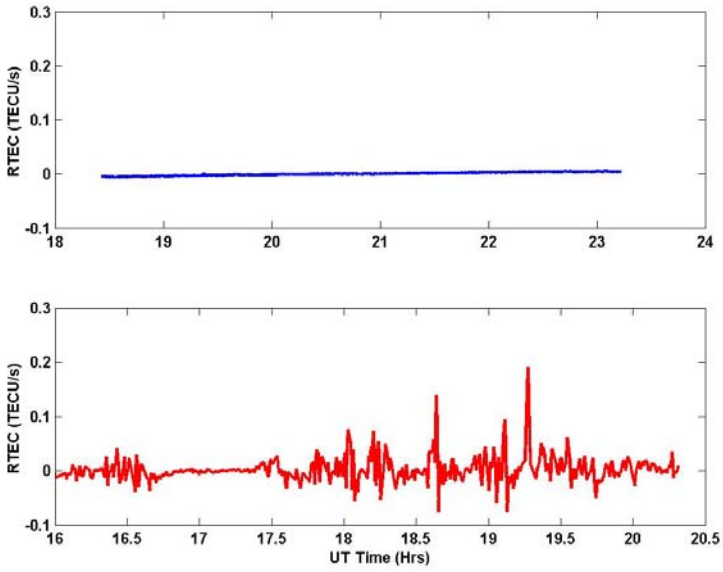

Figure 4.1 RTEC time series for PRN 17 during quiet ionosphere on day 154 of the year 2000 (upper panel), and high ionospheric activity on day 197 of the year 2000 (lower panel) at Yellowknife, Northwest Territories

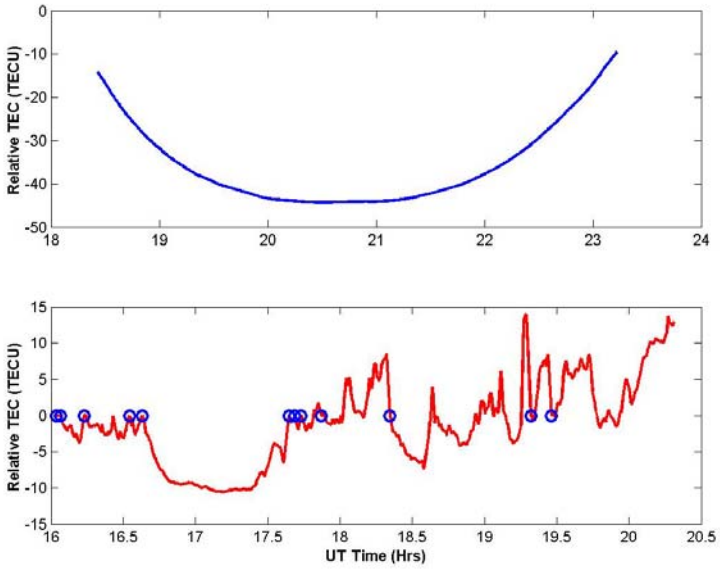

Figure 4.2 Relative TEC time series for PRN 17 during quiet ionosphere on day 154 of the year 2000 (upper panel), and high ionospheric activity on day 197 of the year 2000 (lower panel) at Yellowknife, Northwest Territories. Blue circles represent the occurrences of cycle slips on L2 signal

The RTEC represents the variation of the signal phase for the propagation paths of satellites in view, which can be used to detect the ionospheric disturbances. In this thesis, the ionosphere is monitored using an index to statistically represent the RTEC and detect local ionospheric variability. This index (herein referred to as RTECI) is based on the standard deviation of RTEC observed over a 5-minute time period. The time interval of 5 minutes was chosen such that a reliable statistical representation was derived for a relatively short time interval. Calculation of TEC is presented in detail in Section 3.5. The RTEC and RTECI derivation is discussed in Section 4.1.

4.1 PARAMETERS DERIVATIONS

4.1.1 RTEC Derivation

The RTEC can be measured from precise carrier phase observables. Using the carrier phase observables on L1 and L2, the relative TEC can be derived as follows:

$$\text{TEC} = \frac{-f_1^2 f_2^2}{40.3(f_2^2 - f_1^2)}(\Phi_1 - \Phi_2) \qquad (\text{el/m}^2) \tag{4.1}$$

Where Φ_1 and Φ_2 represent ambiguous carrier phase ranges on L1 and L2, respectively. If the carrier phase ambiguities remain constant over time, such relative TEC observations can be differenced between epochs for each satellite to derive the RTEC as follows:

$$\text{RTEC}_{t,s} = \frac{TEC_{t,s} - TEC_{t-1,s}}{Interval} \tag{4.2}$$

where *TEC* is derived at times *t* and *t-1*, and *s* represents the satellite number. The RTEC values are then normalized from slant to vertical using a mapping factor:

$$M(E) = \left\{1 - \left(\frac{R_E}{R_E + h}\right)^2 \cos^2 E\right\}^{\frac{1}{2}} \tag{4.3}$$

where E is the satellite elevation angle at the reference station (average between epoch t and t-1), h is the altitude of the ionospheric shell above the surface of the Earth (nominally taken as 350 km), and R_E is the Earth radius. The ionosphere layer is approximated as a shell (at altitude 350 km) for simplistic calculation, as based on the discussion in Section 2.4.2. In this discussion, the free electron density as a function of altitudes shows the maximum electron density at altitudes of 350 km [*Davies,* 1990], which validates the assumption of mapping the ionosphere layer to a shell at altitudes of 350 km. An illustration of the ionosphere layer and the assumed ionosphere shell is presented in Figure 4.3.

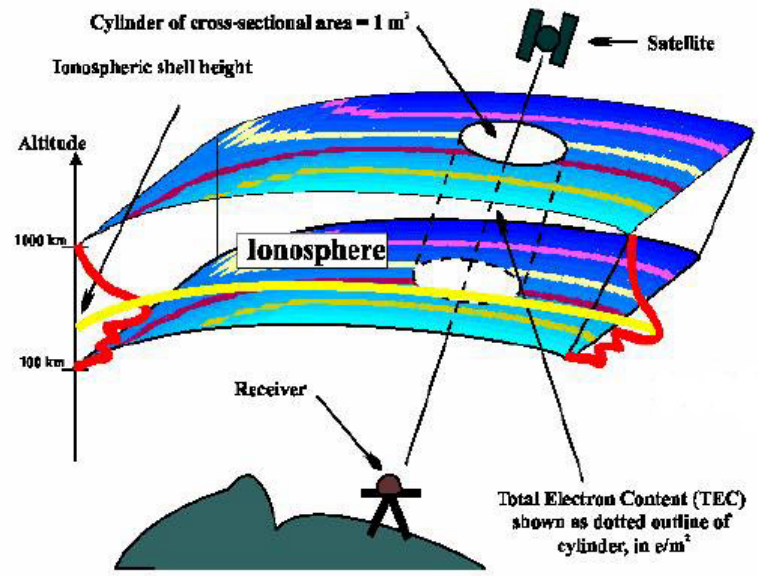

Figure 4.3 Ionosphere layer mapped to shell at altitudes of 350 km

[courtesy of A. Coster and A. Komjathy]

In this thesis the TEC and RTEC derivations are computed using TECANALYS™ software [*Skone,* 2000], which was developed at the University of Calgary.

4.1.2 RTECI Derivation

RTECI is derived as the standard deviation of RTEC observed over a 5-minute time period (Equation 4.4). The 5-minute period provides a reliable statistical representation of RTEC over relatively short time period. The mean of RTEC is expressed in Equation 4.4a. RTECI can be, therefore, expressed in Equation 4.4b as the standard deviation of RTEC observed over a 5-minute interval.

$$\mu = \text{mean } (RTEC)_{5\,\text{min}} = \frac{1}{n}\sum_{i=1}^{n} RTEC_i \tag{4.4a}$$

$$RTECI = \sigma(RTEC)_{5\,\text{min}} = \sqrt{\frac{\sum_{i=1}^{n}(RTEC_i - \mu)^2}{n-1}} \tag{4.4b}$$

where $RTEC_i$ is the rate of change of TEC at a given epoch i for an individual satellite. The sample interval for the data used in this thesis is 30-second. Ten RTEC values are, therefore, available during the 5-minute interval, and n = 10. An extensive data set of TEC and RTECI has been analyzed to monitor the ionospheric activity in the auroral region. Data description and methodology are given in the following sections.

4.2 DATA DESCRIPTION

Dual-frequency data at 30-second intervals were used from the year 2000 at five reference stations in the IGS network. Broadcast ephemeris for every measurement was

obtained from IGS, and used for data processing. It should be noted that the archived data are used in this research in post-mission to develop the ionospheric monitoring technique. Similar methodology will be used in the proposed monitoring service in real-time. The reference stations are located at Churchill, Flin Flon, Lac du Bonnet, Algonquin, and North Liberty as shown in Figure 4.4. The observations were collected using TurboRogue receivers, and the stations satellite-receiver lines-of-sight cover a region extending from 35^{o} N to 65^{o} N of geographic latitude and geographic longitude in the range 110^{o} W – 75^{o} W as illustrated in Figure 4.5. These stations were chosen to provide full coverage of North-South direction in the Canadian sector. This allows full coverage of auroral latitudes and detection of all local ionospheric variations, in order to monitor the auroral oval activity and expansion. Further measurements of more stations covering the East-West direction are analyzed in Chapter 5 to expand the proposed technique across a range of longitudes and for testing purposes.

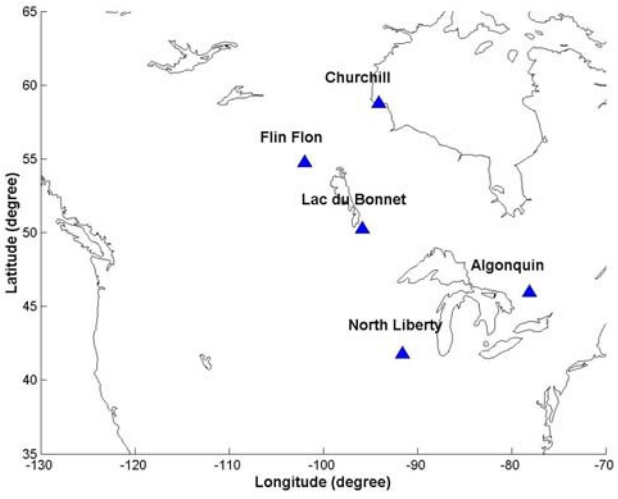

Figure 4.4 Locations of reference stations in IGS network

The coverage of one-day measurements from all stations is illustrated in Figure 4.5. In this Figure, the Ionospheric Pierce Points (IPP) at 350 km altitude for every measurement at all stations are plotted to illustrate the ionospheric coverage allowed from these measurements. An elevation mask angle of 15^{o} was used in all data processing carried out in this thesis.

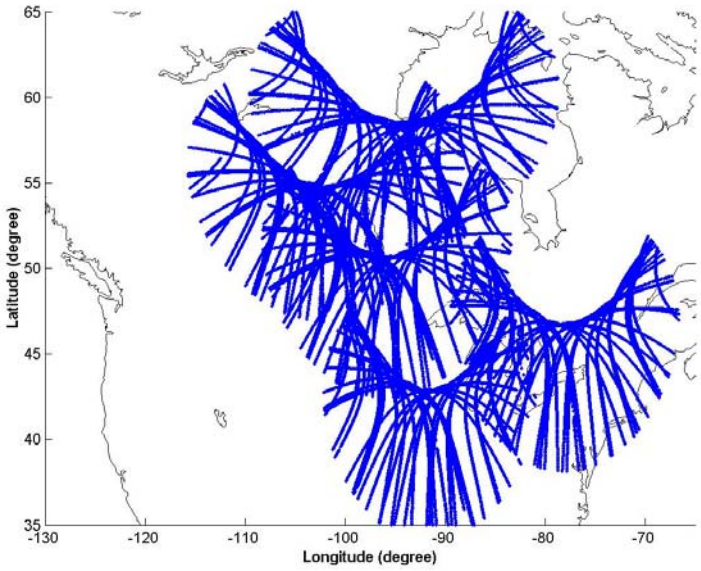

Figure 4.5 IPP distributions

Data of the year 2000 was chosen in this research. This year included a global ionospheric storm that took place on July 15^{th}. This storm is considered as one of the most severe ionospheric storms during the current solar cycle. In addition, this year included another geomagnetic storm on April 17^{th}, as well as a number of occasions with active ionospheric activity. Data of the year 2000, therefore, can represent periods of high, moderate, and quiet ionospheric activity levels. The data are available for 358 days of the

year 2000 at all reference stations. The data availability at each reference station is presented in Figure 4.6, where the black circles indicate missing data.

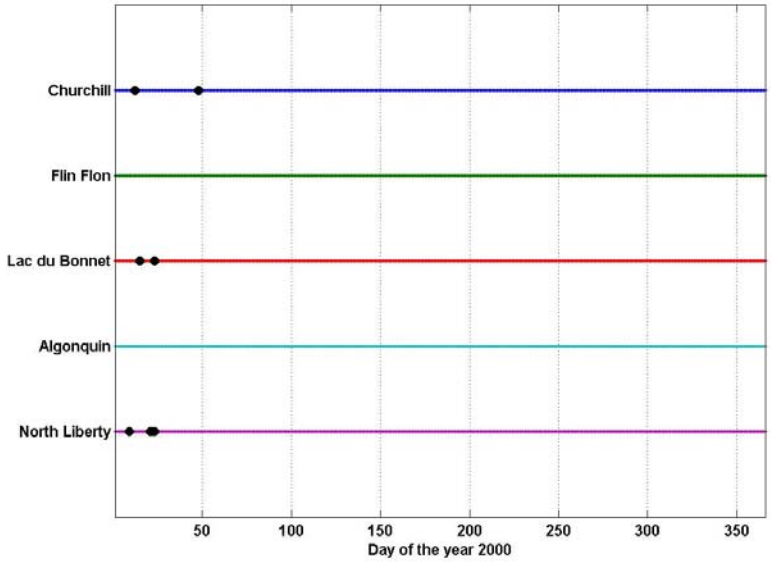

Figure 4.6 Data availability of the year 2000 (black circles indicate missing data)

4.3 OVERVIEW OF METHODOLOGY

An extensive data set of relative TEC time series and the corresponding RTECI values are derived for the analysis from the five stations shown in Figure 4.4. These data are used to develop techniques for monitoring ionospheric effects on GPS measurements in the auroral region.

The first stage of the analysis focuses on a method to define threshold values of the RTECI corresponding to high, moderate, and quiet ionosphere activity levels. The availability of the extensive data set of the relative TEC time series, and corresponding

RTECI values, allows derivation of statistical correlations of RTECI with parameters quantifying the impact on GPS applications. The relative TEC time series and RTECI values are used to define the threshold values of RTECI.

The ionospheric effects on GPS may be inferred from the nature of TEC variations in the ionosphere. If irregularities in electron density exist, the larger spatial and temporal variability of ionospheric TEC will lead to degraded DGPS positioning. The magnitude of such effects may be quantified by deriving correlation times and distances of TEC in the ionosphere. Correlation times and distances can be derived from relative TEC time series. Analysis of the autocorrelation function of the relative TEC time series provides correlation times and distances for each TEC time series, which can be classified according to the corresponding RTECI values of the same time series.

The RTECI threshold values are defined in the first stage. All 5-minute RTECI values for all satellite-receiver lines-of-sight from all reference stations are then profiled in 1-D (i.e. latitude direction) and 2-D (i.e. latitude and longitude directions) for a one-hour time period. The one-hour period is consistent with the times of evolution of auroral storms in the ionosphere that may extend for several hours [*Skone,* 2001]. The spatial modelling of RTECI values allows for identification of the spatial boundaries of regions of different ionospheric activity levels. The second stage (implemented in Chapter 5) of this analysis introduces a technique to profile the RTECI in 1-D and 2-D. The proposed profiling method will allow mapping of RTECI values in latitude-longitude directions covering the Canadian sector, to reach the main objective of monitoring the extent and magnitude of

auroral activity. Consequently, an ionospheric warning and alert system may be provided to GPS users. A discussion of the proposed monitoring and warning technique along with the details of the testing process are provided in Chapter 5. A flow chart of the methodology steps is illustrated in Figure 4.7.

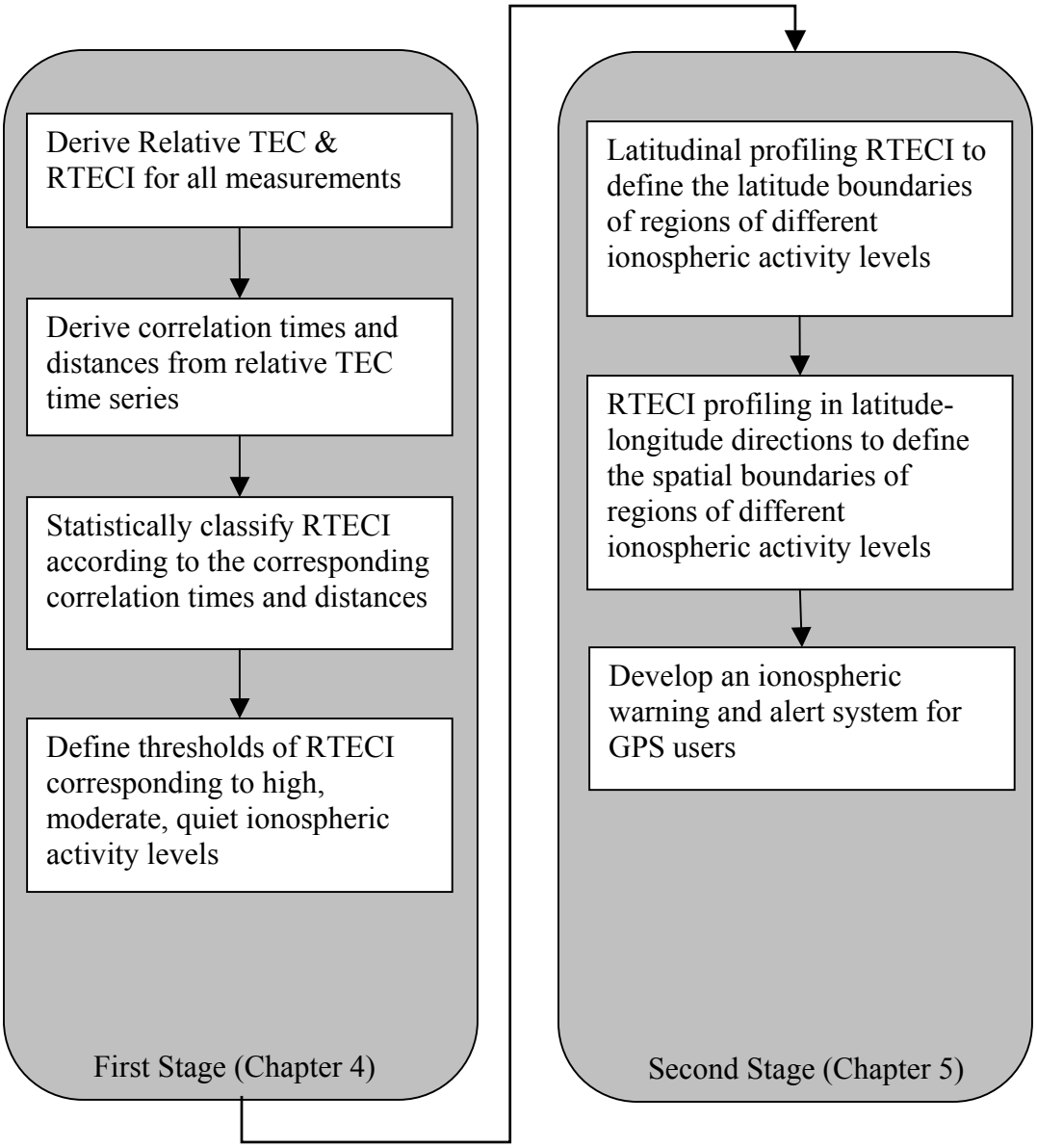

Figure 4.7 Flow chart of the methodology steps

Based on the derived boundary values of RTECI in the first stage, in addition to the profiling technique of RTECI values in 1-D and 2-D, a proposed online service for GPS users may be introduced. The service may be provided in near real time and could be accessed by users via the Internet. GPS users in Canada and Northern United States would benefit from this service. The user would input his/her coordinates and as a result, a sky plot of the user region will be outputted and color-coded according to the ionospheric activity levels. In addition, an estimate of the possible impact on individual satellite measurements will be provided. This service will be based on a network of reference stations covering the Canadian sector, collecting dual-frequency data and ionospheric scintillation parameters in real time and accessed via the Internet.

4.4 CORRELATION STATISTICS

Relationships between features identified in relative TEC time series and the corresponding RTECI values are derived to define the thresholds of RTECI values. The relative TEC time series is derived using Equation 4.1 and contains information on the ionospheric temporal and spatial variation. Thus, these series can be used to analyze relative spatial and temporal variations in TEC. In addition, analyzing the variations in TEC time series during various ionospheric activity levels provides an assessment of the possible impact of the ionosphere on GPS measurements.

The rotational period of the GPS satellites is approximately 12 hours, such that the satellite-receiver line-of-sight crosses through various regions of the ionosphere over time

as shown in Figure 4.8. The TEC time series are therefore derived along the Ionospheric Pierce Points (i.e. IPP_1 and IPP_2), where the ionosphere is assumed as a shell at an altitude of 350 km. The calculation of IPP is described in Appendix A. Variations in TEC time series arise from both temporal changes in the number of ionospheric electrons and the spatial distribution of irregularities in electron density. It is difficult to separate the spatial and temporal effects. It is useful, however, to determine approximate estimates of the correlation times and correlation distances associated with auroral disturbances from such discrete time series through autocorrelation functions.

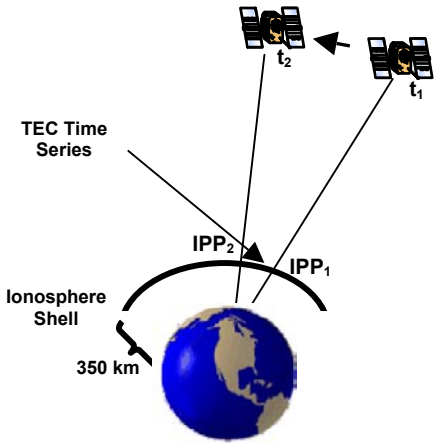

Figure 4.8 Satellite-receiver line-of-sight moves through various regions of the ionosphere over time

The autocorrelation function measures how well the process is correlated with itself, while it is shifted by a constant amount [*Brown and Hawang,* 1997]. Correlation times can be estimated by applying the autocorrelation function to the relative TEC time

series as it is described in Section 4.4.1. The correlation time can be a useful tool for DGPS and regional networks users, where the correlation time allows an approximate measure of the maximum time delay for the reference station to send measurement corrections to the DGPS users, without significant changes in the ionosphere condition.

For correlation distances, using relative TEC series as a function of the traveled distances through the ionospheric shell provides an estimate of the correlation distances by applying the autocorrelation function to such a TEC series. As illustrated in Figure 4.9, the GPS signal crosses the ionosphere at two different points (i.e. IPP_1 and IPP_2) at the same time (t_1) to reach the reference station and the user.

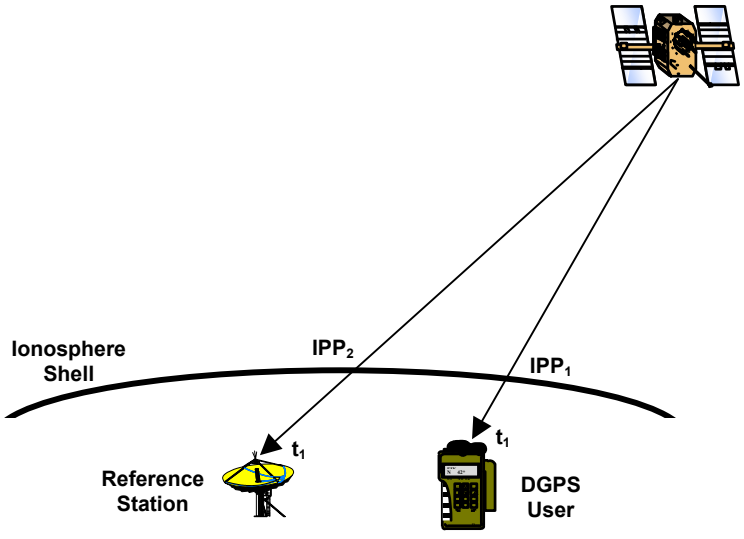

Figure 4.9 GPS signal crosses the ionosphere shell at two different points at the reference station and the user location

Therefore, the correlation distance indicates the maximum distance on the ionosphere shell that the relative TEC series still correlates with itself, which means relatively similar ionospheric conditions at the two IPP. The correlation distances are an important parameter for DGPS and regional network applications. The distance between the DGPS users and the reference station should not be longer than the derived correlation distance, where the ionosphere condition is similar at IPP_1 and IPP_2. The correlation distance represents approximately the maximum distance between the two reference stations that the ionospheric delay errors are still relatively similar at the two IPP. Reference stations spaced larger than the derived correlation distance can result in significantly different ionospheric delay errors at these stations. This can complicate the ambiguity resolution process, and lead to a degradation of accuracies and reliability of precise positioning applications. Details of estimating the correlation distances are discussed in Section 4.4.2.

The autocorrelation function of a continuous process is defined in Equation 4.5a for TEC time series, and in Equation 4.5b for TEC distance series.

$$R(\tau) = \int_{-\infty}^{\infty} X(t)X(t+\tau)dt \tag{4.5a}$$

$$R(\Delta) = \int_{-\infty}^{\infty} X(d)X(d+\Delta)dd \tag{4.5b}$$

where τ denotes the time offset between the process and its shifted version, and Δ denotes the distance offset between the process and its shifted version. It becomes essential to

choose an appropriate model to study the autocorrelation sequence of the relative TEC time and distance series. The most appropriate model to represent the autocorrelation sequence is first order Gauss-Markov process model, which can be expressed as follows:

$$R(t) = \sigma^2 e^{\frac{-t}{\tau}} \tag{4.6a}$$

$$R(d) = \sigma^2 e^{\frac{-d}{\Delta}} \tag{4.6b}$$

where σ^2 is the variance of the relative TEC series. The correlation times are estimated at $t = \tau$, and the correlation distances are estimated at $d = \Delta$. Thus, Equation 4.6 then becomes:

$$R(\tau) = \sigma^2 e^{-1} = \frac{\sigma^2}{e} = \frac{\sigma^2}{2.718} = 0.3678\sigma^2 \tag{4.7a}$$

$$R(\Delta) = \sigma^2 e^{-1} = \frac{\sigma^2}{e} = \frac{\sigma^2}{2.718} = 0.3678\sigma^2 \tag{4.7b}$$

An illustration of estimating the correlation times and distances is presented in Figure 4.10

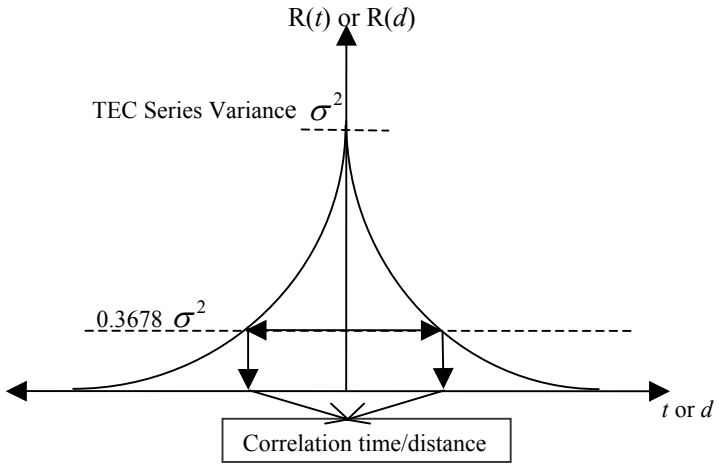

Figure 4.10 Illustration of estimating the correlation times and distances

Relative TEC series are available during the year 2000 for each individual satellite. The vast number of the available relative TEC series should provide reliable statistics during periods of high, moderate, and quiet ionospheric activity. It is important to derive a relationship between the autocorrelation statistics of relative TEC series, and associated RTECI values. Therefore, for each relative TEC series used to derive a given correlation time and distance, the average RTECI value over the time series was also computed. All computed correlation times and distances were then binned according to the corresponding RTECI values in order to derive the threshold values of RTECI for quiet, moderate and high ionospheric conditions.

4.4.1 Temporal Correlation Analyses

Throughout each day of the year 2000, the relative TEC has been derived for each series of satellite measurements at stations in Figure 4.4. RTEC and RTECI are also derived for every relative TEC time series. As an example, one relative TEC time series of PRN 17 for day 197 of the year 2000 is shown in Figure 4.11 (a), for a period of high ionospheric activity at reference station Flin Flon, SK, Canada (at latitude of 54.74^{o} N, and longitude of 101.98^{o} W). The relative TEC time series for the same satellite at the same reference station is presented in Figure 4.11 (b), but during a period of lower ionospheric activity on day 32 of the year 2000.

High frequency variations in the time series of relative TEC arise from temporal and spatial variations in the number of ionospheric electrons observed along the receiver-

satellite line-of-sight (day 197). Low frequency variations dominate the series for day 32; such variations arise from changes in the satellite elevation angle – and associated long-term variations in the line-of-sight path length through the ionosphere.

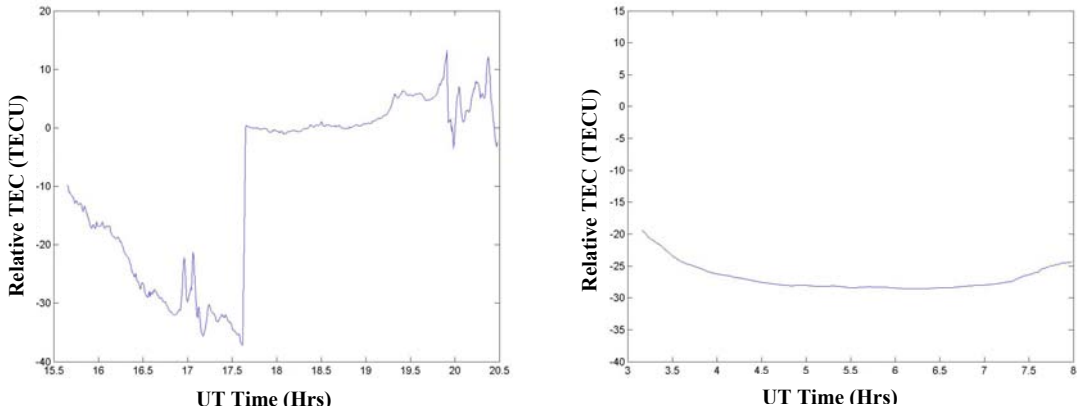

a) **b)**

Figure 4.11 Relative TEC time series for PRN 17 during high ionospheric activity (a), and moderate ionospheric activity (b)

Also, it is noted in Figure 4.11a that there is an occasion of cycle slip occurrence, where the relative TEC time series has been reset to zero. Cycle slip occurrences are greatly associated with high ionospheric activity, due to the ionospheric scintillation effects on the GPS L2 signal. To derive the correlation times and distances using the autocorrelation function, occasions of cycle slips were eliminated from the analyses due to the fact that the sudden reset of the relative TEC time series will strongly affect the results.

The duration of the relative TEC time series itself can greatly affect the derived correlation times and distances. Some TEC time series are 3 hours long or more, which

results in longer correlation times and distances. Alternatively, the shorter correlation times and distances were derived for shorter TEC time series. In order to ensure consistency within the results, one-hour time periods were chosen for processing such that all available TEC time series during the year 2000 were divided into one-hour time intervals. In addition, the proposed near-real time ionospheric warning and alert system will be based on data collected from network GPS reference stations over *one-hour* time periods, and then regions of ionospheric disturbances identified over the network region. Therefore, it is essential to choose one-hour periods of TEC time series for deriving the correlation times and distances.

The correlation analysis was conducted for the relative TEC time series for every individual hour of each satellite-receiver line-of-sight series for the reference stations in Figure 4.4 during the year 2000. All possible ionospheric scenarios have been studied through the available data set, where the latitude separation of the chosen reference stations provides complete North-South coverage of the Canadian sector. An example of a one-hour time frame of relative TEC time series is presented in Figure 4.12 for a single PRN observed simultaneously at all stations – for two different scenarios.

One scenario presents a period of high ionospheric activity (K = 8) on day 197 of the year 2000 (16:30-17:30UT) as shown in Figure 4.12a. The other scenario illustrated in Figure 4.12b presents a period of relatively lower ionospheric activity (K = 1) during day 32 of the year 2000 for a one-hour period (5:00-6:00UT).

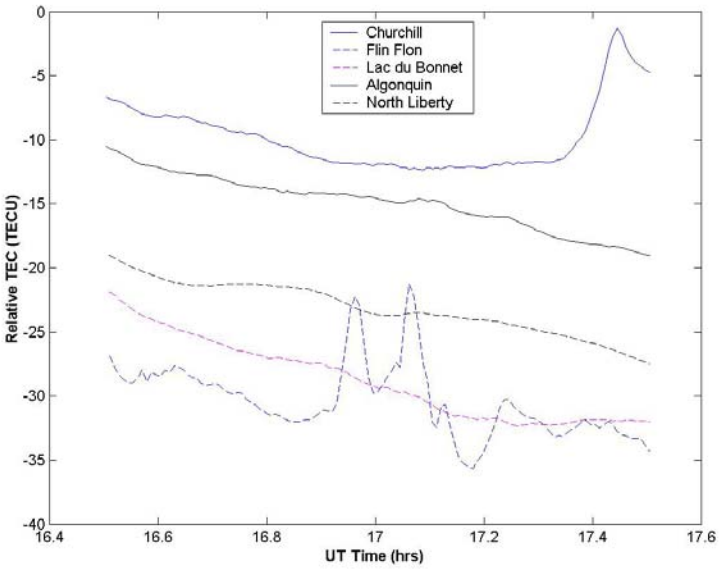

a) During a high ionospheric activity period (16:30-17:30UT) on day 197 of the year 2000

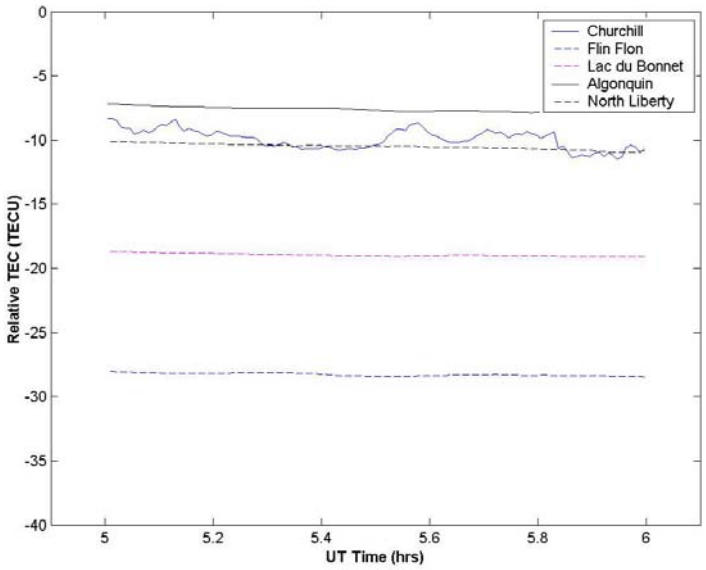

b) During a lower activity period (05:00-06:00UT) on day 32 of the year 2000

Figure 4.12 Relative TEC series for PRN 17 at five stations as a function of UT

Although high ionospheric activity was recorded during the first scenario, not all TEC measurements reflect the same activity. Measurements at Flin Flon reference station reflect the most ionospheric activity during this one-hour period. The high frequency variations in the times series of the relative TEC arise from temporal and spatial changes in the electron density along the signal path through the ionosphere. Measurements at the Churchill reference station reflect lower frequency variations than those observed at Flin Flon, with a significant irregularity observed at the end of the series. The series from the other three stations (i.e. Lac du Bonnet, Algonquin, and North Liberty) observed less significant ionosphere activity during the one-hour time period.

The relative TEC time series presented in Figure 4.12b shows ionosphere variations at Churchill, but the activity was not observed southward at Flin Flon as in the first scenario (Figure 4.12a). The magnitude of the ionospheric effect can be quantified by estimated correlation times and RTECI values for each satellite measurement. The derived correlation times and RTECI values are shown in Table 4.1.

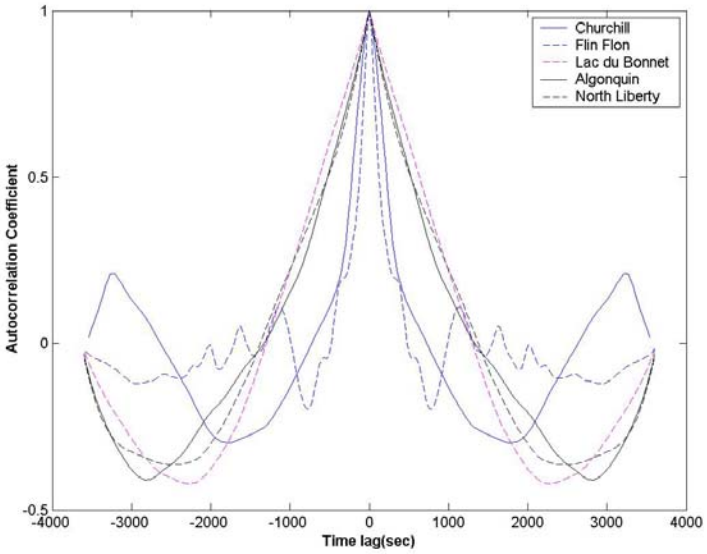

a) During 16:30-17:30UT on day 197 of the year 2000 (period of high ionosphere activity)

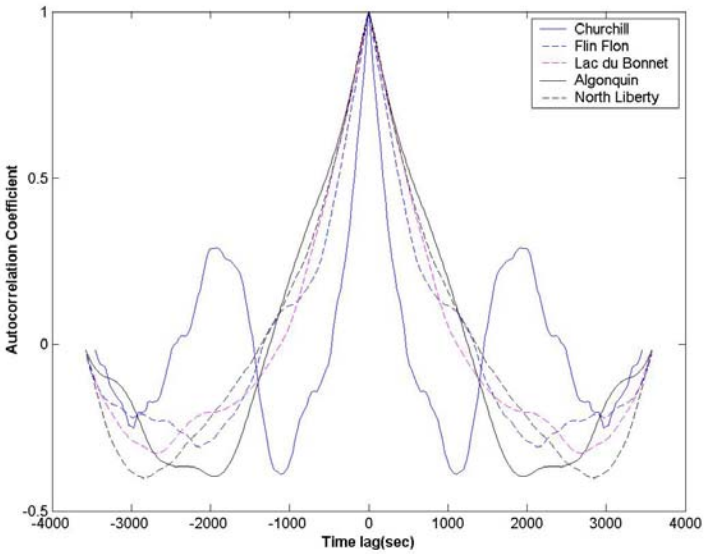

b) During 05:00-06:00UT on day 32 of the year 2000 (period of lesser activity)

Figure 4.13 Normalized autocorrelation functions of the relative TEC time series of PRN 3

The correlation times of the relative TEC time series for both scenarios are derived using the autocorrelation functions illustrated in Figure 4.13. It is assumed that the autocorrelation function has a first order Gauss-Markov distribution (Equation 4.6a). Figure 4.13a presents a high ionosphere activity scenario. The autocorrelation functions at Lac du Bonnet, Algonquin, and North Liberty have first order Gauss-Markov distributions, while Churchill and Flin Flon stations have similar first order Gauss-Markov distributions with significantly shorter correlation times. Therefore, the results of the autocorrelation analysis are consistent with the high frequency variations in TEC time series, and smaller correlation times were derived for Flin Flon and Churchill stations.

A scenario with lower ionospheric activity is presented in Figure 4.13b. All autocorrelation functions approximated as first order Gauss-Markov distributions. At Churchill station, however, the derived correlation time is significantly shorter than the ones derived for the other stations. This is consistent with Figure 4.12b, where high frequency variations of TEC time series are observed only at the Churchill station. Therefore, the smallest correlation time was derived at Churchill. This is consistent with the high latitude location of Churchill, where more auroras are observed.

It becomes evident that the magnitude of the ionospheric activity can be monitored using correlation times and RTECI values (averaged over one hour) as provided in Table 4.1. As shown in Figure 4.13a, and Table 4.1, there is a lower correlation time at Flin Flon due to the fact that the ionospheric activity had moved southward covering the local region of the Flin Flon station (the study of the entire event of day 197 of the year 2000 is

presented in Chapter 5). The other scenario (Figure 4.13b) illustrates that the ionospheric activity remained at high latitudes, in the vicinity of the Churchill station, and did not move southward as in the first scenario.

Table 4.1 Correlation Times and RTECI for Both Scenarios in Figure 4.12

	Day 197 of the year 2000		Day 32 of the year 2000	
	Correlation times (sec)	RTECI (TECU/s)	Correlation times (sec)	RTECI (TECU/s)
Churchill	270	0.004	240	0.006
Flin Flon	180	0.018	510	0.0002
Lac du Bonnet	630	0.001	810	0.0001
Algonquin	660	0.0007	750	0.0002
N. Liberty	690	0.001	780	0.0002

The observed relationship between the derived correlation times and RTECI (and with correlation distance in Section 4.4.2) can introduce a useful method to monitor the extent of the ionospheric activity in the Canadian sector in real time, given the availability of dual-frequency GPS measurements in real-time for a network of reference stations within Canada. Therefore the availability of RTECI in real-time allows monitoring of the ionospheric activity in the auroral and sub-auroral regions (a detailed description of the monitoring technique using RTECI is introduced in Chapter 5).

4.4.2 Spatial Correlation Analyses

In order to illustrate the spatial correlation of the ionosphere, the same sample data used in Section 4.4.1 is presented in this section, but analysed with respect to the line-of-sight motion on the ionospheric shell (at altitude 350 km). Calculation of the distance on the sphere is presented in Appendix C. The relative TEC series of PRN 17 as a function of the traveled distance in kilometres on the ionospheric shell is shown in Figure 4.14 for all five reference stations (i.e. Churchill, Flin Flon, Lac du Bonnet, Algonquin, and North Liberty) during a one-hour time period. These are the same TEC series plotted in Figure 4.12.

The high frequency variations in the relative TEC series as a function of the distance in the ionospheric shell at Flin Flon and Churchill on day 197 (Figure 4.14a) and at Churchill on day 32 (Figure 4.14b) arise from the presence of irregularities in electron density in the ionosphere layer at this region. The low frequency variations that dominate the rest of the TEC series arise from changes in the satellite elevation angle, and associated long-term variations in the line-of-sight path length through the ionosphere.

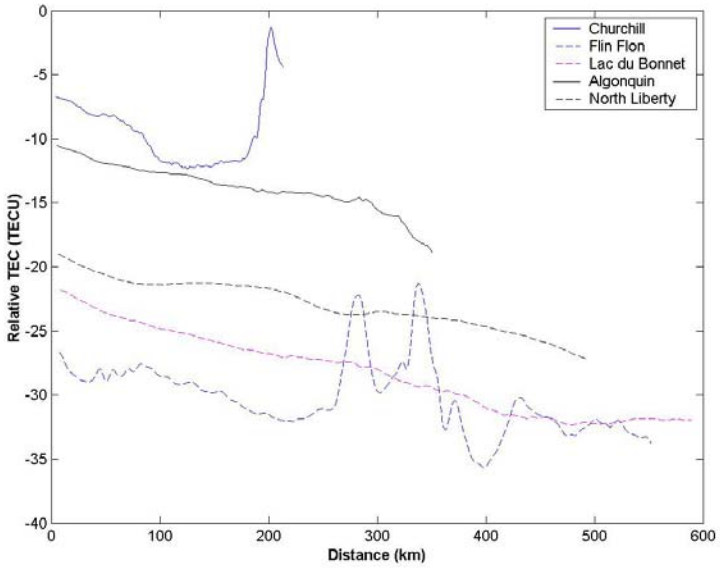

a) During a high ionospheric activity period (16:30-17:30UT) on day 197 of the year 2000

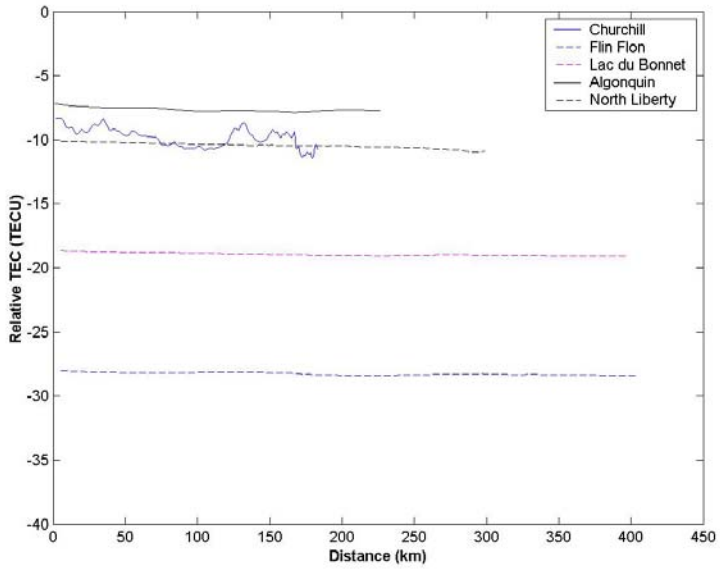

b) During a lower activity period (05:00-06:00UT) on day 32 of the year 2000

Figure 4.14 Relative TEC series for PRN 17 at five stations as a function of the distance in the ionospheric shell

The spatial variations of the ionosphere can be quantified by deriving the autocorrelation function (Equation 4.5b) of the relative TEC time series, but with respect to the distances traveled through the ionosphere layer. An illustration of the autocorrelation functions of both scenarios is shown in Figure 4.15. It is also assumed that the autocorrelation functions have first order Gauss-Markov distribution (Equation 4.6b).

The TEC series for Churchill and Flin Flon in Figure 4.14a, and the TEC series derived for Churchill in Figure 4.15b, have smaller correlation distances and higher RTECI values as presented in Table 4.2. These TEC series have high frequency variations, which results in smaller correlation distances than the TEC series with low frequency at Lac du Bonnet, Algonquin, and North Liberty (Figure 4.14a), and Flin Flon, Lac du Bonnet, Algonquin, and North Liberty (Figure 4.14b). The relationship between correlation distances and RTECI are presented in Table 4.2, and are very similar to the relationship between correlation times and RTECI in Table 4.1 - due to the fact that it is difficult to separate the temporal and spatial effects of the ionosphere.

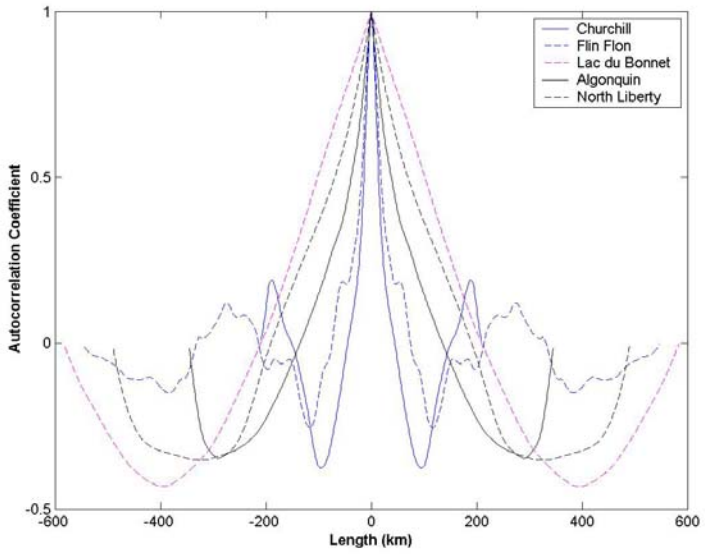

a) During 16:30-17:30UT on day 197 of the year 2000 (period of high ionosphere activity)

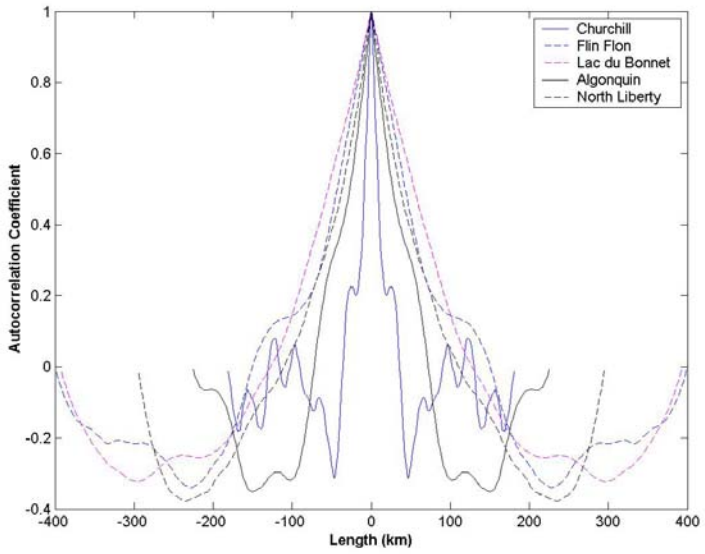

b) During 05:00-06:00UT on day 32 of the year 2000 (period of lesser activity)

Figure 4.15 Normalized autocorrelation functions of the relative TEC series of PRN 3 as a function of distance in the ionospheric shell (at altitude 350 km)

The two scenarios studied during the two different one-hour time periods show high correlations of the RTECI values with the derived correlation times and distances. Therefore, the statistics of the correlation times and distances with associated RTECI can provide an excellent measure of the ionosphere activity in the auroral region as well as provide a useful technique to identify regions of ionospheric disturbances.

Table 4.2 Correlation Distances and RTECI for Both Scenarios in Figure 4.14

	Day 197 of the year 2000		Day 32 of the year 2000	
	Correlation distances (km)	RTECI (TECU/s)	Correlation distances (km)	RTECI (TECU/s)
Churchill	25	0.004	18	0.006
Flin Flon	12	0.018	56	0.0002
Lac du Bonnet	71	0.001	128	0.0001
Algonquin	53	0.0007	100	0.0002
N. Liberty	41	0.001	55	0.0002

4.4.3 Overall Results

A total number of 176,583 TEC series are analyzed from all five stations (Figure 4.4) for the year 2000 to derive the overall statistics. The correlation times and distances are derived and matched with the corresponding RTECIs for each TEC series. Statistics for the correlation times and distances, and the corresponding RTECI, are presented in Table 4.3. The “quiet” statistics were computed using data from intervals during which local North American K indices (from Boulder, Colorado) were less than 2, while the “high”

statistics were computed during intervals of K indices were higher than 7. The “moderate” statistics were computed from periods during which K indices range between 3 and 6. Discussion of K indices is included in Section 2.4.4.

Figure 4.16 presents the probability distributions of RTECI during intervals of quiet, moderate, and high ionospheric activity as identified by the local “K” indices. RTECI values of 0.005 TECU/s and lower were observed for the quiet periods, and for 159,041 TEC time series. For moderate periods of ionospheric activity, RTECI values range between 0.005 TECU/s and 0.015 TECU/s.

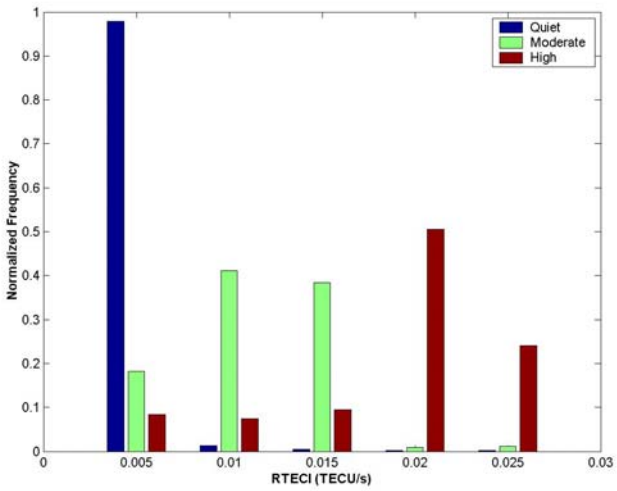

Figure 4.16 Probability distribution of RTECI during intervals of quiet, moderate, and high ionospheric activity

High levels of ionospheric activity were observed for 826 TEC time series. The majority of these TEC series were observed during a major ionospheric storm event

observed on July 15th of the year 2000 where K indices were greater than 7. During these intervals, the majority of RTECI values were greater than 0.015 TECU/s.

The longest correlation times and distances were also observed during the quiet periods, and their probability distributions are illustrated in Figure 4.17. The correlation times and distances have negatively skewed distributions with median (50th-percentile) values of correlation times of 696 sec with standard deviation of 142 sec, while the median value of the derived correlation distances is 75 km with standard deviation of 17 km.

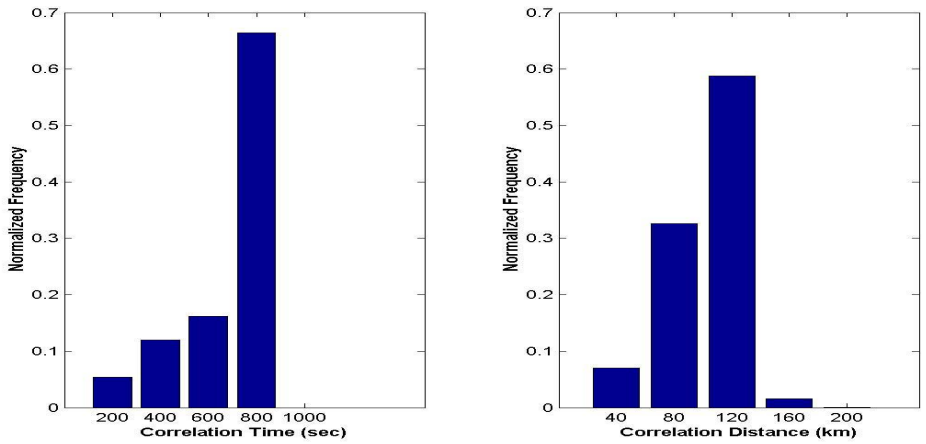

a) **b)**

Figure 4.17 Probability distributions during quiet intervals for a) correlation times, and b) correlation distances

The probability distributions of the correlation times and distances derived during "moderate" and "high" ionospheric activity are presented in Figure 4.18 and Figure 4.19, respectively. Correlation times and distances are positively skewed with median values of

correlation times of 461 sec and 409 sec during “moderate” and “high” intervals, respectively, with standard deviations of 158 sec and 121 sec, respectively. The derived correlation distances during “moderate” and “high” periods have median values of 47 km and 36 km respectively, with standard deviations of 16 km and 12 km respectively.

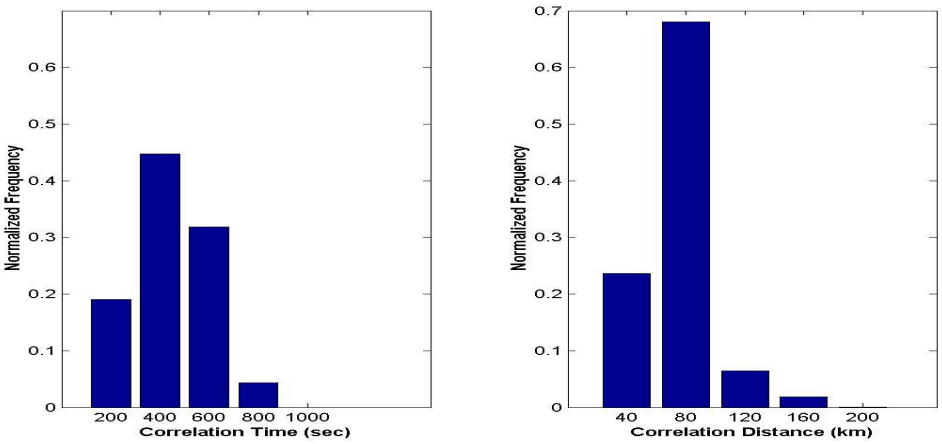

a) **b)**

Figure 4.18 Probability distributions during moderate intervals for a) correlation times, and b) correlation distances

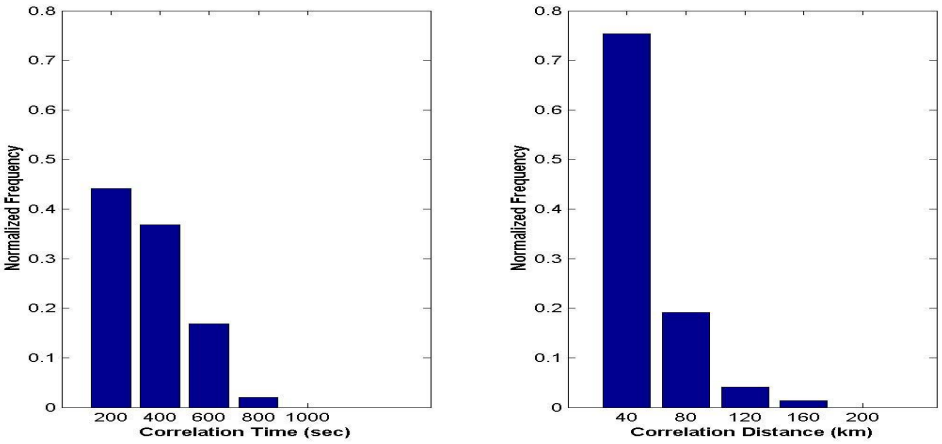

a) **b)**

Figure 4.19 Probability distributions during high intervals for a) correlation times, and b) correlation distances

The median (50th-percentile) values of derived correlation times and distances are presented in Table 4.3 as a function of RTECI.

Table 4.3 Statistics of Correlation Times and Distances and Corresponding RTECI Values for All Data Year 2000

RTECI (TECU/s)	Correlation Distance (km)	Correlation Time (sec)	# of analyzed time series	Activity level
<=0.005	75	696	159041	Quiet
0.005-0.015	47	461	16716	Moderate
>0.015	36	409	826	High

It is also essential to consider amplitudes of the autocorrelation functions for each TEC time series. The mean-squared amplitudes (i.e. variance) can be translated directly into a measure of variations in the ionospheric delay and, therefore, provide magnitudes of the impact on the positioning accuracies. The unit of the mean-squared amplitudes is $TECU^2$. As discussed in Section 3.3, one TECU is equal to 0.16 metres of range delay on L1, and is equal to 0.27 metres of range delay on L2. The amplitudes are derived for the same TEC time series used in the previous analysis during intervals of high and moderate ionospheric activity. During quiet ionospheric activity, the amplitudes are derived for 27246 TEC time series. TEC time series for quiet ionosphere are very similar; therefore, a lower number of series was used in this analysis to reduce the processing time. The probability distributions of the derived amplitude values of the temporal variations during high, moderate, and quiet activity levels are shown in Figure 4.20, with the results summarized in Table 4.4.

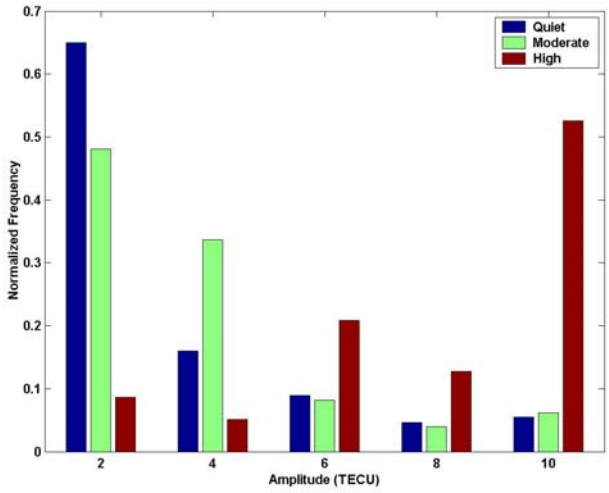

Figure 4.20 Probability distribution of amplitudes of temporal variations of TEC time series during intervals of quiet, moderate, and high ionospheric activity

It must be noted that the amplitudes increase for higher levels of activity. During quiet intervals, the amplitudes have a mean value of 3.03 TECU, which is equal to 0.48 m range delay on L1. The amplitudes increased significantly during high intervals with the mean value of 11.01 TECU that corresponds approximately to 1.76 m range delay on L1. Results of amplitudes of the spatial variations for TEC time series are similar to those for temporal variations.

Table 4.4 Means and Standard Deviations of the Amplitudes of Temporal Variations of TEC Time Series

Activity level	Mean (TECU)	Standard Deviation (TECU)	# of analyzed time series
Quiet	3.03	2.27	27246
Moderate	4.26	2.77	16716
High	11.01	3.79	826

For a network of several GPS reference stations, RTECI values and correlation times and distances will be derived in real-time for all measurements to identify regions of high, moderate, and quiet ionospheric activity over the network region. In addition, the amplitudes of the temporal and spatial variations of TEC time series will be derived to provide a measure of the impact on the positioning accuracies. Details of the proposed technique are presented in Chapter 5 as well as testing the reliability of the technique.

CHAPTER 5

IONOSPHERIC WARNING AND ALERT SYSTEM

The threshold values of RTECI for quiet, moderate and high levels of ionospheric activity have been derived in Chapter 4 in addition to the corresponding correlation times and distances for the ionosphere. By considering Table 4.3, measured RTECI values can be used to characterize the degree of local ionospheric activity, in the region where the given RTECI measurement line-of-sight crosses the ionosphere.

The use of an index such as RTECI is necessary to monitor the extent and the magnitude of the ionospheric effects in the auroral region. Therefore, RTECI values are profiled in 1-D (i.e. latitude) and 2-D (i.e. latitude and longitude) over the auroral zone to identify the spatial extent of regions of high, moderate, and quiet ionospheric activity.

5.1 DATA DESCRIPTION

The 30-second dual-frequency data were collected at 10 stations simultaneously. These stations are part of IGS network, and their locations are shown in Figure 5.1. TurboRogue receivers are used to collect the measurements

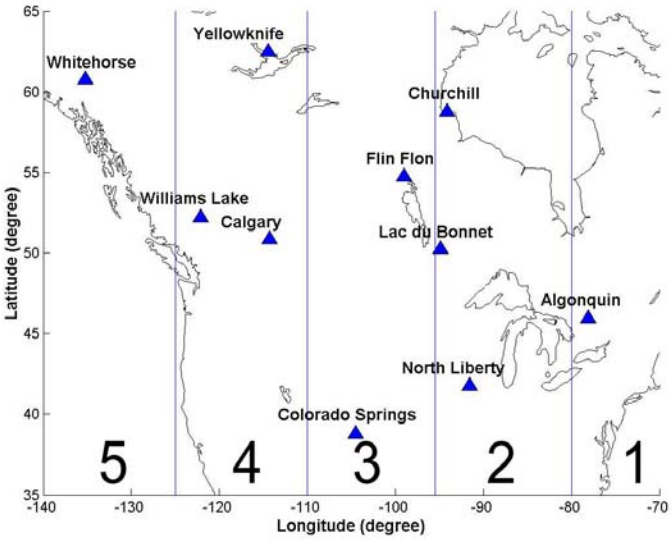

Figure 5.1 Locations of IGS reference stations

Stations that share the same magnetic local hour have been grouped as shown in Figure 5.1, where measurements from every group of stations that falls between the two blue lines are studied to profile the RTECI in the latitude direction. For discussion purposes, the groups are numbered from 1 to 5 as shown in Figure 5.1. It should be noted that some groups contain 3 stations while others contain less stations. The difference in stations number in every group is preferred to allow studying all possible cases for the presented technique.

As stated in Section 4.2, the elevation mask angle of 15 degrees was used in data processing. Figure 5.2 illustrates the ionospheric coverage allowed from one day of measurements from all stations. These measurements cover (65N-35N) in the North-South direction and (150W-70W) in the West-East direction.

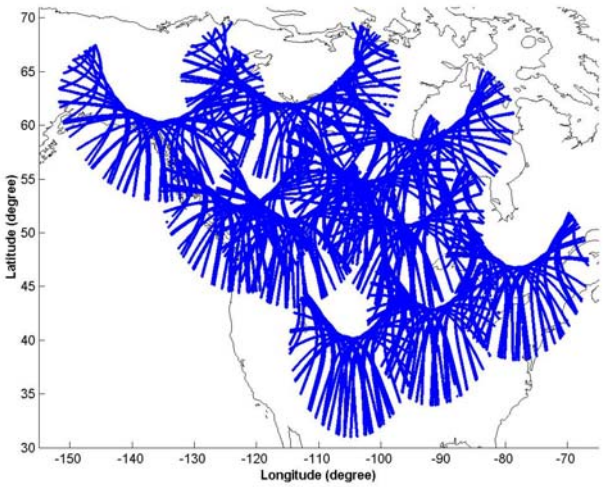

Figure 5.2 IPP distributions over the station network

Measurements from all reference stations are analyzed to estimate latitude-longitude (2-D) boundaries of ionospheric disturbances in the Canadian sector and the northern United States. Estimation of the 2-D boundaries begins with 1-D analyses, where the lower boundaries of ionospheric disturbances are derived, in latitude, for each sector in Figure 5.1. A 2-D boundary is then interpolated in longitude. The implementation of this technique for ionospheric monitoring is presented in the later part of this chapter.

The data availability for each reference station is presented in Figure 5.3. The black circles indicate periods during which no data were available. The data are available for 332 days of the year 2000 at all reference stations.

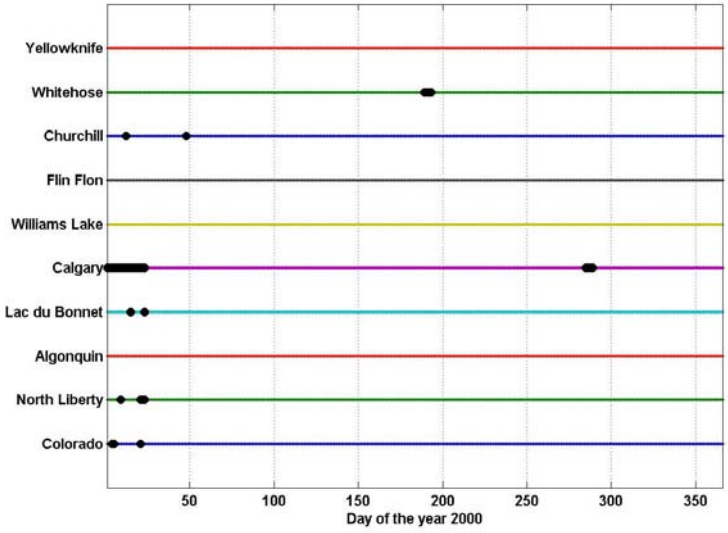

Figure 5.3 Data availability of the year 2000 (black circles indicate missing data)

5.2 METHOD DESCRIPTION

For each satellite-receiver line-of-sight, the IPP are computed (Appendix A) over one-hour time intervals as shown in Figure 5.4. In addition, RTECI values are derived for the given satellite-receiver line-of-sight. There are 12 5-minute RTECI observations available for each one-hour satellite-receiver TEC series. One correlation time and one correlation distance are also derived for each of these series.

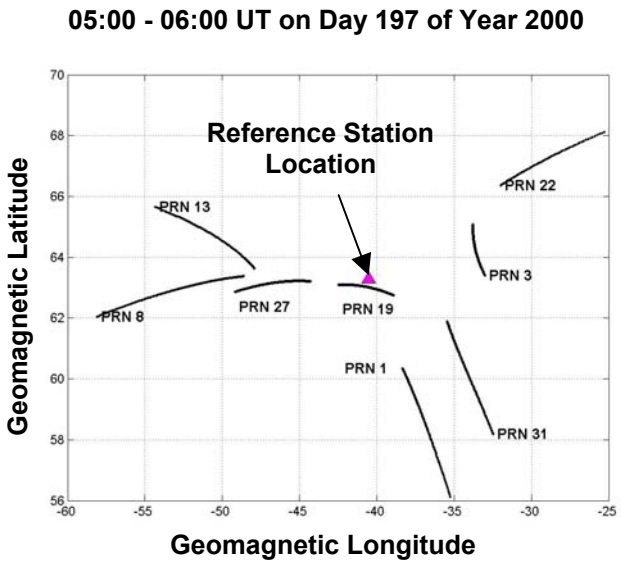

Figure 5.4 One-hour interval of IPP at Flin Flon reference station

During a one-hour time interval, every station is observing several satellites simultaneously (e.g. 4-8 measurements); an example is presented in Figure 5.4. A number of RTECI values will be available for each one-hour series (e.g. 12 values of RTECI). The coordinates of the IPP are also computed for each RTECI estimate. The IPP coordinates are computed at the center of the 5-minute arc. If it is assumed that a given station collects 6 measurements simultaneously (when there are 6 satellites in the view), there are 6x12 = 72 values of RTECI distributed over various regions of the ionosphere during a one-hour period. A full hour of RTECI values is then used to map the 2-D ionospheric activity, and to define the boundary of the high ionospheric activity (e.g. auroral oval). This information can be provided to GPS users to identify the level of ionospheric activity in near-real time.

The 2-D profiles are derived at 60-minute intervals to allow for a sufficient number of RTECI values to be included in the results. In addition, the chosen 60-minute intervals

in this analysis are consistent with the derived correlation statistics in Section 4.4. It is possible, however, to derive profiles over shorter intervals to follow the progression of phenomena such as substorm events.

5.2.1 RTECI Latitude Profiles of the Auroral/Sub-Auroral Regions

A method for identifying the boundaries of high, moderate, and quiet ionospheric regions in 2-D (i.e. latitude and longitude) starts with a latitude profile in 1-D for each sector in Figure 5.1. RTECI values are plotted versus geomagnetic latitude for each group of stations. Five groups of stations are available, extending in the East-South directions. Each group has at least one station. The measurements for each group extend in the North-South direction. Latitude profiles of RTECI for each group are used to determine the latitude extent of the ionospheric activity in the local time zone of the given group. The superposed latitude profiles for all groups defines the boundary of ionospheric disturbances in 2-D.

In 1-D, a test is conducted to choose the appropriate function for fitting the data. Measurements from the Group 2 were chosen for this test. Group 2 has three stations (i.e. Churchill, Lac du Bonnet, and North Liberty), and therefore has the greatest number of measurements during each one-hour time interval.

During periods of low ionospheric activity, all orders of polynomials fit the RTECI values similarly in latitude and provide very similar variance values as shown in Figure

5.5a; results are summarized in Table 5.1. The variance value is the averaged squared deviation of each original RTECI values from the fitted one.

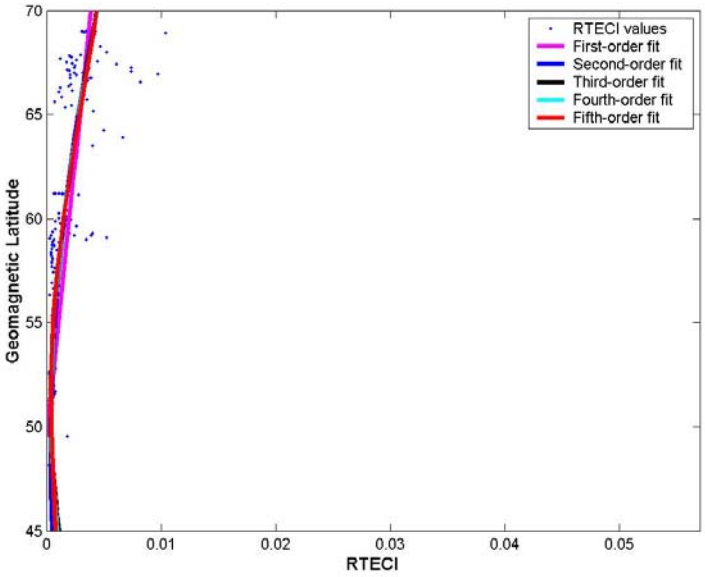

a) At low ionospheric activity K = 3

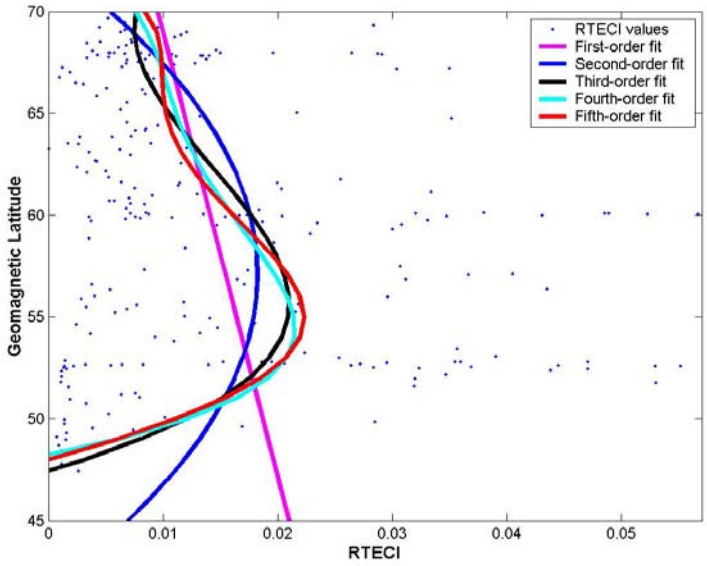

b) At high ionospheric activity K = 9

Figure 5.5 Different orders of polynomials fit to RTECI values

For periods of high ionospheric activity (Figure 5.5b), a third-order polynomial (denoted in black color) fits the data better than first- (magenta) and second- (blue) order polynomials. The variance of the third-order is relatively smaller than the variance of the first- and second-order polynomials. Higher order polynomials are approximately similar to the third-order polynomial as shown in Figure 5.5b, with very close variance values. High ionospheric activity in Figure 5.5 is represented by one-hour (20:00-21:00) on 15 July, 2000, while the low activity is represented by 01:00-02:00 on 15 July, 2000. The Kp index was 9 for the first scenario, and was 3 for the low ionospheric activity period.

Table 5.1 Variance Values $(TECU/s)^2$ for the Various Functions During Low and High Ionospheric Activity

Polynomial degree	First-order	Second-order	Third-order	Fourth-order	Fifth-order
Low Activity	0.000302	0.000295	0.000292	0.000291	0.000291
High Activity	0.0443	0.0401	0.0367	0.0366	0.0364

Fitting a function to the RTECI values allows profiling of the RTECI in latitude. Identification of the latitude boundaries between quiet and moderate and high ionospheric activity regions is done using the threshold values of RTECI derived in Table 4.3.

As an example in Figure 5.6, three colors are chosen to indicate regions of high (red), moderate (yellow), and quiet (green) ionospheric disturbance. Two lines are plotted on every panel (i.e. green and red lines). A green vertical line at the RTECI value of 0.005 TECU/s represents the threshold between quiet and moderate ionospheric activity regions. The threshold between moderate and high ionospheric activity is defined at the RTECI

value of 0.015 TECU/s (red line). The values 0.005 and 0.015 TECU/s were derived in Section 4.4.3 to identify regions of high, moderate, and quiet ionospheric activity. A third-order polynomial fit to RTECI values is presented by a blue curve. The intersection of the blue curve and the red line results in defining the latitudinal extent of the high ionospheric disturbance region. The intersection of the blue curve and the green line provides the latitudinal extent of the moderate ionospheric activity region. The third-order polynomial does not extend in regions where there is no data available. It only represents latitudes with available data.

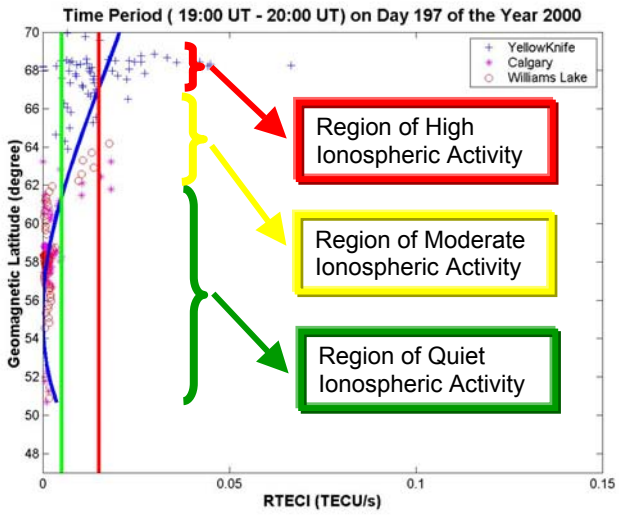

Figure 5.6 Auroral latitude profiles for Group 4 (50°W-65°W) for 1900-2000 UT on day 197 of the year 2000 (K = 9)

The latitude profile shown in Figure 5.6 presents one group of the total of five groups (Figure 5.1). Each group used to create the 1-D latitude profiles covers 15 degrees of geomagnetic longitude. The superposition of results from the five groups covers a total

longitudinal extent of 75 degrees. Latitude profiles of each group provide the boundaries of high, moderate, and quiet ionospheric activity regions.

5.2.2 Two-Dimensional Monitoring of the Auroral/Sub-Auroral

In order to create a 2-D representation of the spatial extent of auroral activity the latitudinal boundaries derived for each group are plotted versus longitude (the center of the 15 degree longitudinal sector for each group).

As an example in Figure 5.7, latitudinal boundaries of each group between quiet and moderate activity regions are plotted as green circles, and the latitudinal boundaries between moderate and high activity regions are plotted as red diamonds. To test the best fit polynomial to latitudinal boundaries, three fits are plotted representing second-order (cyan), third-order (black), and fourth-order (magenta) polynomials. The fourth-order fit does not represent the latitudinal boundaries (data points). The second-order fit does not fit the data points accurately as the third-order fit does. The variance for the second-order fit is 1.3354 $(TECU/s)^2$, while for the third-order fit is 2.6e-27 $(TECU/s)^2$. As a result, the third-order polynomial is chosen to represent the latitudinal boundaries (red diamonds). Similarly, the boundary between the moderate and quiet regions is represented by three types of polynomial; second-order (cyan), third-order (black), and fourth-order (magenta) polynomials. The third-order polynomial is chosen, where its variance is 1.42e-26 $(TECU/s)^2$, and variance of the second-order polynomial is 0.735 $(TECU/s)^2$.

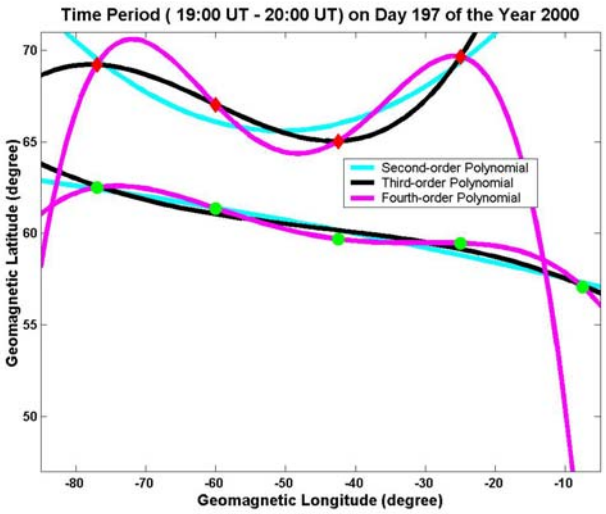

Figure 5.7 Different orders of polynomials fit to latitudinal boundaries

During the one-hour time interval, the magnitude of each RTECI value (as observed for all satellites from all reference stations) is plotted versus the geomagnetic latitude and longitude of the corresponding IPP (computed at the center of the 5-minute arc). It was necessary to linearly interpolate RTECI values in some regions, where there are no RTECI values available. As presented in Figure 5.8, the color bar describes the values of RTECI, with dark blue representing small RTECI values and red represents extreme RTECI values. The boundary between high and moderate activity is represented by a red curve, which is the third-order polynomial fitting of the plotted latitudinal boundaries (red diamonds). The green curve represents the boundary between the moderate and quiet regions, and it is the third-order polynomial fitting of the latitudinal boundaries (green circles). RTECI values smaller than 0.005 (TECU/s) represent the quiet ionospheric activity regions. The values ranging between 0.005 and 0.015 (TECU/s) represent the moderate activity regions. In regions of high ionospheric disturbance, RTECI values are 0.015 (TECU/s) or greater.

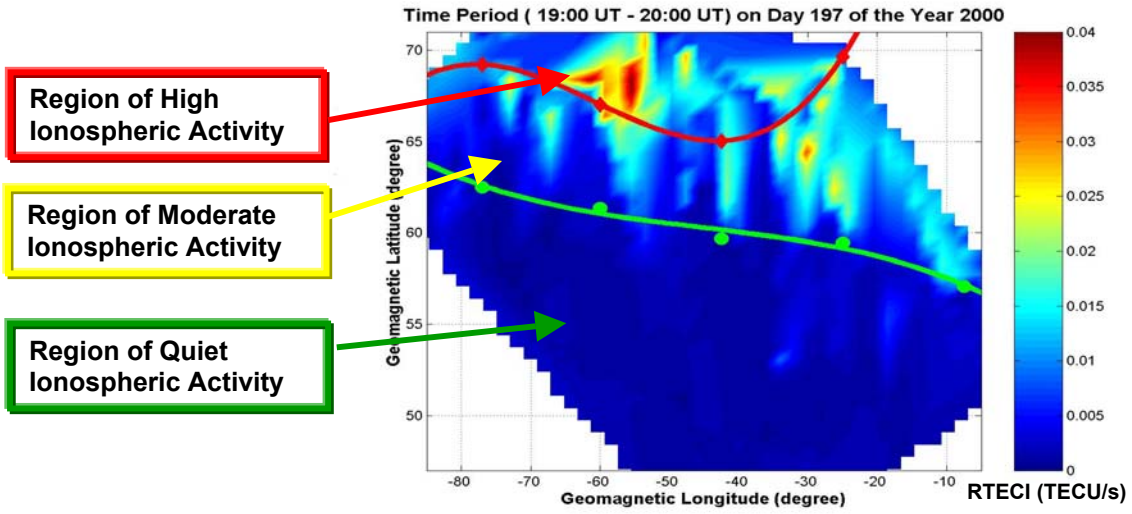

Figure 5.8 Auroral extent in two-dimensions for 1900-2000 UT on day 197 of the year 2000 (K=9)

In order to assess the reliability of estimated latitudinal boundaries for each group, the goodness of fit for all latitude profiles of RTECI is presented by computing the variance. As an example, the variance is derived for each group during the one-hour at 1900-2000 UT on July 15th (day 197) of the year 2000, and presented in Table 5.2. The variances are used to estimate the weight matrix, which is used in the least square adjustment to estimate the longitude third-order polynomial parameters. Weighting the latitudinal boundaries while deriving the two-dimension boundaries can be useful to assure the reliability of estimated longitudinal boundaries.

Table 5.2 Latitude Profiles Variances $(TECU/s)^2$ for Each Group During 1900-2000 UT on Day 197 of the Year 2000

Group 1	Group 2	Group 3	Group 4	Group 5
1.33e-05	5.64e-05	8.29e-05	1.19e-04	1.09e-04

5.3 SAMPLE EVENTS

Three events are studied to demonstrate and discuss the proposed technique. High, moderate, and quiet ionospheric activity events are described in the following sub-sections.

5.3.1 High Ionospheric Activity Event

In late evening of July 15th of the year 2000, a severe geomagnetic storm reached the Earth and led to enhanced ionospheric effects. The global geomagnetic activity index Kp reached a value of 9 for three successive three-hour intervals. High variations of the Earth's magnetic field were observed due to an enhanced solar-terrestrial interaction and strong electric currents in the auroral region. Bright aurora were observed during this event. The auroral oval extended far southward over mid-latitude regions in North America as shown in Figure 5.9.

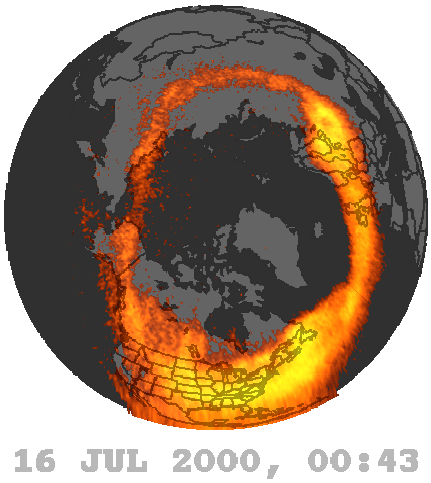

Figure 5.9 The auroral oval extent during storm event on day 197-198 (July 15-16) of the year 2000 [courtesy of Visible Imaging System (VIS), University of Iowa]

The spatial and temporal evolution of this event was monitored using the proposed technique. Four hours (19:00 – 23:00) on 15 July (day 197), 2000 are presented as an example. As shown in Figure 5.1, there are five groups of stations used to derive the 2-D maps. RTECI values are plotted versus geomagnetic latitude for every group. A third-order curve is fit to the RTECI values in order to define the boundary of the auroral oval in latitude and, in turn, define the boundary of ionospheric disturbances.

Group 1

Group 1 contains one station at Algonquin, Ontario. This group's measurements cover geomagnetic longitudes from 5^{o} W to 20^{o} W. Plots of RTECI values versus geomagnetic latitude are shown in Figure 5.10. Each panel in the figure presents a one-hour estimate of the magnitude and extent of the auroral activity at longitudes in the range 5^{o} W – 20^{o} W.

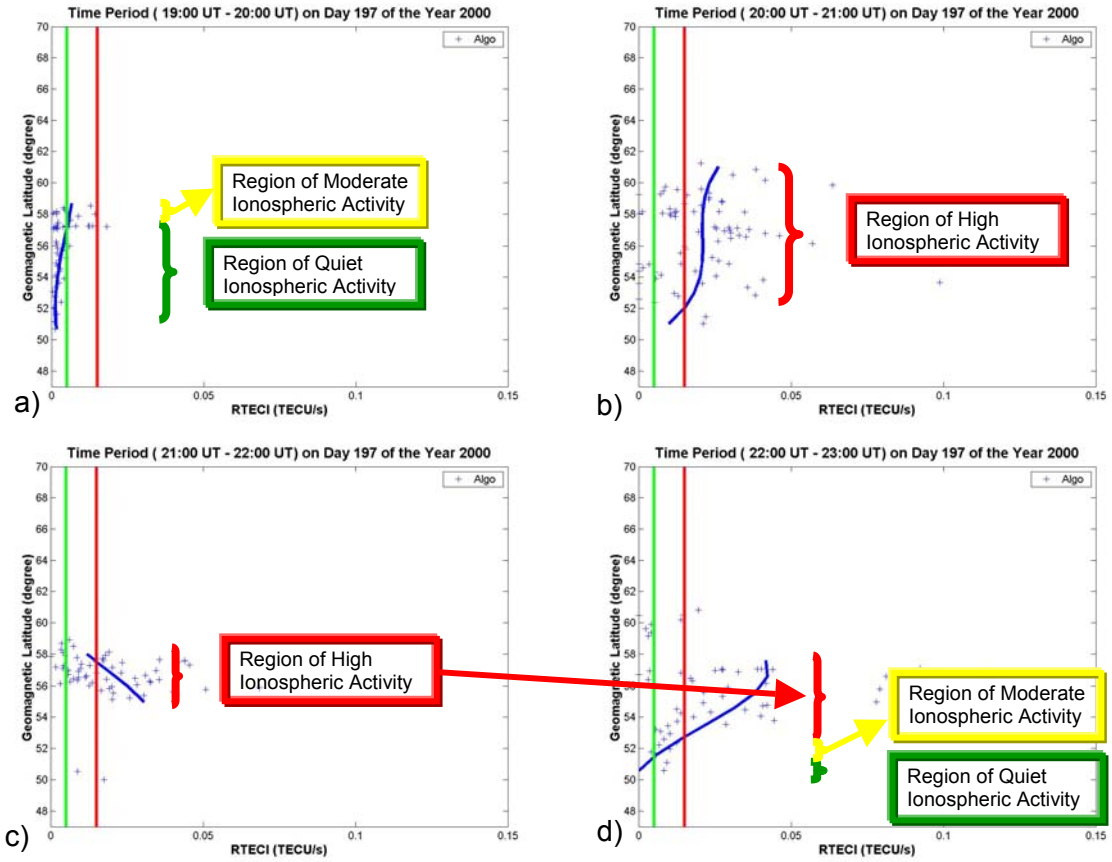

Figure 5.10 Auroral latitude profiles for Group 1 (5°W-20°W) for 1900-2300 UT on day 197 of the year 2000

Figure 5.10a presents a latitude profile for the period 19:00-20:00 UT. The RTECI data are available in the range 51^{o} – 59^{o} geomagnetic latitude, and the third-order polynomial fit is conducted in this latitude range. Moderate ionospheric activity was observed at geomagnetic latitudes of 57^{o} and higher. Latitudes lower than 57^{o} are observed as regions of quiet ionosphere. The latitude profile for the period 20:00 UT – 21:00 UT is presented in the second panel (Figure 5.10b). High ionospheric activity is observed in the region 51^{o} – 61^{o} geomagnetic latitude. The third hour of the study is presented in Figure

5.10c. The highly disturbed region is still observed during this hour, and at geomagnetic latitudes between 55^{o} – 59^{o}. During this hour, it should be noted that there are two RTECI values at latitudes of 50^{o} and 50.5^{o}. These RTECI values are derived for the same satellite, which was only in view for 10 minutes during this one-hour time frame. These values are not taken into consideration when fitting the polynomial to the data points, where the latitude gap between the RTECI values may result in unreliable interpolation of the data points. During the fourth hour presented in Figure 5.10d, RTECI measurements cover geomagnetic latitudes in the range of 51^{o} – 57^{o}. The boundary of the high activity region was estimated as 53^{o} geomagnetic latitude. A region of moderate ionospheric activity was observed at geomagnetic latitudes between 51^{o} and 53^{o}.

Group 2

Group 2 includes three stations. Two stations are located in Manitoba (Churchill and Lac du Bonnet) and the third station is located in North Liberty, Iowa. This group represents the second longitudinal sector that covers geomagnetic longitudes in the range 20^{o} W – 35^{o} W.

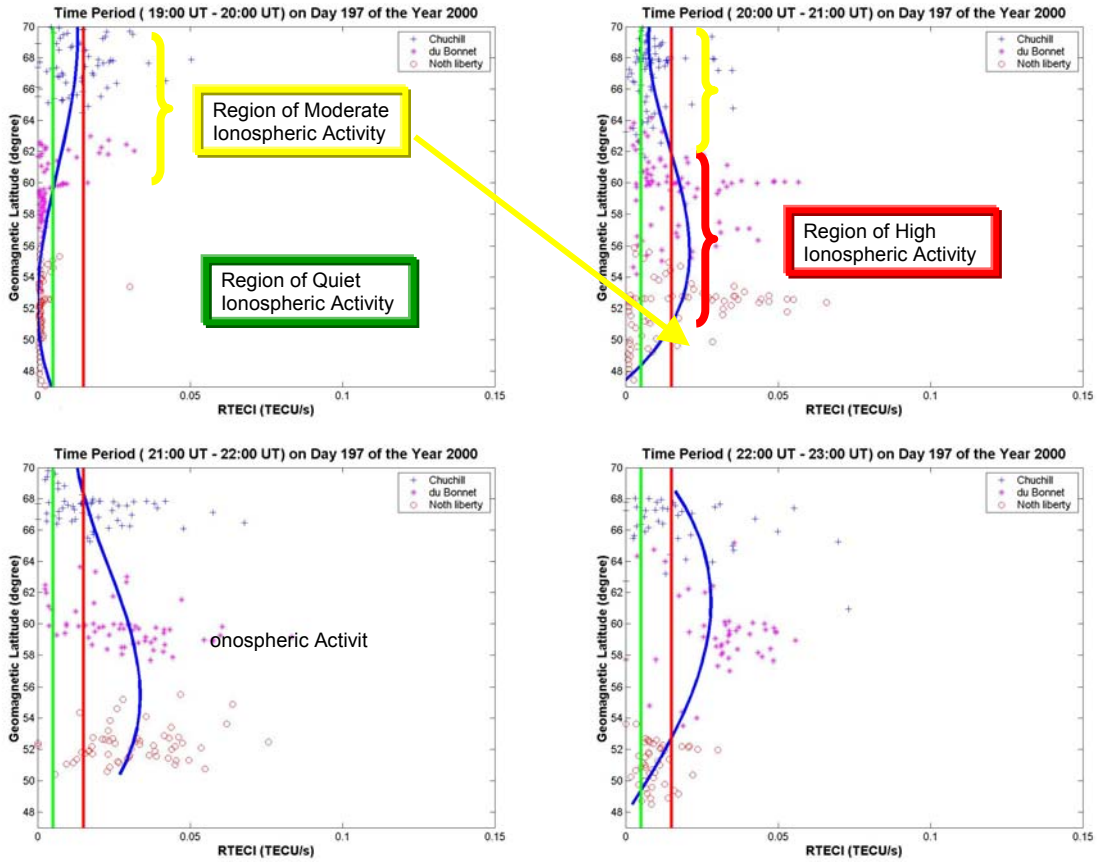

Figure 5.11 Auroral latitude profiles for Group 2 (20°W-35°W) for 1900-2300 UT on day 197 of the year 2000

A latitude profile for the period (19:00 – 20:00 UT) is presented in Figure 5.11a. A region of moderate ionospheric activity was observed at geomagnetic latitudes higher than 60 ^{o}. There was no region with high ionospheric activity observed during this hour. The high ionospheric activity was observed during the second hour between geomagnetic latitudes 51^{o} and 62^{o} as shown in Figure 5.11b. The high activity expanded southwards to 50° latitudes during the third hour (Figure 5.11c), as estimated using the available RTECI values. However, the auroral activity moved northwards to 53 ^{o} of geomagnetic latitude over the period 21:00 UT – 22:00 UT as shown in Figure 5.11d.

Group 3

Group 3 covers geomagnetic longitudes between 35° W and 50° W, and includes measurements at reference stations located in Flin Flon, Manitoba, and Colorado Springs, Colorado.

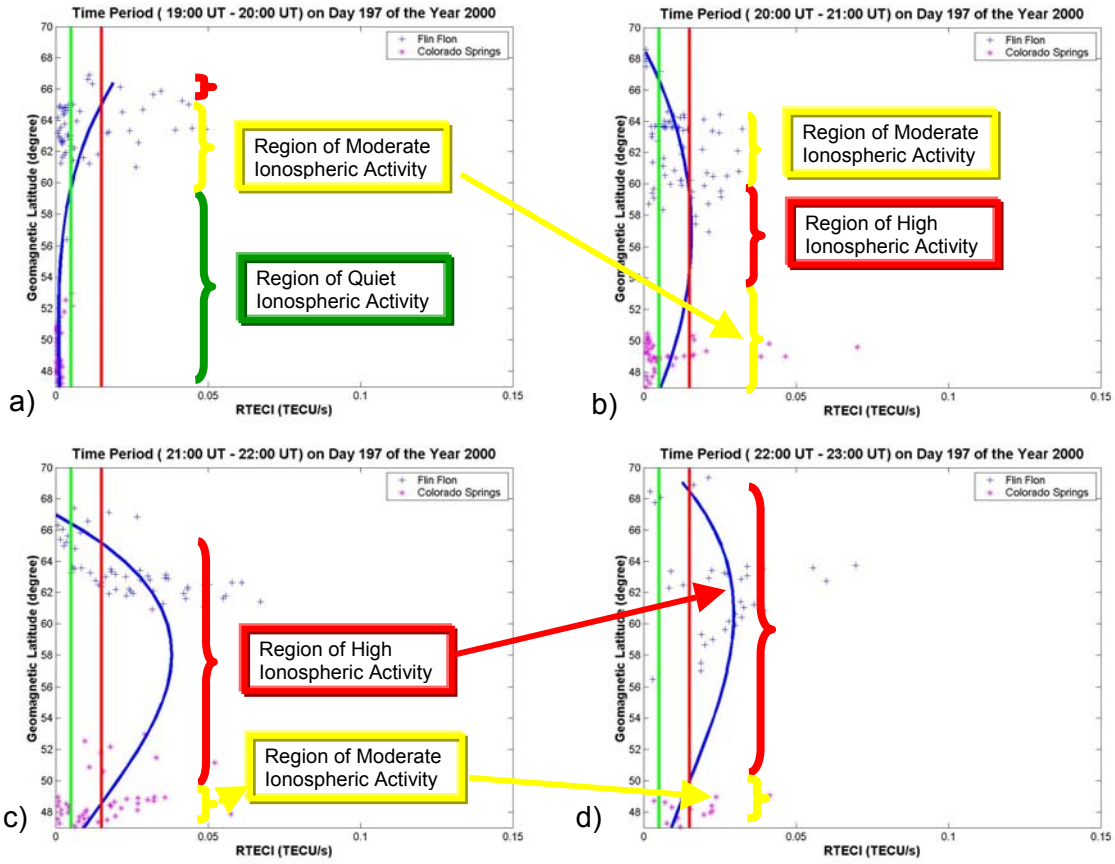

Figure 5.12 Auroral latitude profiles for Group 3 (35°W-50°W) for 1900-2300 UT on day 197 of the year 2000

Regions of high, moderate, and quiet ionospheric activity were observed during the period 19:00 – 20:00 UT. The region with high ionospheric activity was observed at 65° geomagnetic latitude, while a moderate activity region was observed in the geomagnetic

latitude range 59^{o} – 65^{o}, and the quiet region was observed at latitudes south of 59^{o} geomagnetic in Figure 5.12a. The second hour is presented in Figure 5.12b. The high ionospheric activity moved southwards, to the geomagnetic latitude range 53^{o} – 60^{o}. The following hour is presented in Figure 5.12c, where the high disturbance region moved southwards with an equatorward boundary of 49^{o} geomagnetic latitude. During the fourth hour of the study, boundary of high activity slightly moved north at latitude 50^{o}.

Group 4

Group 4 covers the geomagnetic longitudes between 50^{o} W and 65^{o} W. This group includes measurements at Yellowknife (Northwest Territories), Calgary (Alberta), and Williams Lake (B.C.).

Group 4 measurements cover geomagnetic latitudes between 70^{o} N and 50^{o} N. The boundary of high ionospheric activity was observed to extend southwards during the four-hour interval 1900-2300 UT. The boundary of high activity was observed at 67^{o} geomagnetic latitude during the first-hour 1900-2000 UT (Figure 5.13a). The boundary of the high activity then moved southwards to a geomagnetic latitude of 58^{o} during the second hour, as shown in Figure 5.13b. During the third hour, the equatorward boundary of high ionospheric activity extended further southwards to a geomagnetic latitude of 56^{o}. The fourth hour is presented in Figure 5.13d, where the boundary of high activity has moved further southwards to 55^{o} geomagnetic latitude. Moderate and quiet ionospheric activity were also observed during the four-hour interval. Those regions were moving southward with the enhancement of the ionospheric activity in high latitudes.

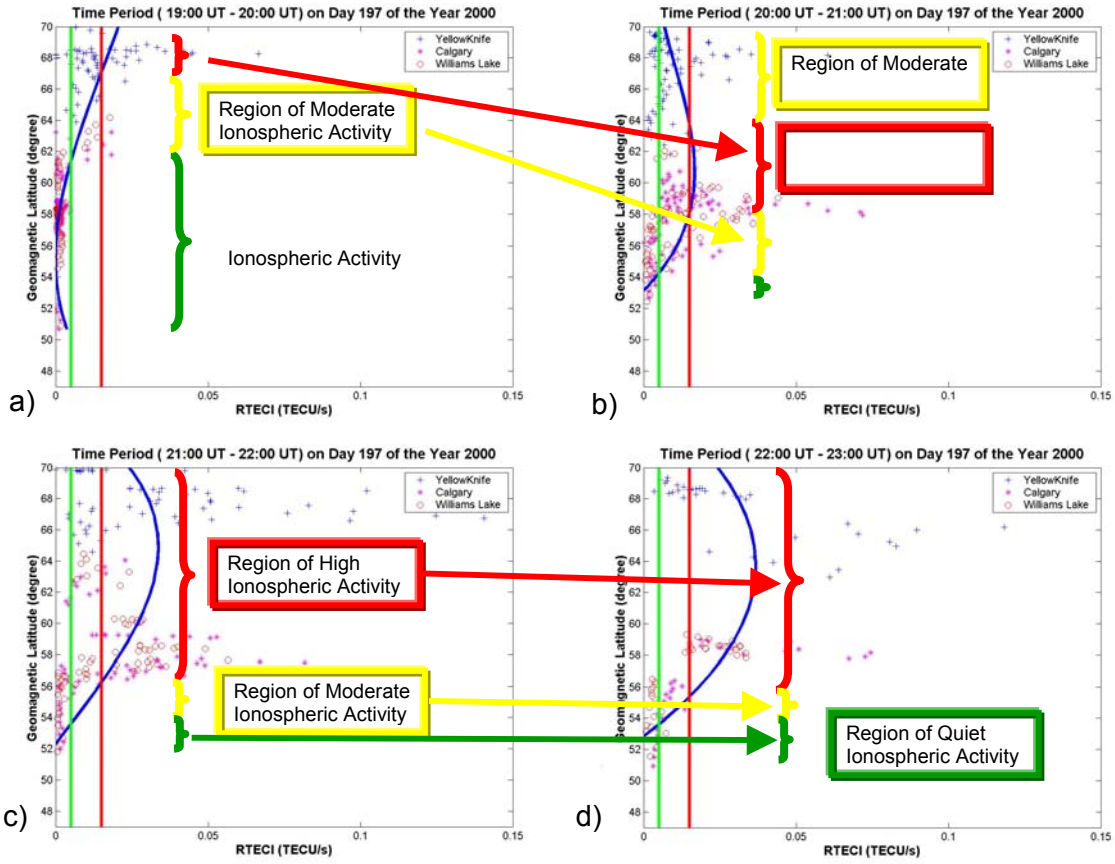

Figure 5.13 Auroral latitude profiles for Group 4 (50°W-65°W) for 1900-2300 UT on day 197 of the year 2000

Group 5

Group 5 includes one station located at Whitehorse, Yukon. This group covers geomagnetic longitudes between 65^{o} W and 80^{o} W, and covers geomagnetic latitudes between 70^{o} N and 58^{o} N.

As shown in Figure 5.14, the boundary of high ionospheric activity was observed at high latitudes (i.e. 69.5^{o} N) during the period 1900-2000 UT, as shown in the first panel.

As the storm grows, the boundary was monitored to extend southwards to 59^{o} geomagnetic latitude during the second hour and the third hour. In the fourth hour, the boundary has moved northwards to a latitude of 63^{o}.

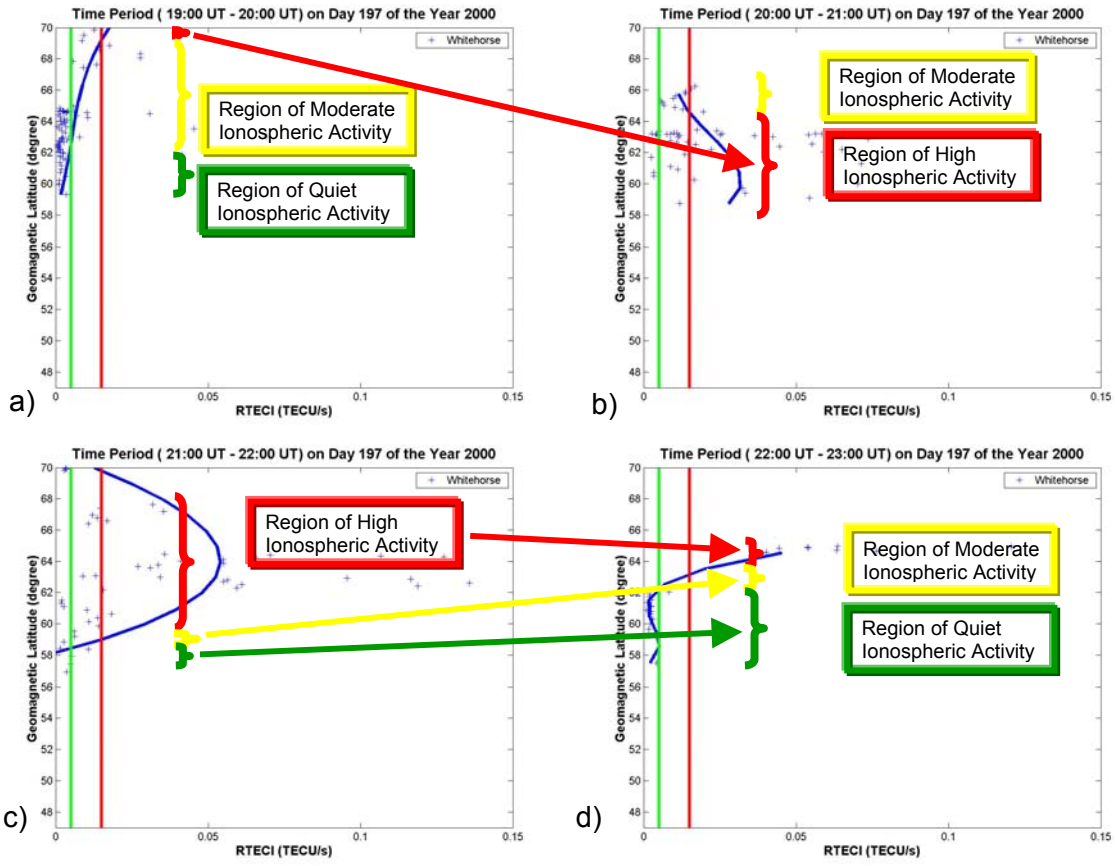

Figure 5.14 Auroral latitude profiles for Group 5 (65°W-80°W) for 1900-2300 UT on day 197 of the year 2000

Overall results for Groups 1-5 are used to extend the monitoring technique in two-dimensions. The boundaries of high, moderate, and quiet ionospheric activity regions are derived by latitude profiles for each group. In order to assess the reliability of estimated boundaries for each group, the variance is computed for the goodness of fit for all latitude

profiles of RTECI. Variances are used to estimate the weight matrix in least square calculations to derive the ionospheric activity boundaries in two-dimensions. The variance is derived for each group during every hour of this event, and presented in Table 5.3.

Table 5.3 Variance Values (TECU/s)^2 Representing the Goodness of Fit of the Boundary Estimation for Each Group

Time on July 15, 2000	1900-2000 UT	2000-2100 UT	2100-2200 UT	2200-2300 UT
Group 1	1.33e-05	2.65e-04	1.86e-04	7.61e-04
Group 2	5.64e-05	1.49e-04	2.19e-04	2.90e-04
Group 3	8.29e-05	9.09e-05	1.63e -04	1.08e-04
Group 4	1.19e-04	1.25e-04	4.32e-04	3.25e-05
Group 5	1.09e-04	3.69e-04	1.20e-03	2.42e-04

The extent of the ionospheric activity in two dimensions is illustrated in Figure 5.15. RTECI distributions are also plotted for the same four–hour period of the July 15-16 (day 197 – 198) storm event.

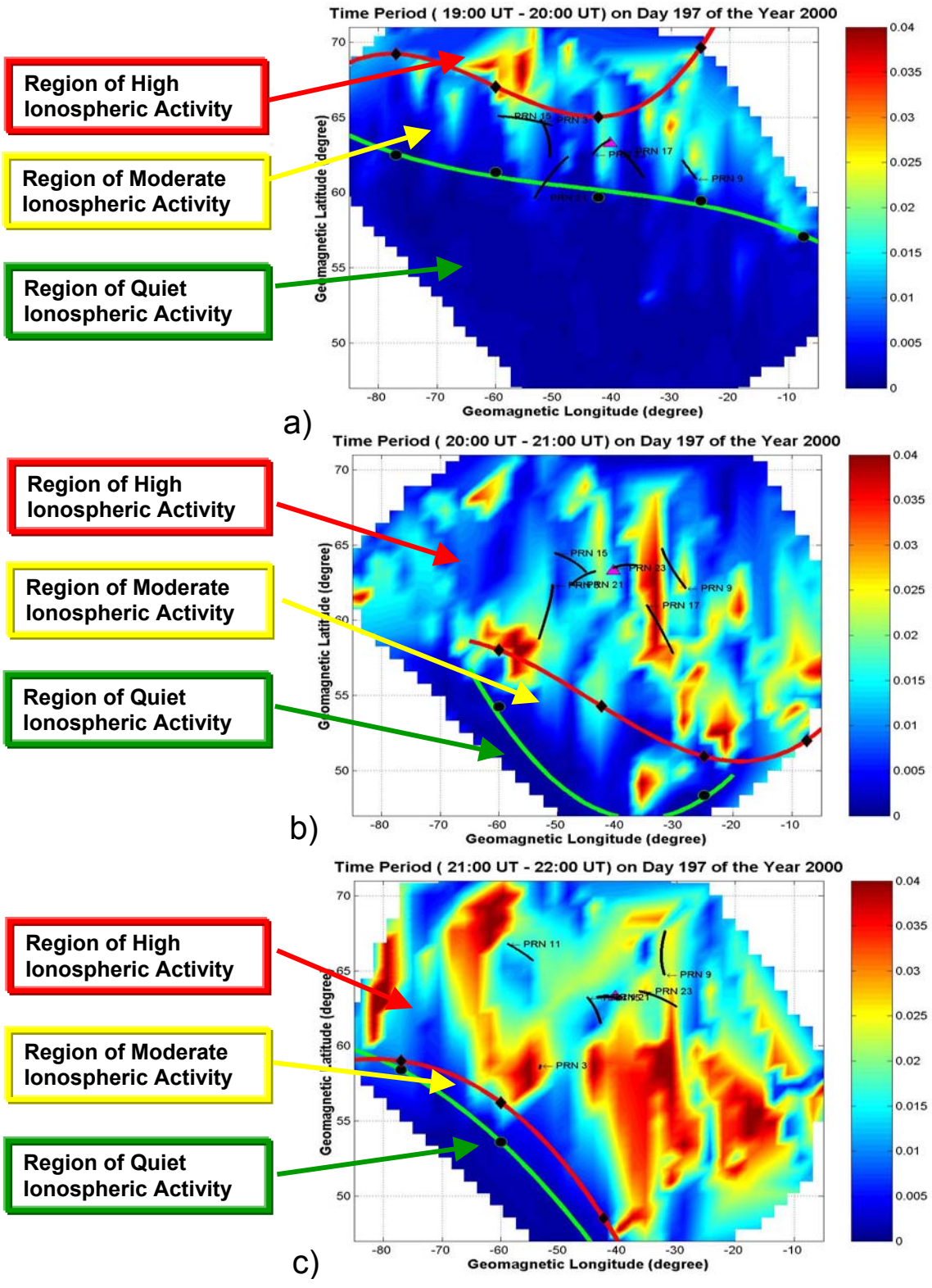
Region of High Ionospheric Activity
Region of Moderate Ionospheric Activity
Region of Quiet Ionospheric Activity
Time Period (19:00 UT - 20:00 UT) on Day 197 of the Year 2000
Geomagnetic Latitude (degree)
Geomagnetic Longitude (degree)
a)
Region of High Ionospheric Activity
Region of Moderate Ionospheric Activity
Region of Quiet Ionospheric Activity
Time Period (20:00 UT - 21:00 UT) on Day 197 of the Year 2000
Geomagnetic Longitude (degree)
b)
Region of High Ionospheric Activity
Region of Moderate Ionospheric Activity
Region of Quiet Ionospheric Activity
Time Period (21:00 UT - 22:00 UT) on Day 197 of the Year 2000
Geomagnetic Longitude (degree)
c)

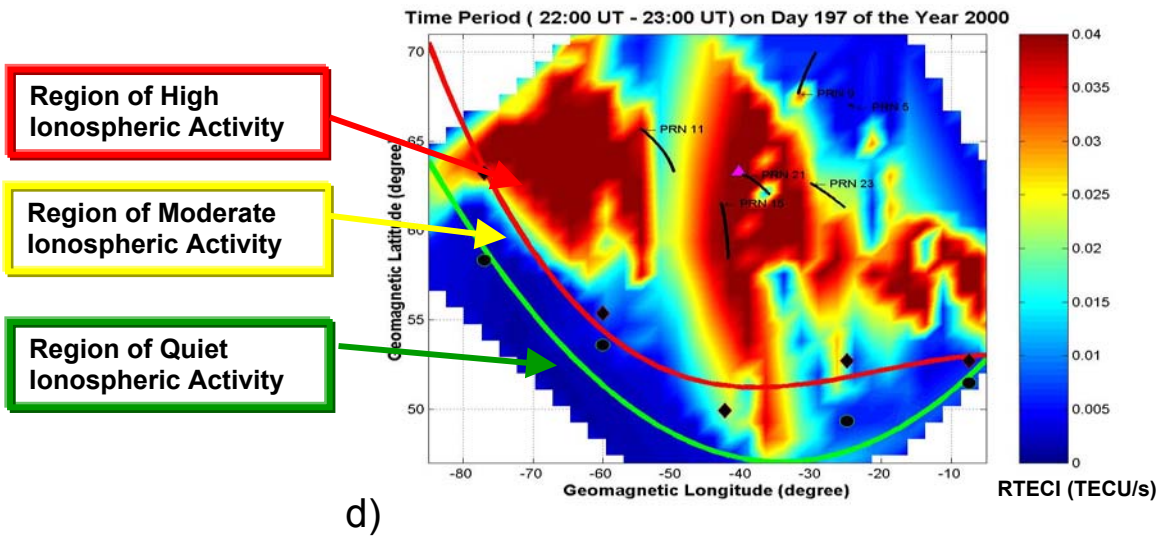

Figure 5.15 Auroral extent in two-dimensions for 1900-2300 UT on day 197 of the year 2000

Although only four hours are presented, the extent of the auroral oval was monitored (within the limitations of a sparse network of GPS stations) successfully. The auroral oval was observed to move equatorward during the storm development, as the boundary of the disturbed region is observed at progressively lower latitudes. GPS observations with satellite-receiver lines-of-sight passing through the disturbed region would be susceptible to enhanced spatial and temporal decorrelations. A warning could be issued to GPS users notifying them of different magnitudes and boundaries of ionospheric activity.

5.3.2 Moderate Ionospheric Activity Event

A moderate ionospheric activity event is presented as an example in this section. The "moderate" level of activity is reflected in the local geomagnetic North American K indices (observed at Boulder, Colorado). Periods of K values ranging from 4 to 6 are assumed to be of moderate activity. Two hour periods are presented in this section in order to demonstrate the proposed technique performance during periods of moderate activity. K values of 4 were observed during the period presented. Observations were collected on August 5th (day 224), of the year 2000 at the stations illustrated in Figure 5.1. Two hours (12:00 – 14:00 UT) are illustrated in the following figures.

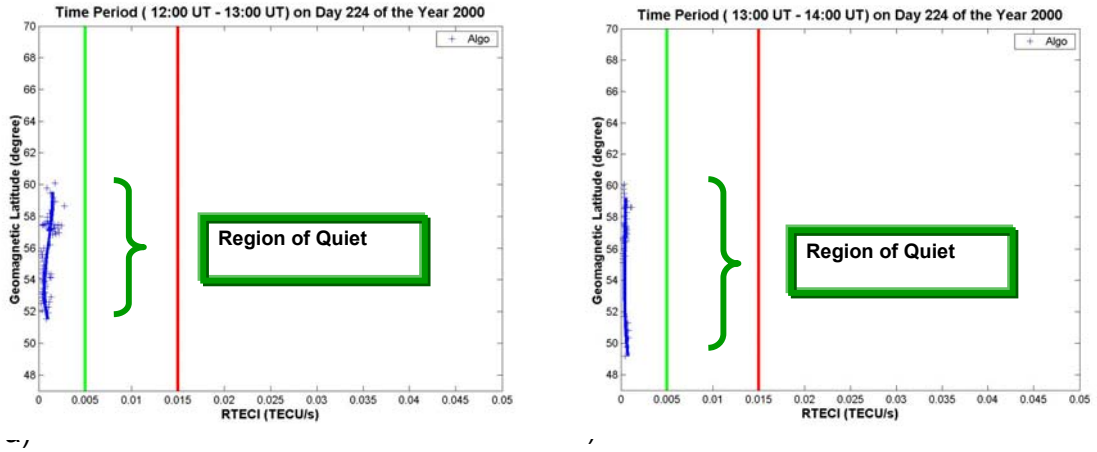

Figure 5.16 Latitude profiles of the Group 1 for 1200 – 1400 UT on day 224 of the year 2000

Latitude profiles of the Group 1 are presented in Figure 5.16. The scale of the x-axis has been changed, compared with latitude profiles presented in Section 5.2.2. The observed RTECI values are significantly lower than the values for the high ionospheric

activity event. During the two-hour period (1200:1400 UT), RTECI values lower than 0.005 (TECU/s) were observed at the Algonquin station.

The derived RTECI values of the Group 2 are plotted in Figure 5.17. The blue curve fits the RTECI values and intersects with the green line to identify the boundary of moderate ionospheric activity. The boundary was observed at a geomagnetic latitude of 60^{o} during the first hour, and at a geomagnetic latitude of 63^{o} during the second-hour.

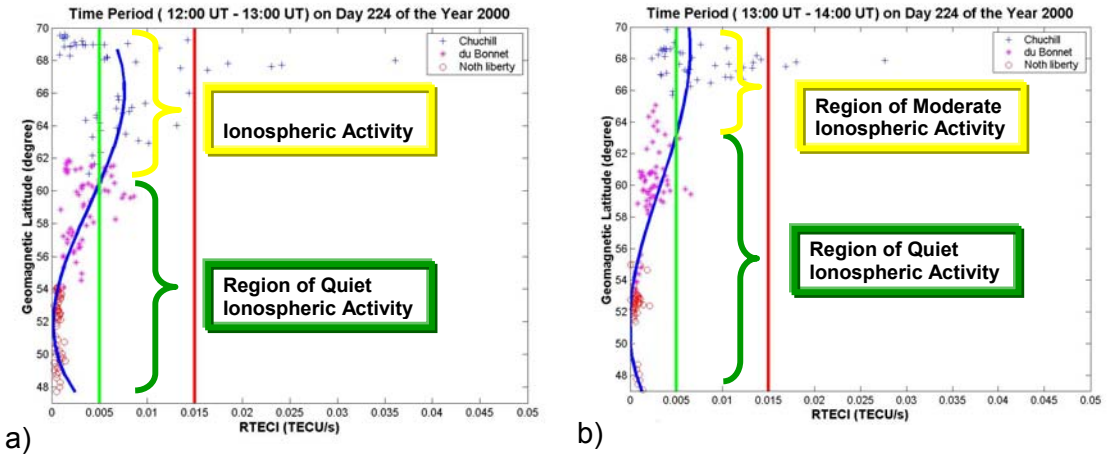

Figure 5.17 Latitude profiles of Group 2 for 1200 – 1400 UT on day 224 of the year 2000

For Group 3, the auroral latitude profiles are presented in Figure 5.18. During the first hour of the presented event, the boundary of the region of moderate ionospheric activity is observed at 59 degrees geomagnetic latitude. During the period 1200 – 1400 UT, the polynomial does not intersect with the threshold between the quiet and moderate activity; however, some RTECI values are higher than 0.005 (TECU/s).

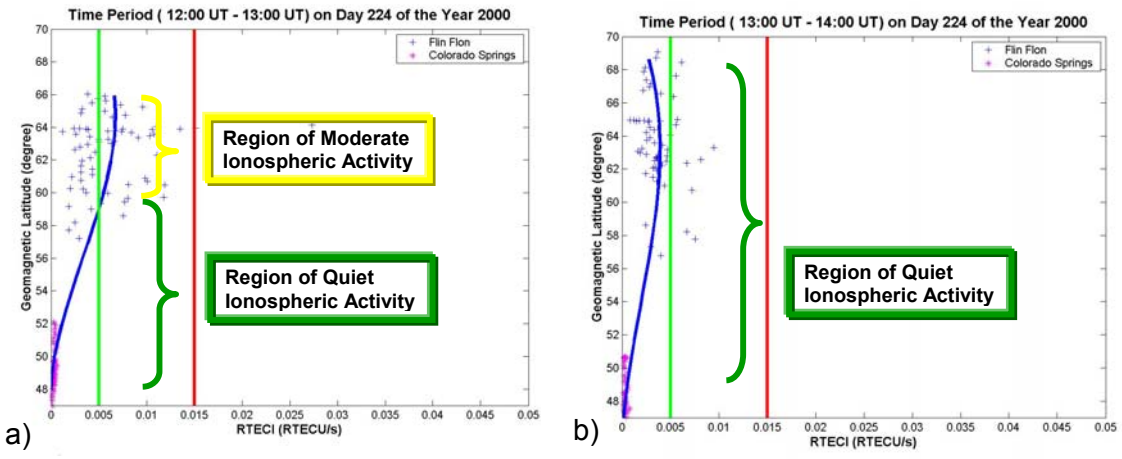

Figure 5.18 Latitude profiles of Group 3 for 1200 – 1400 UT on day 224 of the year 2000

Latitude profiles for Group 4 are plotted in Figure 5.19. The polynomial of the third-degree fits RTECI values and identifies the boundary of the moderate ionospheric activity region. Over the first-hour (1200UT – 1300UT), the boundary of the moderate activity region was observed at a geomagnetic latitude of 62^{o} as presented in Figure 5.19a. The boundary was recorded at a geomagnetic latitude of 60^{o} during the second hour (1300UT – 1400UT) as illustrated in Figure 5.19b.

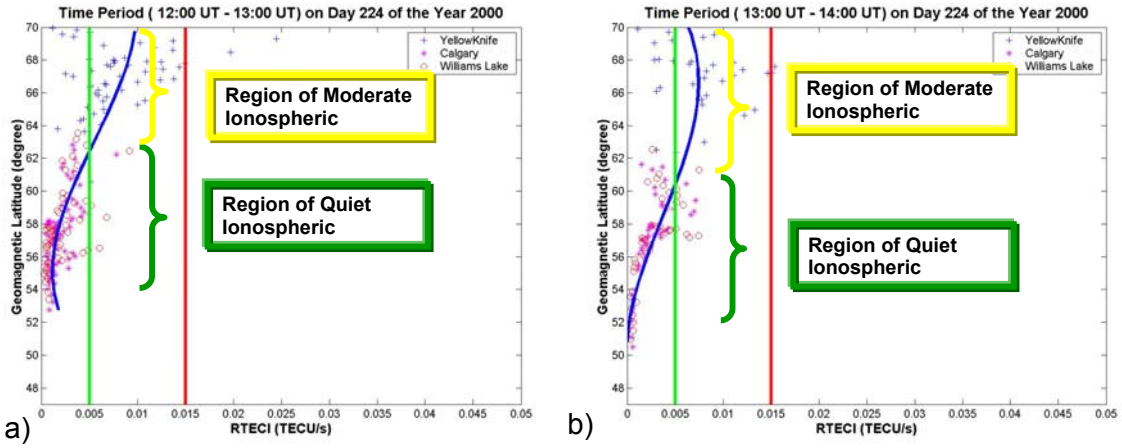

Figure 5.19 Latitude profiles of Group 4 for 1200 – 1400 UT on day 224 of the year 2000

The latitude profiles of Group 5 are presented in Figure 5.20. For time period 1200 – 1300 UT, the observations from Group 5 cover geomagnetic latitudes between 60^{o} and 66^{o}, and the polynomial fit identifies a region of moderate activity. During the second hour (1300 – 1400 UT), the boundary of moderate ionospheric activity region was observed at a geomagnetic latitude of 58 degrees, and the boundary of high activity was observed at a latitude of 60 degrees. It should be noted that only during this hour a boundary of high activity was identified.

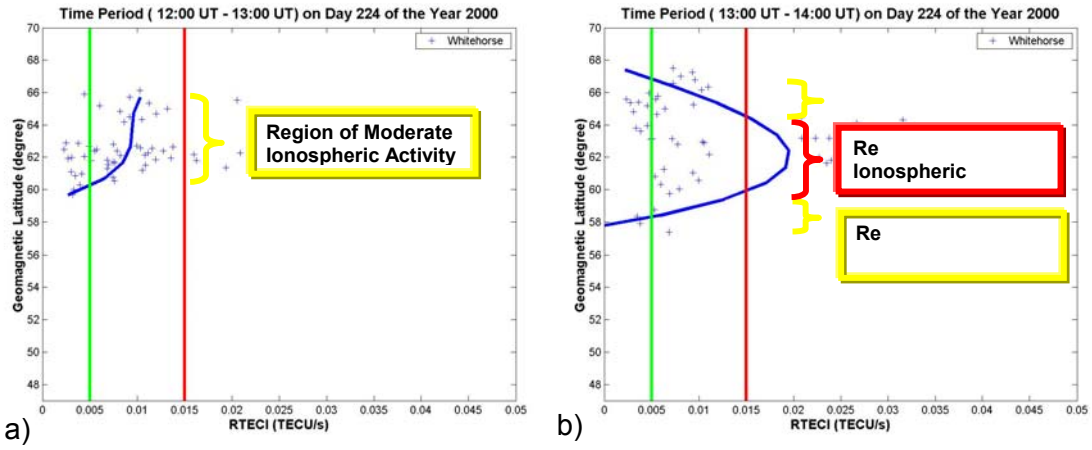

Figure 5.20 Latitude profiles of Group 5 for 1200 – 1400 UT on day 224 of the year 2000

Goodness of fits for the estimated latitudinal boundaries are presented in Table 5.4, where the variance is computed for the fitted polynomial for each group.

Table 5.4 Variance Values $(TECU/s)^2$ Representing Goodness of Fit of the Estimated Boundaries for Each Group

	Group 1	Group 2	Group 3	Group 4	Group 5
1st hour (1200-1300UT)	4.65e-07	1.00e-05	1.95e-05	1.21e-05	3.78e-05
2nd hour (1300-1400UT)	2.04e-07	1.38e-05	8.19e-06	7.64e-06	1.87e-05

Two-dimensional maps of RTECI values are shown in Figure 5.21. Latitude profiles of Groups 1-5 provide the boundary of moderate ionospheric activity (region north of the green curve shown in Figure 5.21).

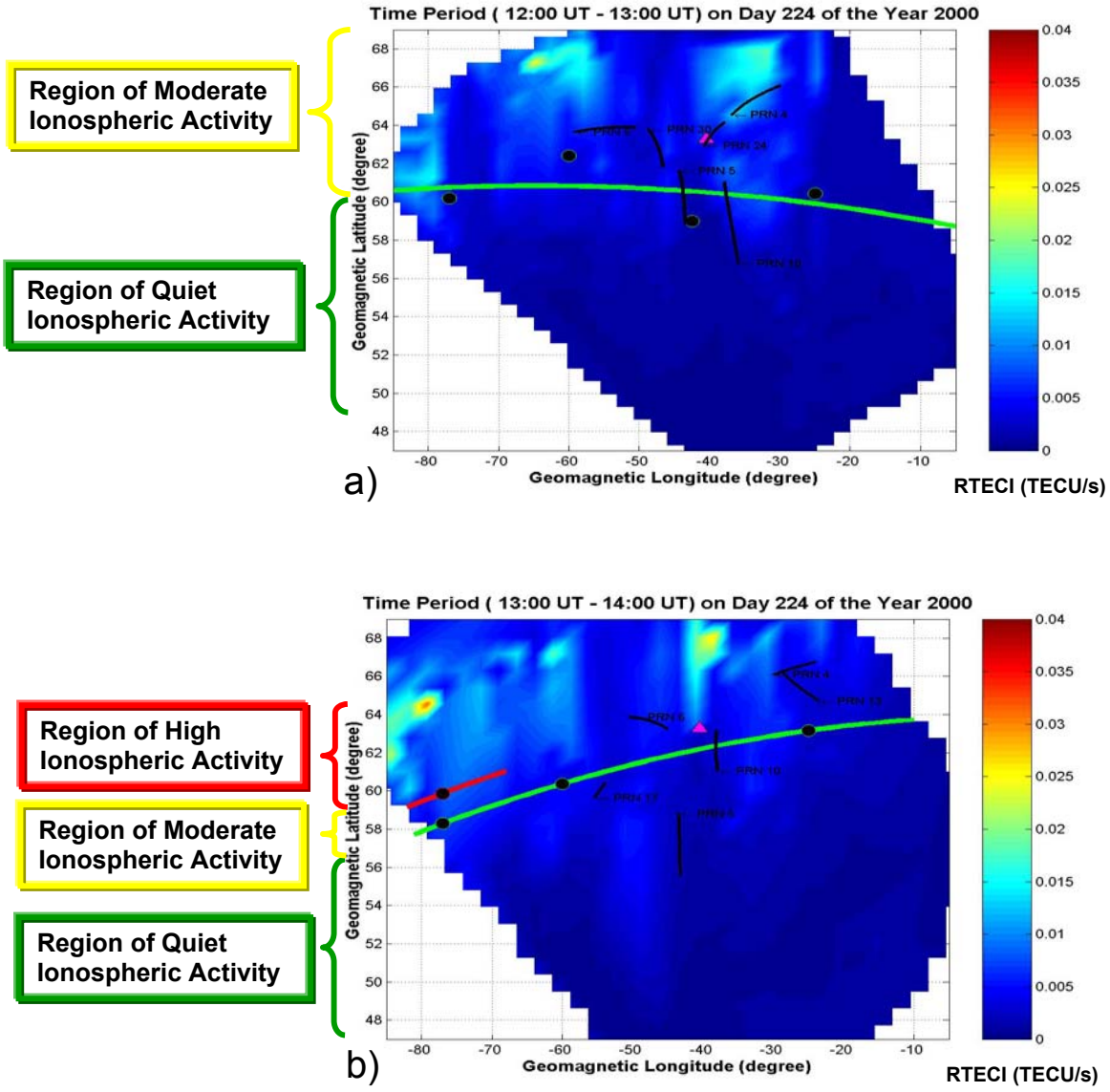

Figure 5.21 Two-dimensional extent of ionospheric activity for 1200 – 1400 UT on day 224 of the year 2000

5.3.3 Quiet Ionosphere Event

In order to illustrate the performance of the ionospheric monitoring technique during periods of quiet ionosphere, a two-hour period has been studied. The quiet periods

are identified according to the local North American geomagnetic "K" indices. Values of K were less than 1 during the two-hour period. Dual-frequency measurements were available on May 18th (day 142) of the year 2000 from reference stations in Figure 5.1. Two one-hour periods are presented from 22:00 – 24:00 UT. RTECI values are derived for each measurement along with the corresponding IPP values.

The series of plots in Figure 5.22 illustrate the latitudinal profiles of RTECI values for the five groups of stations. The observed RTECI values during periods of quiet ionosphere are significantly lower than for moderate and high ionospheric activity. Therefore, the x-axis scale of the latitude profiles has been changed again, compared with figures presented in Section 5.3.1 and Section 5.3.2.

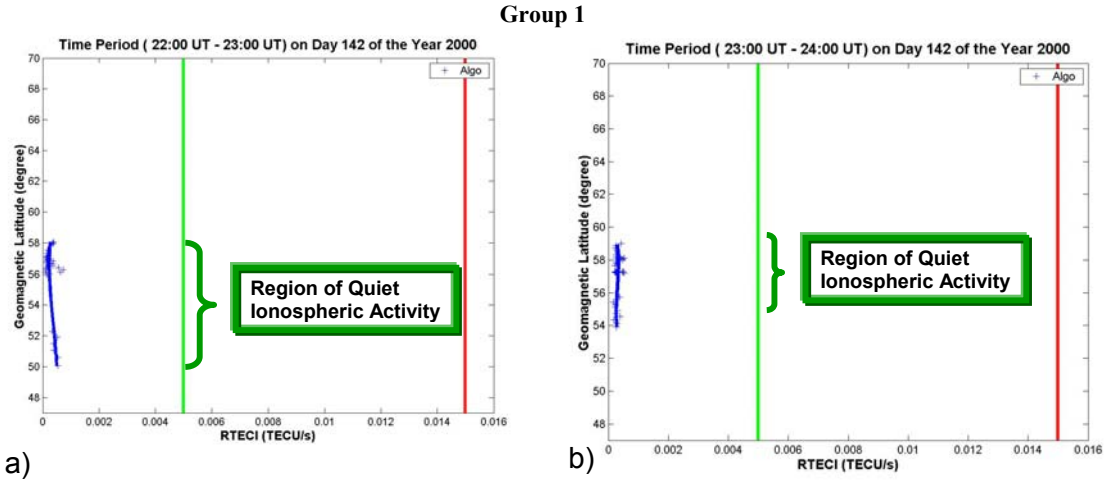

Group 2

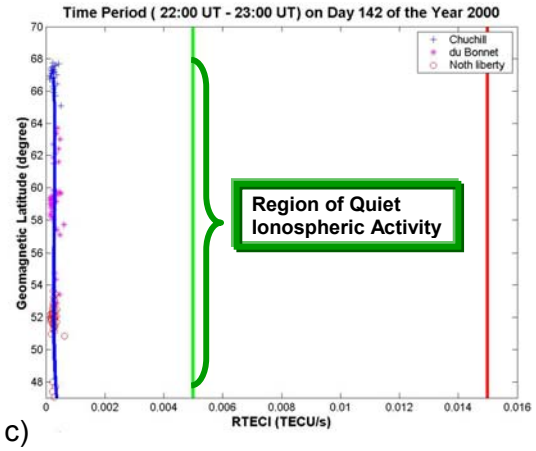

c)

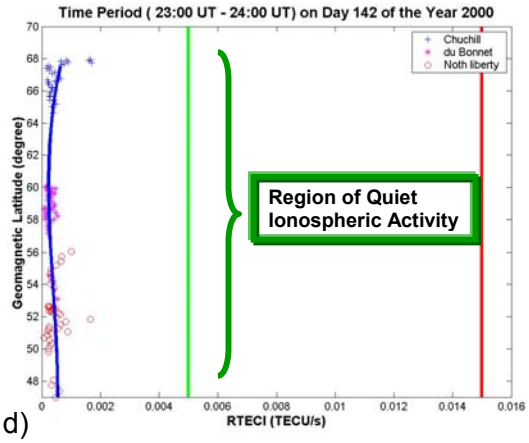

d)

Group 3

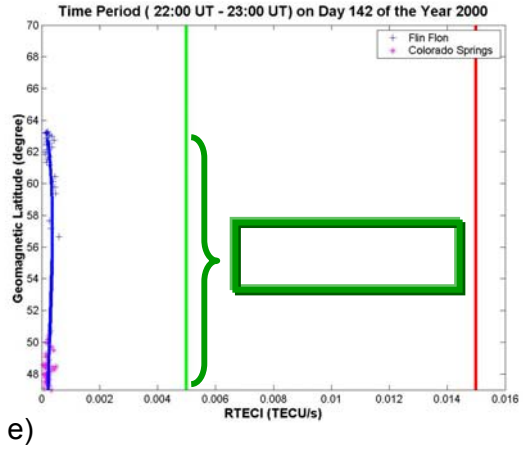

e)

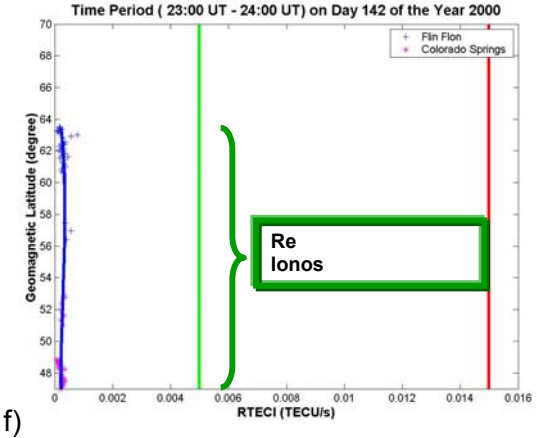

f)

Group 4

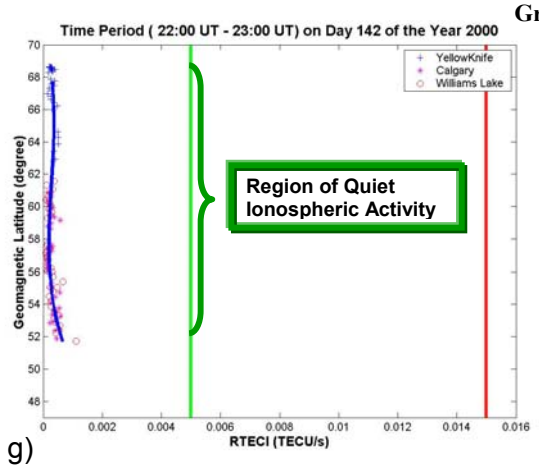

g)

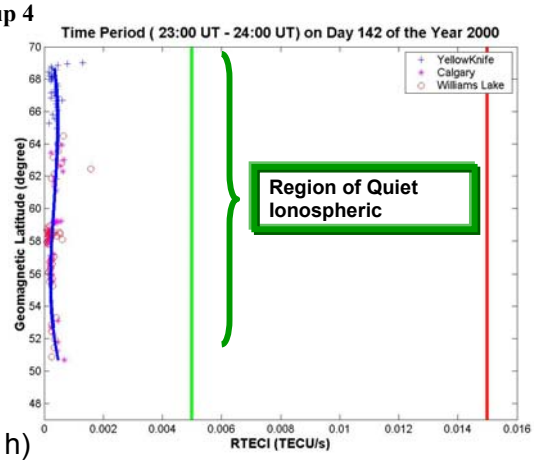

h)

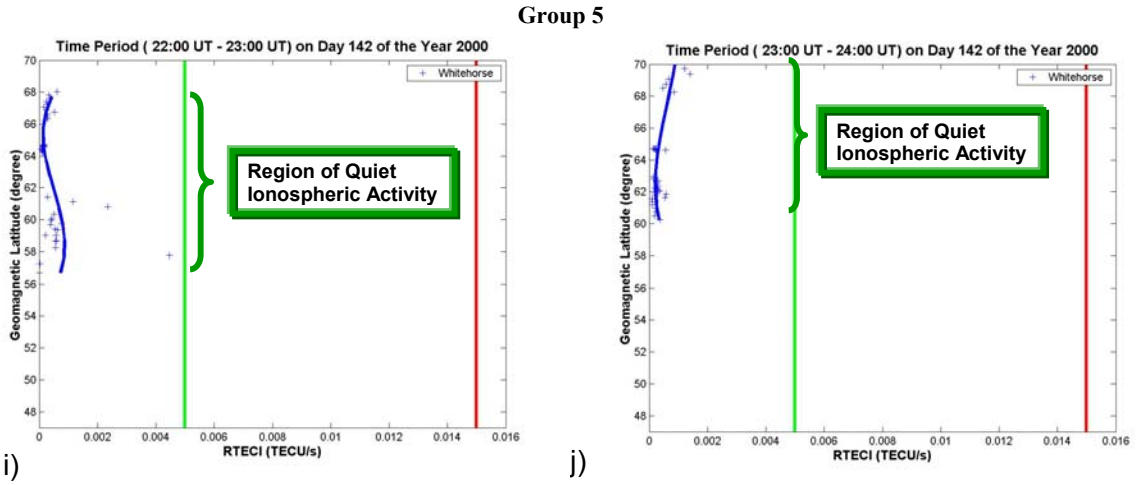

Figure 5.22 Latitude profiles of all groups for 2200 – 2400 UT on day 142 of the year 2000 (K=1)

It must be noted that RTECI values during the presented two-hour period did not exceed the value of 0.002 (TECU/s) for each of the five groups. As derived in Table 4.3, threshold RTECI values of 0.005 (TECU/s) indicate the boundary between quiet and moderate ionospheric activity. Consequently, all derived RTECI values during this event indicate a quiet ionosphere in the auroral region. Therefore, the proposed monitoring technique of the ionospheric activity is consistent with the local K indices.

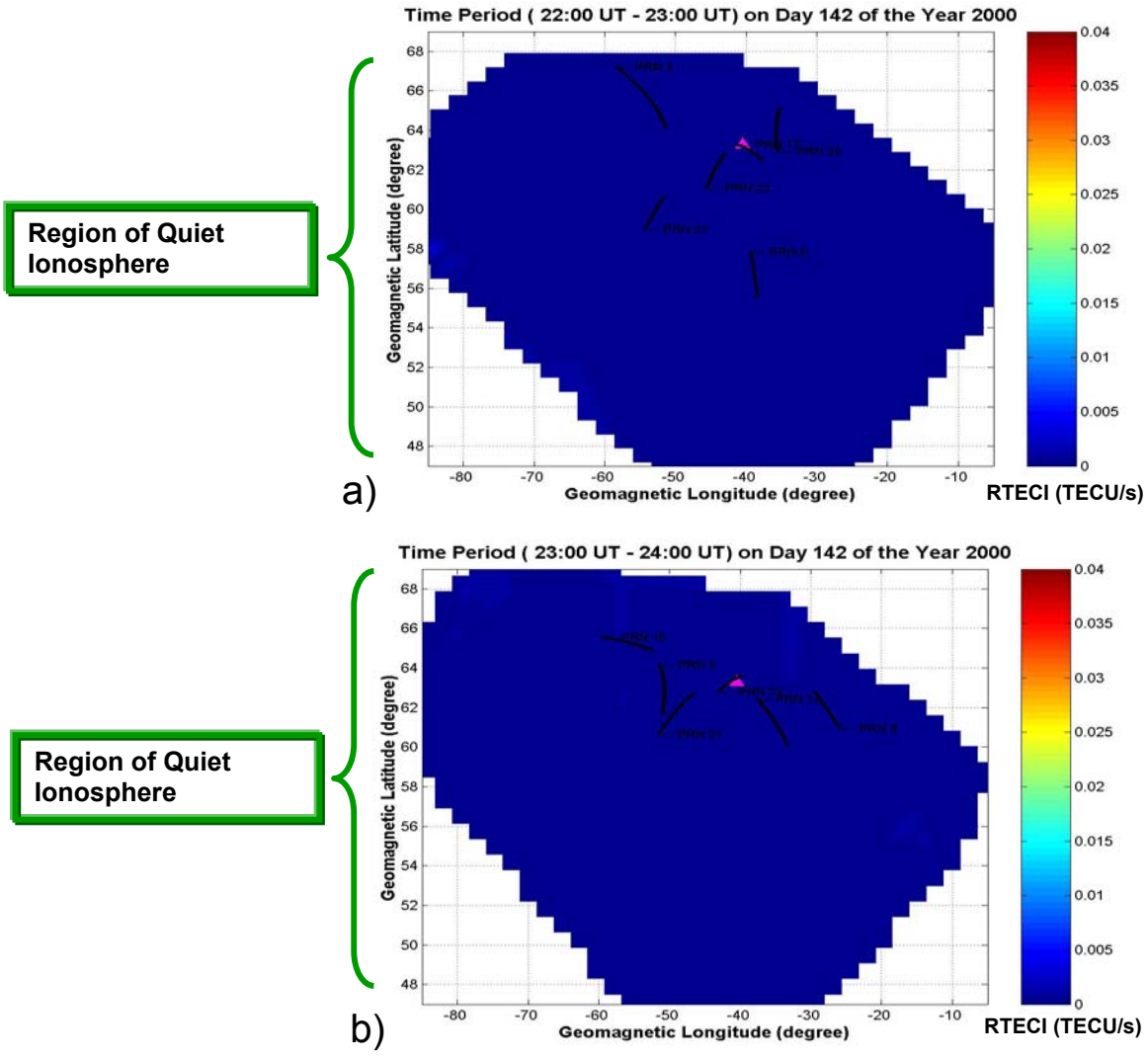

Figure 5.23 Latitudinal and longitudinal extent of the ionospheric activity for 2200 – 2400 UT on day 142 of the year 2000

The RTECI values in two dimensions during this event are presented in Figure 5.21. It is observed that there is no evidence of any ionospheric disturbed regions during these two hours according to the RTECI values. As a result, the entire region is assumed to be a quiet ionosphere region. Results of this section, and Sections 5.3.1 and 5.3.2, suggest

that the magnitude and extent of auroral activity may be monitored using observations from GPS reference stations.

5.4 PROPOSED ONLINE USER SERVICE

An online ionospheric monitoring service will be launched in the near future by the University of Calgary. The service will provide GPS users with near real-time estimates of the magnitude and extent of the auroral oval, as well as providing approximate spatial and temporal correlations in the ionosphere.

This service will be available via the internet, and will be based on data from a network of several Modulated Precision Clock (MPC) receivers. The MPC units consist of an Ionospheric Scintillation Monitor (ISM) integrated with a PC card to allow remote access of the unit via either Ethernet or modem connection. The ISM receiver is a modified dual frequency GPS receiver that extracts amplitude and phase scintillation parameters in real-time. The ISM uses a single-frequency GPS signal [*Van Dierendonck, et al.,* 1996] to derive the scintillation parameters, as well as providing rates of TEC and absolute TEC from dual-frequency GPS measurements. The data will be sent to a central processing facility at the University of Calgary over the Ethernet connection. A flow chart of the proposed online service is presented in Figure 5.24. A methodology similar to the one described in this research will be implemented in the proposed network. It is intended to use scintillation parameters in addition to RTECI - to provide additional information regarding receiver tracking performance.

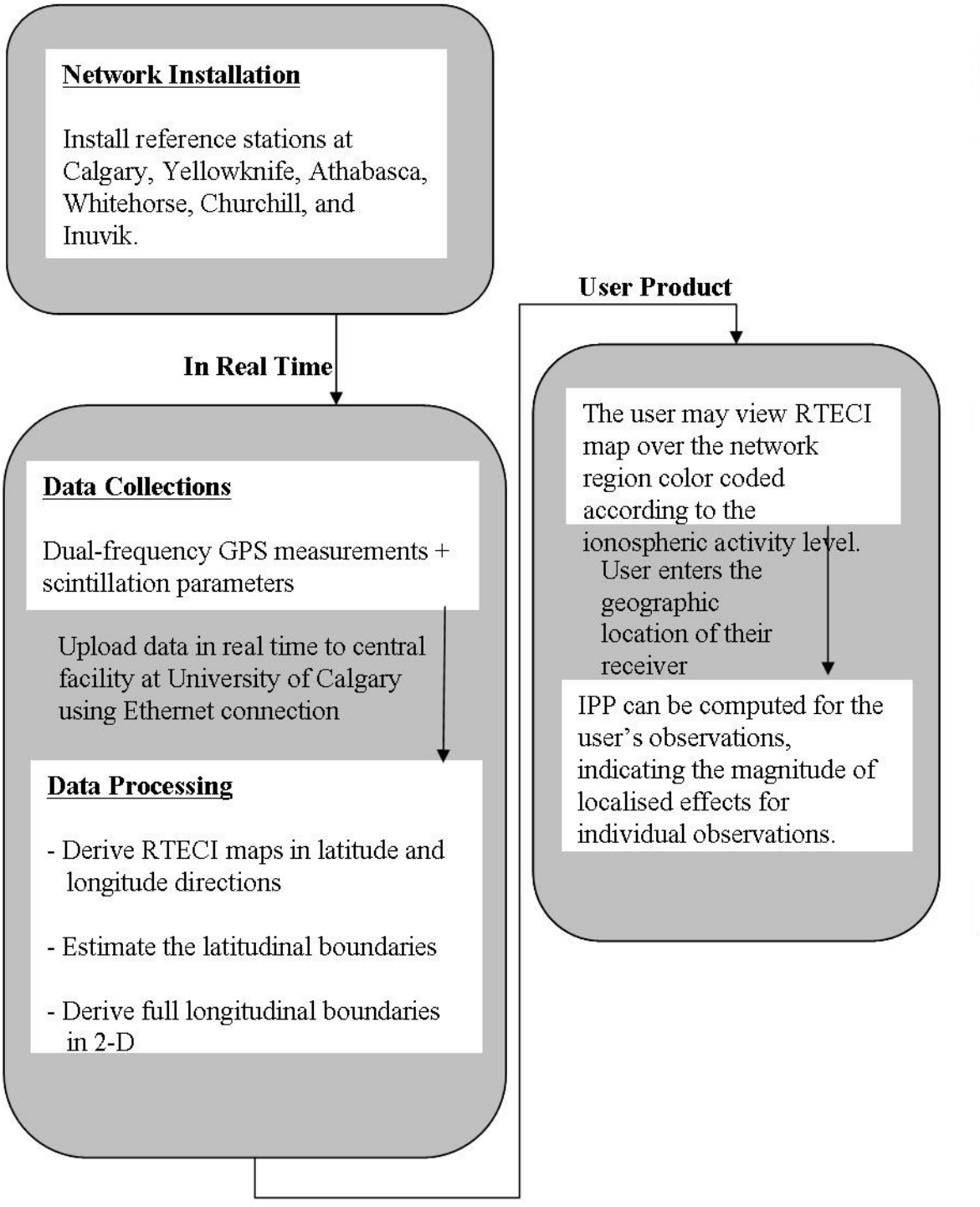

Figure 5.24 Flow chart of the proposed online service

An example of the online service that could be available in near real-time is also illustrated in Figure 5.15, Figure 5.21, and Figure 5.23. A user location is assumed at Flin Flon, Saskatchewan (presented by a magenta triangle in the figures), which is located at a geomagnetic latitude of 63.29^{o} N and a geomagnetic longitude of 40.52^{o} W. If the user enters their coordinates online, the map of RTECI could be provided as in Figure 5.15 for the most recent one-hour period, with the boundaries of high, moderate, and quiet ionospheric activity regions indicated. The IPP for all user observations would also be plotted for reference on the RTECI map. The satellite number of each measurement is indicated in Figure 5.15. For the last hour of the July 15 (day 197), 2000 event (Figure 5.15d), there are measurements available for satellites numbers 5, 9, 11, 15, 21, and 23. All measurements are located in the region of high ionospheric activity. A warning of high ionospheric activity for all measurements could be issued to the user. In addition, estimates of correlation times and distances in the vicinity of each satellite observation could also be provided to the user, based on the statistics derived in Chapter 4. Alternatively, in a non-interactive service the user could simply view plots such as those in Figure 5.15 to determine if the magnitude and extent of current ionospheric activity is an issue for them. Testing of the proposed technique is presented in Section 5.3.

The proposed warning service is also demonstrated in Figure 5.21. During the first-hour of this event, the user was collecting measurements from satellite numbers 4, 5, 6, 10, 24, and 30. According to the proposed technique, all IPP are located in the moderate activity region, with the exception of some measurements from satellites number 5 and 10, as shown in Figure 5.21a. The measurements were collected during the second hour from

satellite numbers 4, 5, 6, 10, 13, and 17. IPP from satellites 4, 6, 13, and 10 are located in the moderate ionospheric activity region. A warning of moderate activity for these measurements would be issued to the user. In addition, estimates of ionospheric correlation times and distances would be provided to identify irregularities in TEC over this region. Extensive testing of this method is essential to ensure the success of the ionospheric activity monitoring, as well as to maintain the reliability of the warning system. Details of the testing methodology and testing results are presented in the next section.

5.5 TESTING THE MONITORING AND WARNING TECHNIQUES

Examples of the monitoring technique have been provided in Section 5.3. The technique has been used to successfully monitor the extent of auroral activity during a substorm event, as discussed in Section 5.3.1. The auroral oval was observed to move equatorward during the storm event, as the boundary of the disturbed region is observed at progressively lower latitudes. During periods of moderate ionospheric activity, as identified by local geomagnetic activity indices K, the technique has also been used to efficiently monitor the level of ionospheric activity, and successfully identified regions of moderate ionospheric activity as discussed in Section 5.3.2.

It is intended that this technique will be used to warn GPS users of regions of high and moderate ionospheric activity. This technique identifies the regions of disturbed ionosphere, as well as identifying the level of disturbance. It becomes essential to test this method, and provide an insight into the reliability of the proposed user service.

Additionally, it is important to investigate the performance of the monitoring technique during large local ionospheric events.

5.5.1 Testing Method

Testing of the proposed user service was conducted for a period of 8 months, which started on January 1st, 2000 and ended on August 31st, 2000. Dual-frequency GPS measurements were collected from the reference stations shown in Figure 5.1. The Flin Flon reference station is assumed to be a GPS user, as illustrated in Figures 5.15, 5.21, and 5.23 (presented by a magenta triangle in the figures).

A similar technique to that described in Section 5.2 was conducted for each one-hour interval, where latitude profiles of RTECI values are derived using data from all groups of stations (with test station Flin Flon excluded). As a result, the boundaries of different ionospheric activity regions are obtained for each longitude sector. These boundaries are then extended in two-dimensions, in latitude and longitude. The Flin Flon reference station is used as an independent test site and, therefore, observations from Flin Flon are not included in the monitoring technique. The availability of Flin Flon data is discussed in Section 5.1.

Using the Flin Flon user's measurements, IPP values are computed for each one-hour interval as shown in Figures 5.15, 5.21, and 5.23 (black lines labeled with the satellite number). Relative TEC time series are also derived for every satellite series observed at

Flin Flon. Correlation times and distances are estimated for every continuous one-hour TEC time series as described in Section 4.4. The user observations are considered to be in regions of quiet, moderate or high activity, when compared with the boundaries derived in two-dimensions. The resulting correlation time and distance of each series is then compared with the statistics derived in Table 4.3 for the appropriate level of ionospheric activity. The statistics presented in Table 4.3 categorize the correlation times and distances according to the ionospheric activity levels. Statistics are computed for different testing scenarios:

5.5.2 Test the Warning of Active Ionosphere

For the purpose of this testing, an "active" ionosphere is defined as follows:

Active ionosphere includes both high and moderate ionospheric activity

In this test, if the one-hour TEC time series is identified as being in a region of active ionosphere (i.e. moderate or high activity regions), and its correlation time and distance are within the range specified in Table 4.3 (e.g. smaller than 696 sec and 75 km respectively), then this is considered to be a correct warning of an active ionosphere. On the other hand, the false alarm is identified if the one-hour TEC time series is in a region identified as having either moderate or high activity, and its correlation time and distance are within the range of quiet activity (greater than or equal to 696 sec and 75 km, respectively) as specified in Table 4.3.

The number of one-hour time series that were derived for testing purposes is 20794. A total of 7,387 time series were identified as being in active ionosphere region (e.g. located in regions of high or moderate ionospheric activity).

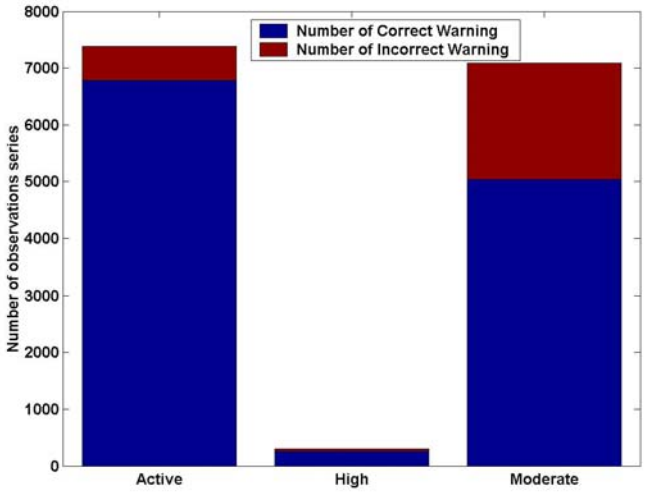

Figure 5.25 Probability of correct warnings (or false warnings) of active, moderate, and high ionospheric activity

Results of this test are summarized in the first column of Figure 5.25. The number of TEC time series that has correlation times and distances consistent with those in Table 4.3 for moderate or high activity is 6788 time series. The probability, therefore, of providing correct warnings of active ionosphere is 91.9%. For the same number of active TEC time series, the percent of false alarms of active ionosphere is 8.1%. For these TEC time series, the warning of ionospheric activity has been falsely issued for undisturbed measurements; the time series were located in regions predicted to be an active ionosphere, but the series have correlation times and distances larger than the values in Table 4.3 for an active ionosphere. The high percent of correct warning of active ionosphere indicates a

good performance of the proposed technique. For periods in which the ionosphere was identified as active by the monitoring technique, the ionosphere activity can be either high or moderate. The following tests presented in Section 5.5.4 and Section 5.5.5 investigate the performance of the monitoring technique for specific periods of high and moderate ionosphere activity, respectively.

5.5.4 Test the Warning of High Ionosphere Activity

Successful warnings of high activity are identified in this test if the one-hour TEC time series is in the region of predicted high activity and its correlation time and distance are in the range identified for high activity in Table 4.3 (smaller than or equal to 409 sec and 36 km, respectively).

The second column in Figure 5.25 summarizes the results. A total number of 297 one-hour TEC time series were identified in regions of high activity according to the monitoring technique. A warning of high activity would be issued for these time series. The derived correlation times and distances were smaller than 409 sec and 36 km, respectively (as identified for high activity regions in Table 4.3), for 85.8 percent of the series. The probability of incorrect warning for high ionospheric activity is 14.2%. In these cases the TEC time series located in a predicted high activity region, but correlation times and distances are larger than the values for high activity in Table 4.3. The derived correlation times and distances for TEC time series for periods of incorrect warning were in the range of the moderate activity.

5.5.5 Test Warning of Moderate Ionosphere Activity

A probability of a successful warning of moderate activity is evaluated in this test. In this case a correct warning is recognized if the one-hour TEC time series is in the predicted moderate activity region (as identified by the monitoring technique), and its correlation time and distance are in the range for moderate activity in Table 4.3 (696 – 409 sec and 75 – 36 km, respectively).

The number of one-hour TEC time series that are located in moderate activity regions is 7,090. The percent of these series that have correlation times and distances in the range of moderate activity is 71.1%, which indicates the probability of correct warnings for moderate ionospheric activity. The number of the TEC time series that were located in predicted moderate activity regions, but have correlation times and distances out of the predicted range for moderate activity is 2056 TEC time series (28.9%). This percent contains false alarms (when the ionosphere was quiet), and missed detections of high ionospheric activity. The false alarms were observed for 599 time series (8.4%), while the number of the missed detections of high activity is 1457 time series (20.5%).

These occasions of false alarms and missed detections of high activity are investigated. The difference between the correlation times (distances) that are outside of the predicted range for moderate activity is presented in Figure 5.26. The differences are binned in groups every 100 sec for correlation times, and every 10 km for correlation distances.

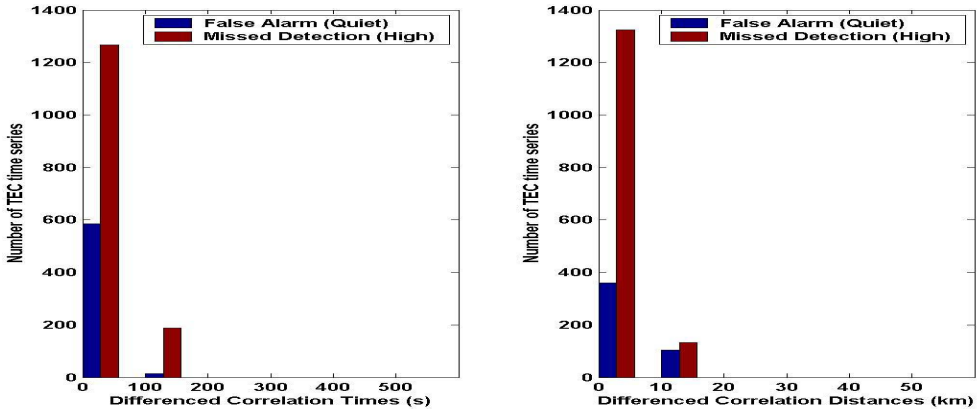

a) **b)**

Figure 5.26 Differences between the false alarm (missed detection) correlation times (a) and distances (b), and the thresholds of moderate ionosphere

For periods of missed detection for high ionospheric activity, the correlation times were shorter by up to 2 minutes, and the correlation distances were shorter by as much as 10-15 km. The number of the false alarms, when the monitoring technique identified the ionosphere activity as moderate and true activity was quiet, is smaller than the missed detection. The false alarms had correlation times longer within 1-2 min, and correlation distances longer within 10-15 km. The ionosphere activity during these periods was quiet, but close to the moderate activity boundaries.

5.5.6 Test Missed Detection of Active Ionosphere

The last test is conducted to examine the probability of not detecting an active ionosphere, when the one-hour TEC time series is in the region of predicted quiet ionosphere (according to the monitoring technique), but its correlation time and distance

are in the range of either moderate or high activity in Table 4.3 (smaller than 696 sec and 75 km, respectively).

There are 13410 one-hour TEC time series located in quiet regions as identified by the proposed monitoring technique. The number of TEC time series that have correlation times and distances in the range of quiet ionosphere (longer than 696 sec and 75 km respectively) is 10580 (78.9%). There are 21.1% of TEC time series located in quiet regions, but with correlation times and distances smaller than the thresholds of moderate ionosphere. The analysis of this 21.1% of the missed detections is presented in Figure 5.27. This figure presents the probability distribution of the missed detection correlation times and distances differenced with respect to the threshold values of moderate ionosphere (696 sec for correlation times, and 75 km for correlation distances).

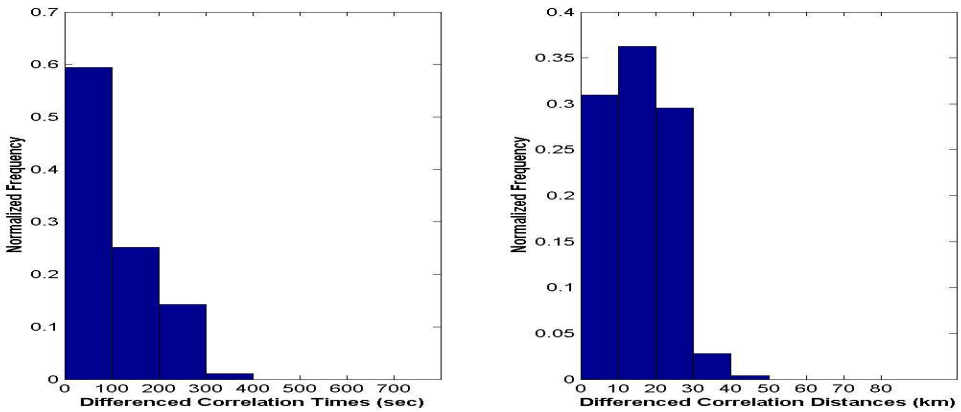

a) **b)**

Figure 5.27 Probability distribution of differences between the missed detection correlation times (a) and distances (b), and the thresholds of moderate ionosphere

Previous statistics summarized in Table 4.3 shows that the threshold values of high activity are smaller than 409 sec and 36 km, respectively. Also, the difference between thresholds for high and moderate activity (Table 4.3) are greater than 287 sec (39 km). In Figure 5.27, the 99^{th} – percentile of the differences, however, are smaller than 287 sec and 39 km. Therefore, the probability distribution presented in Figure 5.27 shows that occasions of missed detection are only when ionosphere has moderate activity.

5.6 SUMMARY

Ionospheric activity can be successfully monitored using GPS measurements [*Wanninger, 1993*]. TEC is one of the major factors that describes the ionosphere activity, where the free electrons in the ionosphere have several effects on GPS measurements as discussed in Section 3.2. The rate of change of TEC (RTEC) may be derived from precise GPS carrier phase observations; this has been used as a measure of ionospheric disturbances at high latitudes [*Stewart and Langley, 1999*]. RTEC has been statistically represented using an RTECI based on the standard deviation of RTEC observed over a 5-minute time period. RTECI values are derived for every satellite-receiver measurement in a network of reference stations, and mapped in latitude and longitude to monitor the extent of the ionospheric activity in auroral and sub-auroral regions. The development of an auroral substorm event has been monitored in real-time using the GPS-based index RTECI as demonstrated in Figure 5.15. Regions of moderate ionospheric disturbance also have been identified successfully using RTECI values as illustrated in Figure 5.21.

Based on the monitoring technique, regions of high, moderate, and quiet ionosphere can be identified. According to the testing conducted for 8 months during year 2000, the proposed method has correctly identified regions of active ionosphere for more than 90% of the total issued warnings. Moreover, the technique has also correctly issued warnings of high ionospheric activity for more than 80% of the warnings issued for high activity. When the technique identified high activity regions, but the correlation times and distances were longer than thresholds of high activity, the ionosphere activity was actually moderate.

Periods identified as moderate activity by the monitoring technique but with correlation times and distances outside of the range for moderate activity were observed 28.9 percent of the time. During these occasions, the correlation times (distances) were within 2 minutes (10-15 km) of the moderate activity thresholds. Periods when the ionosphere was identified as quiet by the monitoring technique but there were missed detections of the active ionosphere occurred 21.1 percent of the time during the 8 months testing period. All the missed detection periods were for moderate ionosphere activity. As a result, high (extreme) ionosphere activity events were always identified and monitored using the proposed technique. There are a few occasions when the monitoring technique might identify the high activity as moderate, but overall an active ionosphere was identified.

CHAPTER 6

CONCLUSIONS AND RECOMMENDATIONS

As discussed in Chapters 1, 2 and 3, enhanced auroral activity is a concern for reliable operations of GPS positioning applications. It leads to variations in ionospheric range delay, with small-scale features causing degraded DGPS accuracies, and the possibility of losing lock on GPS signals during periods of ionospheric scintillations. In recent years, GPS precise positioning applications have been disrupted consistently in Northern Canada – at significant cost to commercial surveying operations. Given the potential auroral effects on GPS applications and the changeable nature of the auroral region, it is essential to monitor the auroral activity and provide GPS users with information about potential impacts in real-time. In this thesis, a GPS-based index is introduced to describe the local ionospheric activity. A technique to monitor the magnitude and extent of the auroral activity is developed, and a warning and alert system for high latitude ionospheric disturbances is introduced. The results of this research are summarized in this chapter with recommendations for future work.

6.1 CONCLUSIONS

Ionospheric activity is conventionally monitored using global geomagnetic indices (i.e. Kp, Dst) derived from ground-based magnetometer measurements. These indices are

not appropriate for local ionospheric activity and are not available in real-time. Due to the dispersive nature of the ionosphere, dual-frequency GPS measurements can provide an alternate measure of the ionospheric activity. Therefore, a GPS-based index (i.e. RTECI) has been defined to describe the local ionospheric activity. RTECI is the standard deviation of RTEC observed over a 5-minute time period. This index allows a measure of the local ionospheric variability, where the time interval of 5-minutes was chosen such that a reliable statistical representation was derived for a relatively short time interval. RTECI values are derived for every satellite-receiver measurement in a network of reference stations, and mapped in latitude and longitude directions to monitor the extent of the ionospheric activity in auroral and sub-auroral regions.

Threshold values of RTECI, corresponding to moderate and high levels of ionospheric activity, are derived by statistically correlating the RTECI values with temporal and spatial properties of the ionosphere derived from individual satellite TEC time series. Increased rates of TEC reflect the presence of structured irregularities in electron density and, in turn, reflect shorter correlation times and distances in the ionosphere. This study was used to identify high, moderate, and quiet ionospheric activity. TEC time series were derived at 5 reference stations for the entire year 2000. The autocorrelation functions were derived for every one-hour of TEC time series, and approximated as first order Gauss-Markov processes to derive the correlation times and distances. It was found that during periods of quiet ionospheric activity the RTECI values are equal to or less than 0.005 TECU/s, with average correlation times of 696 sec, and average correlation distances of 75 km. The RTECI values greater than 0.015 TECU/s were

observed during high ionospheric activity, with average correlation times of 409 sec, and an average correlation distance of 36 km. During moderate periods of ionospheric activity, RTECI values range between 0.005 and 0.015 TECU/s, with corresponding correlation times and distances of 461 sec and 47 km, respectively.

In this thesis, a technique for monitoring auroral activity has been developed by mapping RTECI values in latitude-longitude directions. This method begins with initial latitudinal profiling of RTECI for five individual sectors in the longitude direction, where each strip is 15 degrees in width. Based on the threshold values of RTECI, boundaries of moderate and high ionospheric activity have been defined, and regions of enhanced activity have been identified. Effectiveness of the proposed monitoring technique was demonstrated during a large substorm event on July 15-16 of the year 2000. The substorm evolution was successfully monitored in detail using the proposed technique. Equatorward expansion of the auroral oval over the Northern United States was observed, as the boundary of the disturbed region moved to progressively lower latitudes. The extent of auroral activity during periods of lower ionospheric activity ("moderate") was also effectively monitored using the proposed method.

Based on the monitoring technique, the boundary of the disturbed regions was observed and tests of the proposed monitoring technique were conducted, for a specified user location, for a period of 8 months. It is intended that a warning would be issued to GPS users for events where user's observations have satellite-receiver lines-of-sight passing through disturbed regions. The performance reliability of the warning system has

been established through the testing results. It was concluded that the proposed warning system has correctly issued “active” ionosphere warnings for more than 90 percent of the total issued warnings. Moreover, the warning system has also correctly issued warnings of “high” ionospheric activity for more than 80 percent of the warnings issued for the high activity. When the technique identified high activity regions, but the correlation times and distances were longer than thresholds of high activity, the ionosphere activity was moderate.

During periods in which the ionosphere was identified as moderate by the monitoring technique, the warning system issued false alarms 8.4 percent of the time (when ionosphere was quiet), and missed detection of high activity 20.5 percent of the time. Periods of missed detection of high activity are investigated. The correlation times (distances) derived during these periods are close to the moderate activity thresholds, and were within 2 min (10-15 km) of the moderate activity thresholds.

During periods in which the ionosphere was identified as quiet by the monitoring technique, there were missed detections of active ionosphere for 21.1 percent of the time during the 8 months testing period. All the missed detection periods were for moderate ionosphere activity. Therefore, there were no missed detections of any local high ionospheric activity during the tested 8 months of the year of 2000.

6.2 RECOMMENDATIONS AND FUTURE WORK

In this research, techniques have been developed to monitor auroral activity using dual-frequency GPS measurements, and to provide users with an ionospheric warning and alert system in the Canadian sector and Northern United States. Several areas of future work are proposed here.

Results of testing the proposed technique indicate a limitation of deriving boundaries between quiet and moderate ionosphere activity regions. During periods in which the ionosphere was identified as quiet by the monitoring technique, there were missed detections of moderate activity for 21.1 percent of the time. Therefore, a denser network of reference stations would help significantly to derive the boundaries of high, moderate, and quiet regions accurately. Furthermore, the statistics of the correlation times and distances, and the corresponding RTECI can be investigated using a larger data set to identify more accurate thresholds of RTECI.

Ionospheric scintillation can be investigated by applying a similar methodology using ionospheric scintillation parameters. This may allow monitoring of the ionospheric scintillation, and estimating potential impacts on GPS receiver tracking performance. It is intended to apply a similar method to that presented in this research to the Canadian GPS Network for Ionosphere Monitoring (CANGIM). This network will provide an online ionospheric monitoring service, and will be launched in the near future by the University of Calgary. The service will provide GPS users near real-time estimates of the magnitude and

extent of the auroral oval, as well as providing approximate spatial and temporal correlations in the ionosphere.

This service will be available via the internet, and will be based on data from a network of several Modulated Precision Clock (MPC) receivers. The MPC units consist of an Ionospheric Scintillation Monitor (ISM) integrated with a PC card to allow remote access of the unit via either Ethernet or modem connection. The data are sent to a central processing facility at the University of Calgary over the Ethernet connection at 30-minute intervals. A methodology similar to the one described in this thesis will be implemented in the proposed network.

Three MPC units have recently been installed in Yellowknife, Athabasca, and Calgary covering approximately 1500 km in the N-S direction – with the capability of monitoring the extent of the auroral oval. In the near future, three more MPC units in Whitehorse, Churchill and Inuvik will be installed to expand the network coverage in the Western Canadian sector. Site locations of installed and proposed reference stations are shown in Figure 6.1.

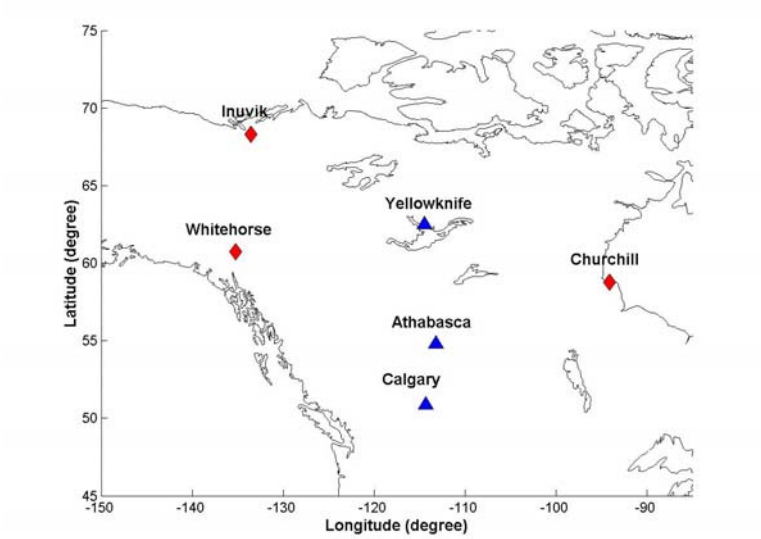

Figure 6.1 Site locations of the installed MPC units (triangles) and the proposed site locations (red diamonds)

The techniques developed here allow near real-time monitoring of ionospheric activity in the Canadian sector. It would be extremely valuable if the system also provided predictive capabilities. Ground-based observations, such as GPS measurements, are adequate for monitoring ionospheric activity. In order to predict ionospheric phenomena, however, the additional measures of solar activity are generally required. Instruments such as space-borne imagers, magnetometers and particle flux sensors provide images of the Sun and the auroral oval, measurements of the interplanetary magnetic field and solar wind velocities, electric field strength, and estimates of particle energies. These data are used by space scientists to monitor the origin of space weather at the Sun and follow its progression towards the Earth. The NOAA Space Environment Center (SEC) has developed "predicted" K indices for a site at Boulder, Colorado – based on both the ground-based magnetometer values and other sources of solar data. The capability of predicting auroral

effects and the extent of auroral activity could be investigated by using these space weather parameters provided by the SEC. The SEC K indices allow several hours advance warning of enhanced ionospheric activity. The correlation between the predicted K indices and RTECI, as well as spatial and temporal correlation properties of the ionosphere derived from TEC time series, may be investigated to evaluate predictive capabilities. This may result in predictions of potential substorm effects for GPS users.

REFERENCES

Appleton, E. V., "The anomalous equatorial belt in the F2-layer", Journal of Atmospheric and terrestrial Physics, 5, 349, 1954.

Basu, S, E. Mackenzie, S. Basu, H.C. Carlson, D.A. Hardy and F.J. Rich, "Coordinated measurements of low-energy electron precipitation and scintillation/TEC in the auroral oval", Radio Science, 19, no.6, 1151, 1983.

Basu, S., E. MacKenzie and S. Basu, "Ionospheric constraints on VHF/UHF communications links during solar maximum and minimum periods", Radio Science, Vol. 23, No. 3, 363, May-June 1988.

Bishop, G., D. Howell, C. Cocker, A. Mazzella, D. Jacobs, E. Fremouw, J. Secan, B. Rahn, C. Curtis, J. Quinn, K. Groves., S. Basu and M. Smithan, " Test Bed for evaluation of GPS receivers' Performance in Ionospheric Scintillation – A Progress Report", Proceedings of ION National Technical Meeting, Long Beach, CA, January 1998.

Black, H. D, "An easily implemented algorithm for the tropospheric range correction", Journal of Geophysical Research, Vol. 83, No. B4, 1825, 1978.

Brown, R. and P. Hwang, "Introduction to Random Signals and Applied Kalman Filtering", John Wiley & Sons, USA, 1997.

Bugoslavskaya, N.Y., “Solar activity and the ionosphere, for radio Communications specialists”, Pergamon Press Ltd., New York, 1962.

Challstrom, C., “The benefits of GPS modernization”, In The Quarterly Newsletter of the Institute of Navigation, vol. 9, no. 2, Summer 1999.

Coker, C., R. Hunsucker and G. Lott, “Detection of auroral activity using GPS satellites”, Geophysical Research Letters, 22, 23, 3259, 1995.

Decker, B. L., “ World Geodetic System 1984”, Proceedings of the Fourth International Geodetic Symposium on Satellite Positioning, Austin, Texas, Vol. 1, 69, 1986.

Davies, K., “Ionospheric radio”, Peter Peregrinus Ltd, London,1990.

Doherty, P. H., S. H. Delay, C. E. Valladares and J. A. Klobuchar, “Ionospheric scintillation effects in the equatorial and auroral regions”, Proceedings of ION GPS, Salt Lake City, UT, 19, September 2000.

Foster, J.C., “Quantitative investigation of ionospheric density gradients at mid latitudes”, Proceedings of ION National Technical Meeting, Anaheim, CA, 447, January 2000.

Foster, A.J., J.C. Foster, P.J. Erickson and F.J. Rich, "Regional GPS mapping of storm enhanced density during the 15-16 July 2000 geomagnetic storm", Proceedings of ION GPS, Salt Lake city, UT, 2531, September 2001.

Gao, Y. and M. Sideris, "Data analysis in engineering", Lecture Notes for ENGO 563, Department of Geomatics Engineering, University of Calgary, Fall 2000.

Goad, C. and L. Goodman, "A modified Hopfield tropospheric refraction correction model", Presented at the Fall Annual Meeting American Geophysical Union, San Francisco, CA, 28, December 1974.

Hapgood, M.A., "Space physics coordinate transformations: a user's guide", Planetary Space Science, 40, 711, 1992.

Hargreaves, J.K., "The solar-terrestrial environment," Cambridge Atmospheric and Space Sciences series, Cambridge University Press, Cambridge, UK, 1992.

Hatch, R., "The synergism of GPS code and carrier measurements", Magnavox Technical Paper, MX-TM-3353-82, January 1982.

Hoffmann-Wellenhof, B., H. Lichtenegger and J. Collins, "GPS: Theory and Practice", Springer-Verlag, New York, Third edition, 1994.

Hopfield, H., “Two-quartic tropospheric refractivity profile for correction satellite data”, Journal of Geophysical Research, Vol. 74, Number 18, 4487, 1969.

Huang, Y. N. and K. Cheng, “Ionospheric disturbances at the equatorial anomaly crest region during the March 1989 magnetic storm”, Journal of Geophysical Research, 96, no. A8, 13953, 1991.

Hunsucker, R.D., “Mini-review: auroral and polar-cap ionospheric effects on radio propagation”, IEEE Transactions on antennas and propagation, 40, no.7, 818, 1992.

Hunsucker, R.D., C. Coker, J. Cook and G. Lott, “ An investigation of the feasibility of utilizing GPS/TEC “signatures” for near-real time forecasting of auroral E propagation at high-HF and low-VHF frequencies”, IEEE Transactions on Antennas and Propagation, 43, 10, 1313, 1995.

International GPS Service (IGS), “International GPS Service Annual Report 2000”, IGS Central Bureau, Jet Propulsion Laboratory. Pasadena, California, 14, 2001.

Jefferson, D. and Y. Bar-Sever, “Accuracy and consistency of broadcast GPS ephemeris data”, Proceedings of ION GPS, Salt Lake City, UT, 438, September 2000.

Kaplan, D., “Understanding GPS principles and applications”, Artech House Publishers, Boston, 1996.

Klobuchar, J.A., “Ionospheric time-delay algorithm for single-frequency GPS users”, IEEE Transactions on Aerospace and Electronic Systems, Vol. AES-23, No. 3, May 1987.

Klobuchar, J.A., “Ionospheric effects on GPS, in Global Positioning System: Theory and Applications”, Vol. I, (ed) B.W. Parkinson and J.J. Spilker, American Institute of Astronautics and Aeronautics, Washington, D.C., 1996.

Knight, M., M. Cervera and A. Finn, “A comparison of predicted and measured GPS performance in an ionospheric scintillation environment”, Proceedings of the ION GPS, Nashville, Tennessee, 1437, September 1999.

Knight, M. and A. Finn, “The impact of ionospheric scintillation on GPS performance”, Proceeding of the ION GPS, 555, September 1996.

Lachapelle, G., “GPS theory and applications”, Lecture Notes for ENGO 625, Department of Geomatics Engineering, University of Calgary, Fall 2001.

Matsushita, S. and W.H. Campbell, “Physics of geomagnetic phenomena”, Vol.II, Academic Press, New York, 1967.

Mayaud, P.N., “Derivation, meaning, and use of geomagnetic indices”, AGU, Washington, D.C., 1980.

Mendes, V., "Modeling the neutral atmosphere propagation delay in radiometric space techniques", Ph.D. Dissertation, Technical Report No. 199, Department of Geodesy and Geomatics Engineering, University of New Brunswick, 1999.

Nichols, J., A. Hansen, T. Walter and P. Enge, "High-latitude measurements of ionospheric scintillation using the NSTB", Journal of The Institute of Navigation, Vol. 47, No. 2, 112, Summer 2000.

NovAtel, "NovAtel's GPS-600 antenna", Product Specification Sheet, 2000.

Parkinson, B.W., "History and operation of NAVSTAR, the Global Positioning System", IEEE Transactions on Aerospace and Electronic Systems, Vol. 30, No. 4, October 1994.

Parkinson, B.W. and P.K. Enge, "Differential GPS", in Global Positioning System: Theory and Applications, Vol. I, (ed) B.W. Parkinson and J.J. Spilker, American Institute of Astronautics and Aeronautics, Washington, D.C., 1996.

Pi, X., A.J. Mannucci, U.J. Lindqwister and C. M. Ho, "Monitoring of global ionospheric irregularities using the worldwide GPS network", Geophysical Research Letters, Vol. 24, No. 18, 2283, September 1997.

Ray, J., "Mitigation of GPS Code and Carrier Phase Multipath Effects Using a Multi-Antenna System", PhD Dissertation, Department of Geomatics Engineering, University of Calgary, 2000.

Rishbeth, H. and O.K. Garriott, "Introduction to Ionospheric Physics", Academic Press, New York, 1969.

Rostoker, G. and S. Skone, "Magnetic flux mapping considerations in the auroral oval and Earth's magnetotail, Journal of Geophysical Reasearch, 98, 1377, 1993.

Saastamoinen, I, "Contribution to the theory of atmospheric refraction", Bulletin Geodesique, 107, 13, 1973.

Shaw, M., K. Sandhoo and D. Turner, "Modernization of the Global Positioning System", GPS World, September 2000.

Skone, S., "Wide area ionosphere grid modelling in the auroral region", PhD Dissertation, UCGE Report No.20123, Department of Geomatics Engineering, The University of Calgary, 1998.

Skone, S., "TECANALYS^{TM}", Operating Manual, Department of Geomatics Engineering, University of Calgary, version 1.0, May 2000.

Skone, S. and K. Knudsen, “GPS receiver tracking performance under equatorial and high latitude ionospheric scintillations”, Proceeding of the 3rd International Symposium on Mobile Mapping Technology, Cairo, Egypt, Jan. 2001.

Skone, S., M. El-Gizawy and S. M. Shrestha, “Limitation in GPS positioning accuracies and receiver tracking performance during solar maximum”, Proceeding of KIS, Banff, Canada, June 2001.

Skone, S., “Atmospheric effects on satellite navigation systems”, Lecture notes for ENGO 633, Department of Geomatics Engineering, University of Calgary, April 2001.

Spilker, J., “Tropospheric effects on GPS”, in Global Positioning System: Theory and Applications, Vol.1, (ed) B.W. Parkinson and J.J. Spilker, American Institute of Astronautics and Aeronautics, Washington, D.C., 1996.

Townsend, B. and P. Fenton, “A Practical approach to the reduction of pseudorange multipath errors in a L1 GPS receiver”, Proceedings of ION GPS, Salt Lake City, UT, 143, September 1994.

Townsend, B., P. Fenton, K. Van Dierendonck and R. van Nee, “Performance evaluation of the multipath eliminating delay lock loop”, Journal of the Institute of Navigation, Vol. 42, No. 3, 503, Fall 1995.

Van Dierendonck, A.J., P. Fenton and T. Ford, “Theory and performance of narrow correlator spacing in a GPS receiver”, the ION National Technical Meeting, San Diego, January1992.

Van Dierendonck, A. J., Q. Hua, P. Fenton and J. Klobuchar, “Commercial ionospheric scintillation monitoring receiver development and test results”, Proceedings of The ION 52nd Annual Meeting, Cambridge, MA, June 1996.

Wanninger, L., “Ionospheric monitoring using IGS data”, Proceedings of the 1993 IGS workshop, Berne, March 1993a.

Wanninger, L., “Effects of the equatorial ionosphere on GPS”, GPS World, 48, July1993b.

Weisenburger, S., “Effect of constraints and multiple receivers for on-the-fly ambiguity resolution”, M.Sc. Thesis, Report Number 20109, University of Calgary, Department of Geomatics Engineering, Calgary, 1997.

Wells, D., N. Beck, D. Delikaraoglou, A. Kleusberg, E. Krakiwsky, G. Lachapelle, R. Langley, M. Nakiboglu, K. P. Schwarz, J. Tranquilla and P. Vanicek, “Guide to GPS positioning”, 2nd printing with corrections, Canadian GPS Associates, 1987.

Wooden, W.H., “Navstar Global Positioning System”, Proceedings of the First International Symposium on Precise Positioning with the Global Positioning System, Rockville, Maryland, 1985.

APPENDIX A

IONOSPHERE PIERCE POINT CALCULATION

Ionospheric Pierce Point (IPP) is the intersection point between the satellite-receiver line-of-sight, and the ionosphere shell. The ionosphere is assumed to be a thin shell at fixed altitude (nominally taken as 350 km). IPP location can be computed by providing reference station coordinates (ϕ_r, λ_r), and satellite ephemeris [*Skone, 2000*] as illustrated in the following figure:

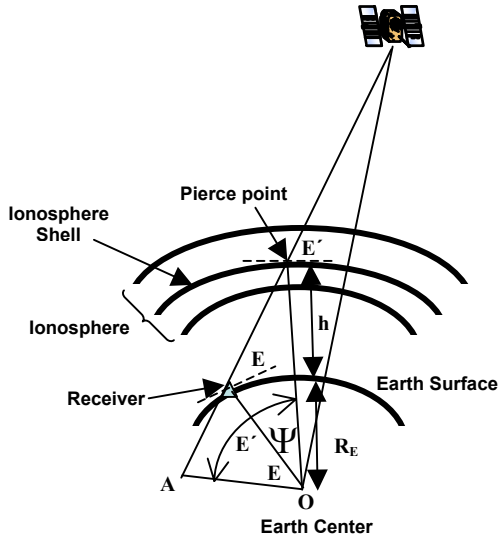

Figure A.1 Geometry of ionospheric pierce point calculation

In Figure A.1, E' and E are elevation angles at the IPP and the user's receiver, respectively. R_E is the mean radius of the spherical Earth (6371.0 km) and h is the height of IPP (nominally taken to be 350 km). The angle Ψ is defined from the center of a spherical Earth, and it is the offset between the IPP and the user's receiver. This angle is computed as follows:

$$\Psi = E' - E \tag{A.1}$$

The following relationship can also be derived from the figure geometry:

$$OA = (R_E)\cos E = (R_E + h)\cos E' \tag{A.2}$$

An approximate expression for the elevation angle E' can be derived from Equation A.2 as follows:

$$E' = \cos^{-1}\left(\left(\frac{R_E}{R_E + h}\right)\cos E\right) \tag{A.3}$$

Equation A.1, therefore, can be expressed as

$$\Psi = \cos^{-1}\left(\left(\frac{R_E}{R_E + h}\right)\cos E\right) - E \tag{A.4}$$

Given the user's receiver coordinates (ϕ_r, λ_r) and the offset angle Ψ, the pierce point coordinates $(\phi_{IPP}, \lambda_{IPP})$ are then derived by the following expressions:

$$\phi_{IPP} = \phi_r + \Psi \cos(Azim) \tag{A.5}$$

$$\lambda_{IPP} = \lambda_r + \frac{\Psi \sin(Azim)}{\cos(\phi_{IPP})} \tag{A.6}$$

where *Azim* is the azimuth angle of the satellite.

APPENDIX B

GEOMAGNETIC COORDINATES CALCULATIONS

The geomagnetic poles can be computed as a function of the Modified Julian Day (*MJD*) [*Hapgood, 1992*], and can be expressed as follows:

$$\phi_{dip} = 78.8 + 4.283 \times 10^{-2} \left[\frac{MJD - 46066}{365.25} \right] \tag{B.1}$$

$$\lambda_{dip} = 289.1 - 1.413 \times 10^{-2} \left[\frac{MJD - 46066}{365.25} \right] \tag{B.2}$$

The geomagnetic coordinates (Φ, Λ) are calculated by converting the geographic coordinates (ϕ, λ) as expressed in the following equations [*Matsushita and Campbell, 1967*]:

$$\sin\Phi = \sin\phi\cos\phi_{dip} + \cos\phi\sin\phi_{dip}\cos(\lambda - \lambda_{dip}) \tag{B.3}$$

$$\sin\Lambda = \frac{\cos\phi\sin(\lambda - \lambda_{dip})}{\cos\Phi} \tag{B.4}$$

APPENDIX C

DISTANCE CALCULATION ON IONOSPHERE SHELL

Given the coordinates of the two Ionospheric Pierce Points (ϕ_1, λ_1) and (ϕ_2, λ_2), the distance that the GPS signal travels through the ionosphere shell can then be computed using the Law of Cosines for Spherical Trigonometry. The distance can be derived as follow:

$$A = \sin(\phi_1)\sin(\phi_2) \quad \text{(B.1)}$$

$$B = \cos(\phi_1)\cos(\phi_2)\cos(\lambda_2 - \lambda_1) \quad \text{(B.2)}$$

$$C = \arccos(A + B) \quad \text{(B.3)}$$

$$d_{IPP} = (R_E + h) \times C \quad \text{(B.4)}$$

Where d_{IPP} is the traveled distance by the signal through the ionosphere shell, R_E is the mean radius of the Earth (6371.0 km), and h is the altitude of the ionosphere shell (350km).